ACE Deliverable *2.3D03*

Catalogue of Models and Methods for Reflector Surface Modelling

Project Number: FP6-IST 508009

Project Title: Antenna Centre of Excellence

Document Type: Deliverable

Document Number: WP2.3-2-01

Contractual date of delivery: 1 July 2004

Actual Date of Delivery: 31 December 2004

Workpackage: 2.3-2

Estimated Person Months: 6

Security (PP,PE,RE,CO): PP

Nature: Report

Version: 1

Total Number of Pages: 106

File name: ACE_2.3_D3_Reflector_Surface_Modelling_Catalogue.doc

Editors: Knud Pontoppidan

Participants: TNO FEL, Chalmers University of Technology, University of Siena, Politecnico di Torino, Lund University, TICRA Engineering Consultants

Abstract

The present document is a comprehensive collection of methods and models for the analysis and prediction of surface reflection and transmission characteristics. The different types of surfaces are discussed and various accurate and approximate analysis methods of the partners are presented. Chapter 5 gives a number of specific applications of the more general methods presented. Here the applications are ordered according to the surface type.

Keyword List

FSS, Strip Grids, Wire Grids, EBG, PMC

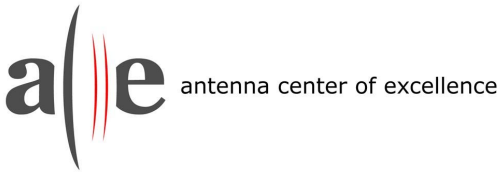

Catalogue of Models and Methods for Reflector Surface Modeling

ACE WP2.3-2 Reflector Surface Models

July, 2004 WP2.3-2-01

Prepared by:

G. Gerini, TNO FEL
P. -S. Kildal, Chalmers University of Technology
S. Maci, University of Siena
Z. Sipus, Chalmers University of Technology
D. Sjöberg, University of Lund
D. Trinchero, Politecnico di Torino
K. Pontoppidan, TICRA
P.E. Frandsen, TICRA

TABLE OF CONTENTS

1. INTRODUCTION

Reflector surfaces for communications and future medical applications often use special materials such as frequency and polarisation sensitive surfaces to separate different frequency bands or orthogonal polarisation. It is expected that reflector antennas will continue to be used in particular for geostationary satellites.

In the general reflector antenna program, GRASP9, provided by TICRA a number of simple and approximate models for reflector surface materials are included, such as strip grids, dielectric layers etc. However, in many cases these models are not sufficiently accurate and this is especially the case for frequency selective surfaces (FSS). It is the purpose of the present catalogue to assist the user of reflector antennas and radomes to find the relevant information on available methods and software.

The practical realisation of surface materials can be carried out in different ways. One approach is to laser etch a thin conducting layer into the desired pattern. This is the most general technique and can be used for both strip grids and FSS. Another approach is to cut narrow strips from a planar sheet of the material and then arranging them on the surface side by side.

Dual curved reflectors give rise to special problems. Such reflectors are not unfurlable and this means that a planar surface material cannot be bent into the shape of the reflector without wrinkling. Consequently, the parameters of the surface must inevitably vary across the reflector with a possible impact on the resonance frequency and the polarisation performance.

It may be difficult to model the precise layout of a particular design and in most cases one will have to accept the approximations assuming the same material parameters and the same orientation all over the reflector surface.

The work described in this report has been carried out as Work Package 2.3-2 under the ACE (Antenna Centre of Excellence). The partners of this work package are

TICRA (WP Leader), Denmark
Politecnico di Torino, Italy
University of Siena, Italy
TNO, Netherlands Org. for Applied Scientific Research
Lund University, Sweden
Chalmers Tekniske Högskola, Sweden

The material is organised as follows. Chapter 2 subdivides the different types of surfaces into the following categories: perfect magnetic conductors, hard/soft surfaces, impedance surfaces, electromagnetic band gap surfaces, non-linear surfaces and penetrable surfaces.

Chapter 3 presents the various analysis methods developed by the partners. Both methods in the time domain and in the frequency domain are included and equivalent transmission line models play an important role in many of the methods described.

The methods in Chapter 3 are all relying on variations of the Method of Moments and the required computer time ban be substantial, depending on the complexity of the problem. For a realistic design problems it may be necessary to use faster and perhaps more approximate solvers, especially if they are used inside an optimisation procedure. Chapter 4 presents some solutions to this problem.

Chapter 5 gives a number of specific applications of the more general methods presented in Chapter 3. Here the applications are ordered according to the surface type. Non-resonant surfaces comprise strip and wire grids as well as dielectric layers. Resonant surfaces include both thin and thick FSS structures and both single layer and multi-layer configurations are treated. Artificial and complex surfaces show examples of Perfect Magnetic Conductors (PMC) and electronic band gap (EBG) structures. Special surfaces are dealt with in Section 5.4 and cover Carbon Fibre Reinforced Plastic (CFRP) and honeycomb structure and here also the new light-weight triangular CRFP mesh is dealt with together with the tricot mesh for unfurlable reflectors. Advanced topics are collected in Section 5.5 and include combinations of FSS and arrays, curved surfaces, edge effects and manufacturing tolerances.

Each section in the report is written by only one partner in the team and the name of the partner is added to the heading of the section. In the case where several partners have contributed to the same topic these contributions are arranged as subsections with the heading being the name of the partner.

Many of the methods presented in this report have been implemented in software packages. These computer programs are described in a separate volume of this report: “Catalogue of software for Reflector Surface Modelling”, Report WP2.3-2-02.

2. REFLECTOR SURFACE CATEGORIES

2.1 Perfect Magnetic Conductor (PMC) – (Chalmers).

The concept of surfaces that are made from perfect electric conductor (PEC) is used very often in electromagnetics. For example, when designing a reflector antenna or a reflector surface, one will make the assumption that the metal surface is made from PEC. This is a reasonable assumption since various metals (copper, aluminium, silver, gold) have very good conducting properties and the losses due to finite conductivity are often negligible or can be estimated separately. A similar concept can be made for surfaces made from perfect magnetic conductor (PMC). PMC surfaces have the characteristic that electric current sources such as dipoles can be located at the surface and still radiate well. Thereby very low profile antennas can be realized [1], [2]. Other applications of PMCs are to realize waveguides that can support TEM waves [3]. For example, the dominant mode of a rectangular waveguide with two opposite PEC walls and two opposite PMC walls is a TEM mode with uniform field distribution and constant polarization over the cross-section. Unfortunately, there are no materials in nature that sufficiently well approximate a PMC at microwave frequencies. Therefore, there are attempts to realize an artificial surface (usually a periodic structure) that will act as a PMC in some frequency band. Such a structure is called an artificial magnetic conductor (AMC).

References

[1] T.H. Liu, W.X. Zhang, M. Zhang, and K.F. Tsang, "Low profile spiral antenna with PBG substrate," Electron. Lett. Vol. 36, pp. 779-780, Apr. 2000.

[2] F. Yang, Y. Rahmat-Samii, "Reflection phase characterizations of the EBG ground plane for low profile wire antenna applications," IEEE Trans. Antennas Propagat., vol. 51, pp. 12691-2703, Oct. 2003.

[3] F-R. Yang, K-P. Ma, Y. Qian, T. Itoh, "A novel TEM waveguide using uniplanar compact photonic-bandgap (UC-PBG) structure", IEEE Trans. Microwave Theory Tech., Vol. 47, No. 11, pp 2092 –2098, Nov. 1999.

2.2 Hard/Soft (PEC/PMC strip) (Chalmers)

The concept of PEC/PMC surfaces has been extended by considering electromagnetic waves propagating along the considered surface. Vertically polarized waves (i.e. plane waves with electric field normal to the surface)

propagate easily along a PEC surface (so-called GO-characteristic), but they cannot propagate along the PMC surface (so-called STOP-characteristic). Horizontally polarized waves have the opposite property (table 1).

Surface name		Polarization	
new	classical	VER	HOR
	PEC	GO	STOP
AMC	PMC	STOP	GO
PBG	Soft	STOP	STOP
EBG	Hard	GO	GO

Table 1. Characteristics of different types of surfaces with respect to propagation of surface waves for different polarizations.

The soft and hard surfaces are anisotropic surfaces that for one polarization behave as a PEC surface and for the other like a PMC surface [1], [2]. The soft surface behaves like a perfect electric conductor (PEC) for a horizontally polarized wave, and as a perfect magnetic conductor (PMC) for a vertically polarized wave. The hard surface behaves opposite, see Table 1. In other words, the soft surface has STOP-characteristics for both polarizations, and the hard surface have GO-characteristics for both polarizations. The physical picture of an ideal soft-hard surface is a PEC/PMC strip grid with zero strip period, or in other words a surface with electric and magnetic conductivity in one (and the same) direction only, see Figure 2. One way to artificially realize PMC strips is to use a quarter-wavelength transformer with a short circuit (PEC shunt) at the end of the transformer. In practice, this can be done by using corrugations or a strip-loaded grounded dielectric slab.

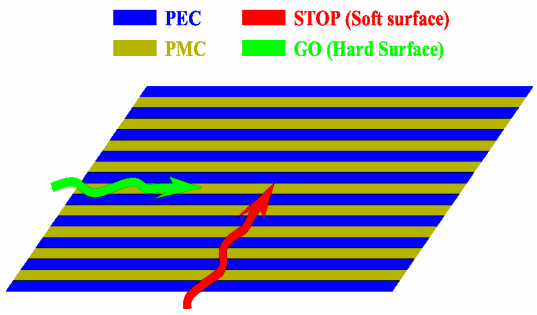

Figure 2 PEC/PMC strip representations of ideal soft and hard surfaces. The red and green wave-shaped arrows represent the direction of propagation of the waves that makes the PEC/PMC strip surface soft and hard, respectively.

Recently, the concept of photonic band-gap (PBG) or electromagnetic band-gap (EBG) structures has been introduced in electromagnetics to describe periodic structures along which or through which there is no propagation of electromagnetic wave in some frequency band [3]. There is a large similarity between concepts of EBG/PBG structures and soft/hard surfaces. If practical realizations are considered, the soft/hard surfaces are structures with periodicity in one dimension, while the EBG/PBG structures have periodicity in two or three dimensions.

References

[1] P.-S. Kildal, "Definition of artificially soft and hard surfaces for electromagnetic waves", Electron. Lett., vol. 24, 3, pp. 168 -170, Feb. 1988.

[2] P.-S. Kildal, "Artificially soft and hard surfaces in electromagnetics", IEEE Trans. Antennas Propagat., vol. 38, pp. 1537-1544, Oct 1990.

[3] E. Yablonovitch, “Inhibited spontaneous emission in solid state physics and electronics,” Phy. Rev. Lett., vol. 58, pp. 2059-2062, 1987.

2.3 Impedance (Siena)

The usually approximate boundary condition in electromagnetic scattering has been an area of research for at least 40 years. Approximate Boundary Condition (ABC) can be used to eliminate many of the difficulties associated to the computation of the scattering of coated bodies. The concept of ABC is the postulate that the relationship between tangential electric and magnetic fields at any point between the exterior of the coated body and free space is a purely local one depending only on the coating directly below the point in question. Once the relationship of the field of the coated body is known it is not necessary to consider the field inside the coating has unknowns. The only true unknown is either tangential electric or magnetic field of the free space boundary, the other being obtained through the boundary condition. The simplest and the most widely used ABC is the Standard Impedance Boundary Condition (SIBC) [1]. In this case the tangential components of electric field are related to those of the magnetic field by a simple multiplication factor. This factor is obtained by solving the problem of the reflection of a normally incidence plane wave at the infinite grounded plane coated with the appropriate material. In its simplicity, this approximate boundary condition is accurate for some situation. This condition is met by very thin coatings as well as by coating made up of material with high values of the reflective index or with significant loss. For coating with reflection characteristics strongly dependent of the angle of incidence the Standard Impedance Boundary Condition fails. The restriction of independence from angle of incidence can be mitigated by incorporating derivatives of the field components in the boundary conditions. In this case the ABC are referred to generalized BC (GABC). Such BC introduced in [2] and more recently treated in [3]

References
[1] M.A. Leontopich “Investigations of radio wave propagation part 2”, Moskow , Academy of Sciences, 1948
[2] S.N. Carp and F.C. Karal “Generalized impedance BC with applications to surface wave structure” Electromagnetic Theory Part 1, pages:479-483, pergamon press, NY, 1965
[3] J.L.Volakis, and T.B.A. Senior, ”Application of generalized BC to scattering to metal backed dielectric half plane”, proceedings of the IEEE, 77(5): 796-895, May 1989

2.4 Electromagnetic Band Gap surfaces (Lund*)*

Electromagnetic Band Gap surfaces make use of a resonant structure to create band gap behaviour, i.e., for a band of frequencies no fixed frequency solutions can exist in the material. With the acronym EBG we also include Frequency Selective Surfaces (FSS) and Photonic Band Gap (PBG).

The main characteristics of EBG materials are contained in the dispersion relation, i.e., the relation between w and k, which usually has to be calculated numerically. It is usually represented in a band diagram as in the figure below. The main design issue when dealing with EBG is to design the microstructure such that the band gap is broad enough for all angles of incidence (k vectors). Often one has to be satisfied with only a partial band gap, valid only for certain polarizations or angles of incidence.

EBG materials have been a hot topic in the electromagnetic community for more than a decade, and have an even longer history in physics, originating in the early quantum mechanics. The major analytical tool is the Floquet-Bloch representation, which transforms an arbitrary function into a periodic one, depending on the wave vector **k**. Most EBG designs are two-dimensional.

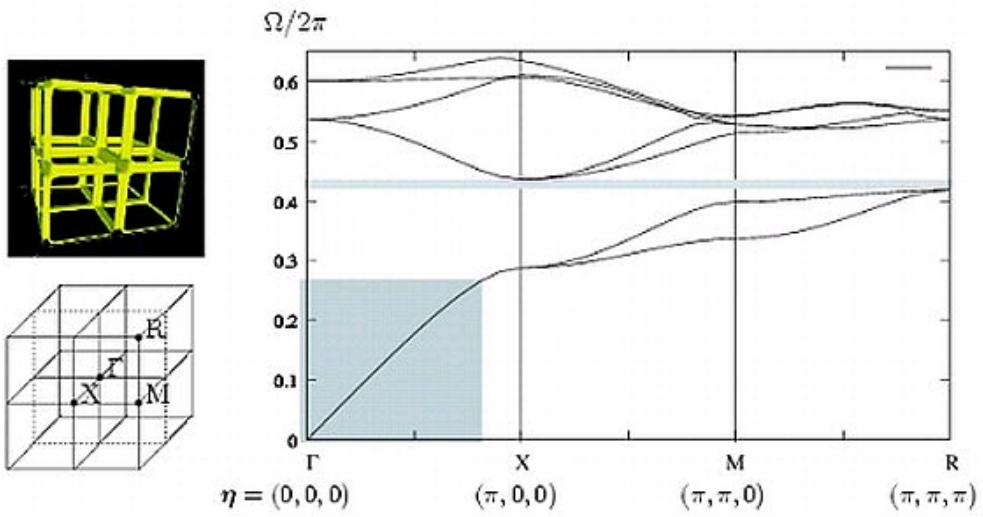

Figure 1 A typical band plot, where normalized frequencies $\Omega = a\omega / c$ and wavevectors $\eta = a\boldsymbol{k}$ are used, a being the physical size of the unit cell. The unit cell is depicted on the top left and has side 1, and the reciprocal unit cell (first Brillouin zone) has side 2π. The thin, shaded strip is the band gap, and the shaded region near the origin indicates where the dispersion relation is similar enough to that of a homogeneous material, i.e., a straight line, so that it can be considered homogeneous.

In electromagnetics, EBG materials find applications such as Perfect Magnetic Conductors (PMC), which can be used to reduce the size of patch antennas; a typical realization is the mushroom surface due to Sievenpiper, see also the above section on PMC. The band gap in EBG materials also prohibits surface wave propagation, which can be used to reduce edge diffraction and mutual coupling between elements in an antenna array. Recently, there has also been a huge interest in designing so-called meta-materials with negative permittivity and permeability.

References

[1] E. Yablonovitch. Photonic Band Gap Crystals. J. Phys.: Condens. Matter, Vol. 5, pp. 2443-60, 1993.

[2] IEEE Transactions on Antennas and Propagation, Special issue on meta-materials, part I. Vol. 51, No. 10, 2003.

2.5 Penetrable Surfaces (Siena)

In some cases the Impedance Boundary Condition cannot be applied because of strong interaction between the interface material surface and the medium

behind. In this case one may resort to some approximations, which any way simplify any boundary value problems based on equivalent transmission line orthogonal to the surface. This transmission line may be applicable, for instance, to periodic printed structure in stratified media as Frequency Selective Surfaces (FSS). Within the periodicity representation imposed by the Floquet theorem it is possible to represent the dominant propagating Floquet reflected plane wave in terms of an impedance in a transmission line. This approximation is valid for describing the interaction of this dominant Floquet wave (FW) with the stratification behind and to account for the storage of reactive energy associated to evanescent FW. Although a more accurate description of periodic structure is framed in the MoM solution scheme described in Sec. 3.1, the impedance representation could be useful for the Pole-Zero Matching technique described in Sec. 3.5

3. ANALYSIS METHODS

3.1 MOM Solution Framework - spectral (POLITO)

The spectral formulation represents the natural way to analyse the scattering problem of an arbitrary planar array of patches or aperture [1]-[2]. This formulation is based on the introduction of a vector transmission line representation, where voltages and currents are the two-dimensional Fourier transforms of the transversal electric and magnetic fields, respectively.

$$\underline{E}_t(\underline{\rho}, z) = \frac{1}{2\pi} \int \underline{V}(\underline{\alpha}, z) \exp(-j\underline{\alpha} \cdot \underline{\rho})\, d\underline{\alpha} \quad (1)$$

$$\underline{H}_t(\underline{\rho}, z) \times \hat{z} = \frac{1}{2\pi} \int \underline{I}(\underline{\alpha}, z) \exp(-j\underline{\alpha} \cdot \underline{\rho})\, d\underline{\alpha} \quad (2)$$

$$\underline{J}_t(\underline{\rho}, z) = \frac{1}{2\pi} \int \underline{i}(\underline{\alpha}, z) \exp(-j\underline{\alpha} \cdot \underline{\rho})\, d\underline{\alpha} \quad (3)$$

$$\underline{M}_t(\underline{\rho}, z) \times \hat{z} = \frac{1}{2\pi} \int \underline{v}(\underline{\alpha}, z) \exp(-j\underline{\alpha} \cdot \underline{\rho})\, d\underline{\alpha} \quad (4)$$

Two solution approaches are possible: the patch approach, where the unknown is the current induced on the metallization, and the aperture approach, where the aperture electric field is chosen as unknown. The array generalized Scattering Matrix (GSM) is subsequently derived in the Floquet mode basis.

Power dissipation in a FSS can take place in the dielectric support structure and in the metal patches. While the former process can be easily modelled by introducing complex permittivities, the latter requires a reformulation due to the modification of the boundary conditions.

To solve the problem, a vector transmission line formalism [3] can be introduced, where the voltage and current are the 2D Fourier Transforms of the transverse electric and magnetic field, respectively. Hence, the impedances and scattering matrix elements are dyadic.

The general FSS scattering problem is solved by a network approach. The metal elements, assumed to be of zero thickness, are removed by means of the Equivalence theorem and substituted with an unknown distribution of

electric current, equal to the magnetic field jump. Applying the transmission line technique, the structure is represented by a network, where the electric current induced on the patches is accounted for by the shunt current generator.

The dielectric stratifications are represented by means of their scattering matrices, whereas the voltage generator is the Fourier transform of the incident electric field.

The functional equation is solved by the method of moments applied directly in the spectral domain. A suitable set of basis functions is introduced to represent the strength of the current generator $\underline{i}(\sigma)$ and to project the functional equation (Method of Galerkin). In the case of a periodic arrangement of patches with a plane wave incidence the spectrum becomes discrete (Floquet modes) and the solution is obtained in a scattering matrix form.

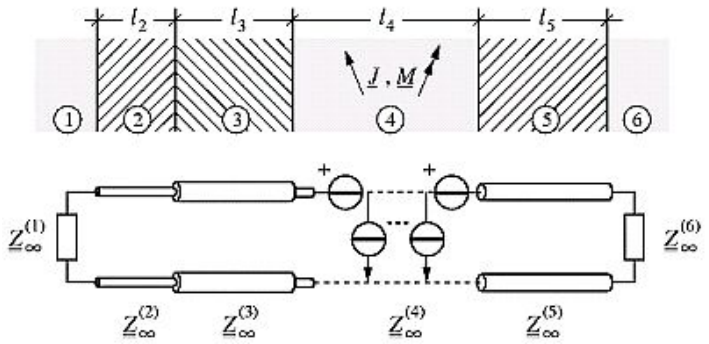

References

[1] R. Orta, R. Tascone and R. Zich, "A unified formulation for the analysis of general frequency selective surfaces", Electromagnetics, vol. 5, no. 4, 1985, pp. 307-329.

[2] R. Orta, R. Tascone and D. Trinchero, "A spectral approach for the modelling of planar periodic structures", in Recent Res. Devel. Microwave Theory & Tech.}, edited by S. G. Pandalai, Transworld Research Network Press, Trivandrum, India, vol. 1, 1999, pp. 133-157.

[3] L. B. Felsen and N. Marcuvitz, Radiation and Scattering of Waves, Prentice Hall, 1973.

3.2 MOM Solution Framework – spatial (Siena)

The rigorous analysis of printed circuit elements, such as microstrip interconnects terminated by complex loads, microstrip discontinuities, patch antennas and printed dipoles, requires the use of the vector and scalar Green's

functions for a substrate layer backed by a ground plane. It is well-known that the Green's functions for microstrip geometries are improper integrals [I], also called Sommerfeld integrals, whose integrands are oscillatory and slowly decaying functions; hence, their calculation is very time-consuming if not impractical for many configurations of interest. Using the closed-form expressions for the spatial domain Green's functions in a variational technique, e.g., the method of moments (MoM), can result in a substantial savings of computation time when analysing planar microstrip structures. Once the improper infinite range in over finite supports associated with the basis and testing functions. In view of this, it would be instructive to demonstrate the difficulties that one may face in the application of the conventional moment method approach to microstrip geometries, before starting the derivation of the closed-form Green's functions for the vector and scalar potentials.

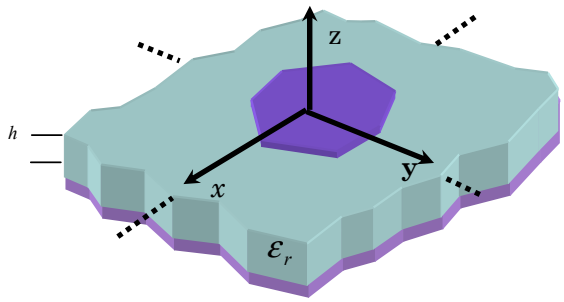

Figure 1 General microstrip structure

It is well known that MOM can be applied either in the spatial domain [4] or in the spectral domain [5], the latter being more suitable for planar geometries unless the spatial domain Green's functions can be approximated in closed-forms [6], [7]. Both approaches will be briefly examined here with a view to comparing their computational efficiency.

An important issue that merits examination in the MOM formulation is the convergence problem of the integrals representing the MOM matrix. Consider, for the sake of illustration, a general microstrip structure shown in Fig. 1 where it is assumed that the substrate layer extends to infinity in the transverse directions. Let the thickness and the permittivity of the substrate be denoted by d and e_r, respectively. Although the Green's functions discussed herein pertain to the geometry shown in Fig. 1, the comments appearing in this section apply to more general geometries as well. The tangential electric fields on the plane of the patch ($z = 0$) can be written in terms of the surface current density J and the Green's functions for the vector and scalar potentials G_{xx}^{A}, and G_q, respectively;

$$E_x = -j\omega G_{xx}^A * J_x + \frac{1}{j\omega}\frac{\delta}{\delta x}\left[G_q * \nabla \cdot J\right] \tag{1a}$$

$$E_y = -j\omega G_{yy}^A * J_y + \frac{1}{j\omega}\frac{\delta}{\delta y}\left[G_q * \nabla \cdot J\right] \tag{1b}$$

where * implies convolution.

To solve for the surface current density on the patch by the MoM, the first step is to expand the surface current densities in terms of a linear combination of the basis functions as follows:

$$J_x = \sum_n A_n J_{xn}(x,y) \tag{2a}$$

$$J_y = \sum_n B_n J_{yn}(x,y) \tag{2b}$$

where A_n and B_n are the unknown coefficients of the basis functions, J_{xn} and J_{yn}. Next we substitute (2) into (1) and test the resulting equations using some testing functions T_{xm} and T_{ym} and a suitable definition of inner product, e.g.,

$$\langle f, g \rangle = \iint dxdyf(x,y)g(x,y) \tag{3}$$

Since the testing functions and the tangential electric fields have non zero values over complementary regions, the left hand sides of (la) and (lb) become zero after the testing, and the following algebraic equations are obtained for the coefficients A_n and B_n:

$$\sum_n A_n \left\{ \left\langle T_{xm}, G_{xx}^A * J_{xn} \right\rangle + \frac{1}{\omega^2} \left\langle T_{xm}, \frac{\delta}{\delta x} \left[G_q * \frac{\delta}{\delta x} J_{xn} \right] \right\rangle \right\}$$
$$+ \sum_n B_n \left\{ \frac{1}{\omega^2} \left\langle T_{xm}, \frac{\delta}{\delta x} \left[G_q * \frac{\delta}{\delta y} J_{yn} \right] \right\rangle \right\} = 0 \tag{4a}$$

$$\sum_n B_n \left\{ \left\langle T_{ym}, G_{yy}^A * J_{yn} \right\rangle + \frac{1}{\omega^2} \left\langle T_{xm}, \frac{\delta}{\delta y} \left[G_q * \frac{\delta}{\delta y} J_{yn} \right] \right\rangle \right\}$$
$$+ \sum_n A_n \left\{ \frac{1}{\omega^2} \left\langle T_{ym}, \frac{\delta}{\delta y} \left[G_q * \frac{\delta}{\delta x} J_{xn} \right] \right\rangle \right\} = 0 \tag{4b}$$

The first inner product term is written below as an example

$$\left\langle T_{xm}, G_{xx}^A * J_{xn} \right\rangle = \iint_{D(T)} dxdy T_{xm}(x,y) \iint_{D(B)} dx'dy' \cdot G_{xx}^A (x-x', y-y') J_{xn}(x', y') \tag{5}$$

where D(T) and D(B) represent the domain of the testing and basis functions, respectively, and

$$G_{xx}^A(\rho) = \frac{1}{4\pi} \int_{-\infty}^{+\infty} dk_\rho k_\rho H_0^{(2)}(k_\rho \rho) \tilde{G}_{xx}^A(k_\rho) \tag{6}$$

In general, each inner product term in the spatial domain, e.g., the one given in (5), is a five-dimensional integral: one of these is associated with the Green's function itself which is an improper integral (Sommerfeld integral) over an infinite domain and is given in (6); two of these are convolution integrals; and, the remaining two are inner products. Since the numerical integration of the five-dimensional integrals is computationally intensive, the convolution integral over the Green's function and the basis functions is often transferred over to the basis and testing functions, enabling one to carry out this integral analytically. With this step, the order of integration can be reduced to three. In spite of this, the evaluation of the inner product is still very time-consuming because of the slow convergence behaviour of the integrands of the Green's function. Recently an approach to circumventing this problem has been developed on the basis of complex equivalent images which leads to closed form expressions for the spatial domain Green's functions corresponding to the vector and scalar potentials associated with a horizontal electric dipole (HED) located over a thick substrate [1],[2],[3]. This approach allows treating the spatial domain MoM in the same fashion as that for free space environment. On the other hand the use of the small

domain basis function imply a very flexible and general scheme, which takes advantage by a fast calculation of the mutual impedances. The spectral domain approach analysed in Sec 3.1 is indeed suitable for entire domain base functions, which exhibit a reduced spectral bandwidth. It is indeed worth noting that the MoM impedance of the electric field integral equation assumes the expression, for instance:

$$\int_{-\infty}^{\infty}\int_{-\infty}^{\infty} T_{xm}\left(-k_x,-k_y\right)G_{xx}^{EJ}\left(k_x,k_y\right)J_{xn}\left(k_x,k_y\right)dk_x dk_y$$

where $G_{xx}^{EJ}\left(k_x,k_y\right)$is the spectral domain Green's function for the electric *x*-oriented dipole source and *x*-directed observed electric field.

References

[1] M. Axun, R. Mittra, "Derivation of close form for Green's functions for a general microstrip geometry," IEEE Trans. on Microwave Theory and Techniques, Vol 40, No 11 , Nov 1992

[2] M.I. Aksum, "A robust approach for the derivation of close Green's Functions", IEEE transaction on Microwave Theory and Techniques, Vol.44, no.5, May 1996

[3] R.E.Jorgenson, R.Mittra, "Efficient Calculation of the periodic Green's Functions in layered dielectric Media", IEEE transaction on Microwave Theory and Techniques, Vol.41, no.3, March 1993

[4] R. F. Harrington, "Field computation by Method Moment", NY; MacMillan; Florida; Krieger Publishing, 1983

[5] T. Itho, R. Mittra, "Spectral Domain approach for calculating the dispersion characteristics of microstrips line", IEEE transaction on Microwave Theory and Techniques, Vol.21, 1973

3.3 Multimode Analysis (Y,S) – (TNO)

In the last few decades, several approaches have been proposed for the analysis of complex multilayer FSS structures, mostly evolutions of the Method of Moments (MoM) technique. An in depth discussion about the various methods can be found in [1]-[3]. In most of these cases, the response of the multilayer FSS to plane wave incidence, in terms of reflection and transmission coefficients, is obtained by solving a single integral equation and, in a second step, characterizing the fields reflected and transmitted at the two most outer transitions. This approach provides global information about the electromagnetic response of the complete layered structure, but not about the field distribution at each internal discontinuity.

On the contrary, the Generalized Scattering Matrix (GSM) and the Multimode Equivalent Network (MEN) approaches characterize each periodic surface/dielectric slab in the structure, in terms of a multimode representation based on the scattering parameters, (GSM), or impedance/admittance parameters, (MEN). These methods treat each layer as an open waveguide, where the fields are represented as a superposition of Floquet's Waves (modes). The multilayer FSS is then seen as a cascade of scattering or impedance matrices, retaining the information about the field distribution at every section of the structure. For both the GSM and the MEN approaches, a significant improvement in the numerical stability has been achieved by following the concept, originally introduced in [4], of separating the modes in accessible and localized ones. The accessible modes propagate or stay below cut-off, but with a low enough attenuation to be still significant when they reach the adjacent transition. The latter do not leave the transition area and are associated to the reactive energy stored in the vicinity of the discontinuities. Accordingly the number of input and output ports in the equivalent network, characterizing the transition between two discontinuity free regions, is equal to the number of accessible modes on the two sides of the discontinuity.

A first fundamental advantage of these approaches is given by their intrinsic modularity. In fact, complex multilayer structures can be analysed as a cascade of different blocks each one characterized by its own equivalent network independent from the others. Therefore, only those parts of the complete structure that have actually been modified need to be characterised again, keeping unchanged the representation of the rest of the structure. Moreover, if the tuning is mainly achieved by acting on the longitudinal dimensions of the waveguide sections, there is no need to re-compute the modes and the coupling integrals, which have been evaluated and properly stored in previous iterations. Clever exploitation of the above features allows for substantial speed-up in optimisation procedures when many iterations are required to meet the design specifications.

Even though the GSM and the MEN approach share many features a key difference arises. With the GSM approach the scattering parameters are calculated by solving a single Integral Equation (IE) pertinent to each transition, [1], [5]-[9]. This is different in the MEN approach, where the problem formulation leads to a set of IE's, whose number is equal to that of the selected accessible modes. These IE's will be referred to as reduced Kernel IE's. In fact each one of them has a Kernel, which is associated to the non-accessible portion of the Green's Function (GF). In other words, the contribution corresponding to the selected accessible modes is subtracted from the Green's function expression.

The MEN method, that was originally proposed for the analysis of planar two dimensional gratings [10]-[12] has been extended to the study of

waveguide transitions [13]-[15], therefore allowing the analysis of thick perforated metal screens and FSS directly integrated with the array aperture (open-ended waveguide radiators), and recently to three dimensional FSS's of slots or patches [16].

One of the most significant advantages of the MEN representation with respect to commercial codes is its versatility, in particular, its capability to extract the dominant EM behaviours and to make use of this information in order to reduce the total computational time. The number of full wave simulations that are necessary to characterize the complete FSS structure, depends on the speed of the variation of the observed parameters as a function of the frequency. It can be observed that the input impedance of the overall multilayer FSS structure is varying fast as a function of the frequency. In fact, all the fast frequency dependencies are associated to the transmission-line-type interactions between the two FSS's that in the MEN are accounted for at equivalent network level rather than at full wave analysis level. This property is systematic and holds also for aperture based FSS's. On the contrary, looking only at the impedance/admittance matrixes of the slot/patch transition, it can be observed that the variation of the impedance matrix elements as a function of the frequency is much smoother and therefore their interpolation is very simple. This important property can be observed also by using a GSM method to calculate the scattering parameters of each FSS and deriving then the generalized impedance or admittance matrix through a standard parameter conversion method. However, a first key feature of the MEN method with respect to GSM approaches is that it intrinsically provides more physical insight to the phenomena at hand. This is due to the fact that admittance or impedance matrix elements are essentially weak versions of the GF's, while the scattering parameters are artificial compacting tools. If one wishes to simplify the numerical evaluation of the GF's of periodic structures excited by non periodic sources this property is extremely useful. Moreover, it is clear that the slow variation of the MEN impedance matrix elements is associated to the use of the non-accessible GF in the Kernel of the IE's. A less singular Kernel indeed provides less variation with the frequency.

References

[1] R.Mittra, Chi H.Chan and T.Cwik, “Techniques for analyzing frequency selective surfaces-a review”, Proc. IEEE, vol. AP-76, no.12, 1988.

[2] B.A.Munk, Frequency Selective Surfaces: theory and design. New York: John Wiley and Sons, 2000.

[3] J.C.Vardaxoglou, Frequency Selective Surfaces. New York: John Wiley and Sons, 1997.

[4] T.E.Rozzi and W.F.G.Mecklenbrauker, ”Wide-band network modeling of interacting inductive irises and steps”, IEEE Trans. on MTT, vol.23, pp. 235-244, 1975.

[5] R.Orta, R.Tascone and R.Zich, “A unified formulation for the analysis of general frequency selective surfaces”, Electromagnetics, vol.5, no.4, 1985.

[6] S.Contu and R.Tascone, “Scattering from passive arrays in plane stratified regions”, Electromagnetics, vol.5, pp. 285-306, 1985.

[7] R.Orta, P.Savi and R.Tascone, “Numerical green's function technique for the analysis of screens perforated by multiply connected apertures”, IEEE Trans. on Ap, vol. AP-44, no.6, pp. 756-776, 1996.

[8] A.K.Bhattacharyya, “Analysis of multilayer infinite periodic array structures with different periodicities and axes orientation”, IEEE Trans. on AP, vol.48, no.3, pp. 357-369, 1996.

[9] M.Bozzi and L.Perregrini, “Analysis of multilayered printed frequency selective surfaces by the mom/bi-rme method”, IEEE Trans. on AP, vol. AP-51, no.10, 2003.

[10] M.Guglielmi and A.A.Oliner, “Multimode network description of a planar periodic metal-strip grating at a dielectric interface - part I: Rigorous network formulations”, IEEE Trans. on MTT, vol.37, no.3, pp. 534-540, 1989.

[11] M.Guglielmi and A.A.Oliner, “Multimode network description of a planar periodic metal-strip grating at a dielectric interface - part II: Small-aperture and small-obstacle solutions”, IEEE Trans. on MTT, vol.37, no.3, pp. 542-552, 1989.

[12] M.Guglielmi and A.A.Oliner, “Multimode network description of a planar periodic metal-strip grating at a dielectric interface - part III: Rigorous solution”, IEEE Trans. on MTT, vol.37, no.3, pp. 902-909, 1989.

[13] G.Conciauro, M.Guglielmi and R.Sorrentino, Advanced Modal Analysis, John Wiley and Sons, 2000.

[14] G.Gerini and M.Guglielmi, “Full-wave cad of a rectangular waveguide filter with integrated coaxial excitation’, IEEE Trans. on MTT, vol.49, no.5, pp. 986-989, 2001.

[15] G.Gerini, L.Zappelli, “Phased Arrays of Rectangular Apertures on Conformal Cylindrical Surfaces: a Multimode Equivalent Network Approach”, IEEE Trans. on AP, vol.52, no.7, 2004.

[16] S. Monni, N. Llombart Juan, A. Neto, G. Gerini, “A closely spaced waveguide phased array integrated with a frequency selective surface: modeling and design”, 2003 IEEE International Antennas and Propagation Symposium, June 2003, Columbus, Ohio.

3.4 Homogenisation of boundary conditions (including asymptotic boundary conditions) (Lund)

When the applied wavelength is much larger than the geometric variations of the structure, only the first few Floquet modes contribute to the reflected field. This causes the reflection characteristics of the surface to be similar to that of a fictitious, homogeneous medium. By manipulating the geometry of

the microstructure, it is possible to control the properties of this fictitious medium.

General homogenisation: The typical geometry is given by a periodic (or statistically homogeneous) surface, where the period is small compared to the wavelength. There are then two characteristic scales in the problem: one is the wavelength, and the other is the period. Denoting these scales by $\boldsymbol{x}$ and $\boldsymbol{y}$, respectively, we are typically looking for solutions on the form $\boldsymbol{E}(\boldsymbol{x},\boldsymbol{y}) = \boldsymbol{E}(\boldsymbol{x},\boldsymbol{x}/\delta)$, periodic in the second argument, where δ is the ratio between the microscopic and the macroscopic scale, i.e., a small dimensionless parameter. The classical way of analysing the problem is to make an asymptotic series expansion [1],

$$\boldsymbol{E}(\boldsymbol{x},\boldsymbol{x}/\delta) = \boldsymbol{E}_0(\boldsymbol{x},\boldsymbol{x}/\delta) + \delta\boldsymbol{E}_1(\boldsymbol{x},\boldsymbol{x}/\delta) + \delta^2\boldsymbol{E}_2(\boldsymbol{x},\boldsymbol{x}/\delta) + \ldots$$

As the scale $\delta \to 0$, we expect $\boldsymbol{E} \to \boldsymbol{E}_0$. Inserting this ansatz into Maxwell's equations and collecting terms of different powers in δ, the result is that the lowest order field $\boldsymbol{E}_0$ should satisfy the equations

$$(1) \qquad \nabla_y \times \boldsymbol{E}_0 = \boldsymbol{0} \Leftrightarrow \boldsymbol{E}_0 = \langle \boldsymbol{E}_0 \rangle - \nabla_y u \text{, and } \nabla_y \cdot [\boldsymbol{\varepsilon}(\boldsymbol{y}) \cdot \boldsymbol{E}_0] = 0$$

The physical interpretation of these equations is that the mean value part $\langle \boldsymbol{E}_0 \rangle$ corresponds to the macroscopic field, i.e., the field that is observable at scales comparable to the wavelength, and the gradient part ∇u corresponds to the microscopic fluctuations. The effective permittivity is defined by the relation

$$\langle \boldsymbol{D} \rangle = \boldsymbol{\varepsilon}_{eff} \cdot \langle \boldsymbol{E}_0 \rangle \text{, or } \langle \boldsymbol{\varepsilon}(\boldsymbol{y}) \cdot (\langle \boldsymbol{E}_0 \rangle - \nabla_{\boldsymbol{y}} u) \rangle = \boldsymbol{\varepsilon}_{eff} \cdot \langle \boldsymbol{E}_0 \rangle$$

This shows that the effective permittivity can be calculated by choosing the mean value $\langle \boldsymbol{E}_0 \rangle$ and solving the local problem (1). Although the expansion in an asymptotic series is only formal, it can be rigorously justified by the concept of two-scale convergence [2]. The equations can also be generalised to apply to statistically homogeneous, random media [3].

An important alternative to solving the local problem is the use of bounds [4]. These are analytical expressions, which can be used to give estimates of the homogenised permittivity based on only limited geometrical information of the microstructure, such as volume fractions and other statistical parameters. These bounds often coincide with classical mixture formulas, such as the Maxwell-Garnett formula.

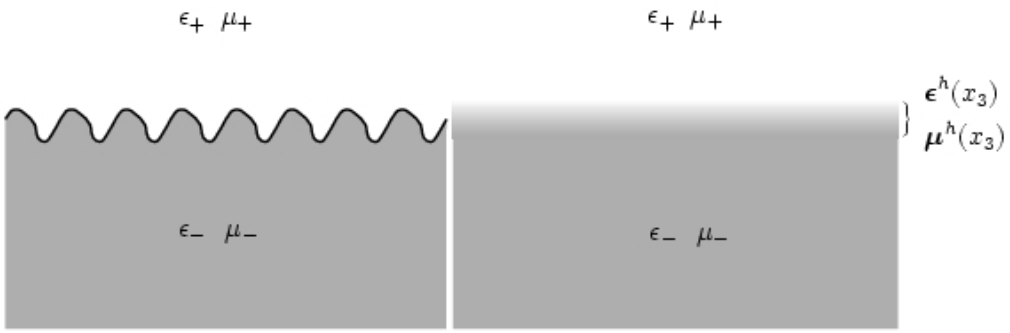

Figure 1 Typical geometry for surface homogenisation.

Application to surfaces: Let the medium be periodic in the dimensions parallel to the surface, for instance as in Figure 1. The homogenisation procedure can be applied in each cross section, i.e., for a given height coordinate x_3. This transforms the corrugated surface to a stratified medium, in which the wave propagation is described by a set of ordinary differential equations in the x_3 coordinate. By solving these differential equations, it is possible to calculate the surface impedance or reflection coefficient of the surface.

A common case is when the medium is periodic in only one direction, typically realised by grooves in a metallic surface. These are the soft and hard surfaces [5], which can also be analysed by considering the fields inside the grooves as modes in a parallel plate waveguide. The only propagating mode is then the one with electric field orthogonal to the grooves, and choosing grooves with depth corresponding to a quarter of a wavelength means the corresponding tangential magnetic field at the top of the groove is zero. See the section on Soft and Hard Surfaces in this catalogue for applications.

It is important to remember that asymptotic boundary conditions are defined by a limit process, where a microscopic scale is becoming infinitesimally small compared to the wavelength. Another common limit process is when the conductivity of a metal is becoming very large. An important result is that these two limit processes do not commute, i.e., we end up with different results depending on if we homogenise a PEC surface, or if we homogenise a finite conductivity surface and then send the conductivity to infinity.

Another problem with homogenisation is that it is difficult to estimate the range of validity for the results. The old rule of thumb is that the microscopic scale should be at least ten times smaller than the wavelength. However, recent results show that homogenised properties give good results for surprisingly large microscopic scales. For reflection from surfaces this is par-

ticularly true if the observation point is sufficiently far from the surface, since then the evanescent modes do not contribute to the total field.

References
[1] A. Bensoussan, J.-L. Lions, and G. Papanicolaou. Asymptotic Analysis for Periodic Structures. North Holland, Amsterdam, 1978.
[2] G. Allaire. Homogenization and two-scale convergence. SIAM J. Math. Anal., Vol. 23, No. 6, pp. 1482-1518, 1992.
[3] V. V. Jikov, S. M. Kozlov, and O. A. Oleinik. Homogenization of Differential Operators and Integral Functionals. Springer-Verlag, Berlin Heidelberg, 1994.
[4] G. W. Milton. The Theory of Composites. Cambridge University Press, Cambridge, UK, 2002.
[5] P. S. Kildal. Artificially soft and hard surfaces in electromagnetics. IEEE Trans. Antennas Propagat., Vol. 38, No. 10, pp. 1537-1544, 1990.

3.5 Impedance representation of FSS (Siena)

As anticipated in Sec. 2.6, an FSS printed in stratified region may be represented by an equivalent impedance in parallel to a z-transmission line (z being the abscise orthogonal to the surface). Several authors [1], [2], [3], [4], have treated this impedance via equivalent LC-circuit to characterize both the reflection and the dispersion properties. The lumped parameters are based on a quasi-static approximation and are capable to gracefully model the surface reflection properties in a certain limited frequency range. Although in some cases the same LC-topologies catch the dominant dispersion physics, the same parameters, which are used for the reflection, are not able to describe the band gap properties. This motivates the demand for a network derivation, which is rigorous, systematic, and uniformly valid in a broad range of frequency and wavenumber from the visible to the non-visible region.

Let us consider a simple case of a periodic FSS constituted by thin dipoles printed on a grounded slab, and illuminated by a plane wave. The geometry is shown in Fig. 1. The dipoles are directed along the x axis of a reference system with z axis along the normal, and origin at the dielectric-air interface. The periodicities of the FSS are d_x and d_y along x and y, respectively. Two different cases of incident plane wave are considered, which are sketched in Fig. 2a. In a first case, the plane wave direction of propagation belongs to the y-z plane, and forms an angle θ with the z axis. Only the TE (with respect to z) polarization provides the interaction with the FSS, being the E-field aligned with the electric dipoles. Since the dipoles are thin, the TM polarized wave essentially feels a bare (unprinted) grounded slab. When the plane wave is incident in the x-z plane, the TM field interacts with the dipoles, while the TE field feels the bare slab. The interesting cases are

therefore TE for H-plane incidence (Fig. 2a) and TM for E-plane incidence (right hand side of Fig. 2a).

Consider first the TM case. The imposed plane wave establishes a dominant phasing $k_x=k\sin\theta$ (k=free space wavenumber) and $k_y=0$, so that the field may be expanded in terms of Floquet waves (FW) with wavenumbers $k_{xm}=k_x+2m\pi/d_x$, $k_{yn}=2n\pi/d_x$. Assume that all the FW's are evanescent along z, except for the dominant one. At a certain distance from the surface, where the evanescent FW's are completely attenuated, we can assume that the field in the x-y plane is uniform in amplitude. Thus, the total field may be rigorously described by a z-transmission line network [15] (Fig.2b), where the effect of the FSS accounted for by a shunt impedance $Z_{FSS}^{TM}(k_x,\omega)$ placed at z=0. According to the description of unprinted dielectric stratified media, the rest of the network is described by pieces of TM transmission line with propagation constants associated to the dominant (propagating) FW: $k_z=\sqrt{k^2-k_x^2}$ for the free-space semi- infinite line and $k_{z1}=\sqrt{\varepsilon_1 k^2-k_x^2}$ for the short-circuited dielectric line. The TM characteristic impedances are, $Z_0^{TM}=k_z/\omega\varepsilon_0$ and $Z_1^{TM}=k_{z1}/\omega\varepsilon_1$.

An analogous network can be given for the TE case, where the FW expansion leads to wavenumbers $k_{ym}=k_y+2n\pi/d_y$, $k_{yn}=2n\pi/d_x$. The corresponding network (Fig. 2b) has propagation constants $k_z=\sqrt{k^2-k_y^2}$, and $k_{z1}=\sqrt{\varepsilon_r k^2-k_y^2}$, characteristic impedances $Z_0^{TE}=\omega\mu_0/k_z$ $Z_1^{TE}=\omega\mu_0/k_{z1}$, and shunt impedance $Z_{FSS}^{TE}(k_y,\omega)$.

We denote by "FSS equivalent impedance" the uniform *impedance* $Z_{FSS}^{TM}(k_x,\omega)$ placed at z=0 which recovers the exact field *far enough* from z=0. (we will often refer to $Z_{FSS}^{TM}(k_x,\omega)$ for simplicity, understood that analogous considerations apply to $Z_{FSS}^{TE}(k_y,\omega)$). More rigorously, the FSS impedance can be defined as the ratio between the E-field and the discontinuity of the H-field (ΔH) associated to the dominant Floquet mode.

It is worth emphasizing the following points.

i) The FSS impedance is *not* associated to the ratio between *total* E and ΔH contribution at z=0, since these quantities are not uniform along the x-y plane, but to contributions proper of the dominant FW. These latter may be considered as associated to an average field concept [13].

ii) The network is not valid for any z-level. The total field has indeed non uniform amplitude in the x-y plane at z-levels where the higher order FW's are not completely vanished.

iii) The *homogenisation process* we have defined for the FSS impedance doesn't require high number of printed dipoles in terms of a wavelength; it has been only assumed to deal with *only one propagating Floquet mode* for any incidence angle.

iv) For the concerned dipole FSS, and for both the polarization cases, the *dominant* propagating FW has the same polarization (TE or TM) of the incident plane wave. This property is not satisfied by the higher order, *z*-evanescent FW's, which are of both TE and TM types for each individual case shown Fig 2.

v) If the direction of incidence does not belong to the principal planes, the dominant propagating FW is depolarized.

Concerning with the points ii), iii), and iv), the present method can be generalized by using a multiport network scheme [16]

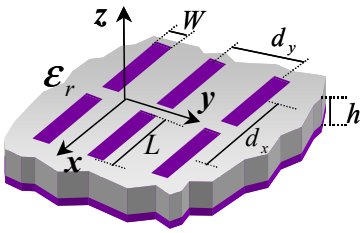

Figure 1

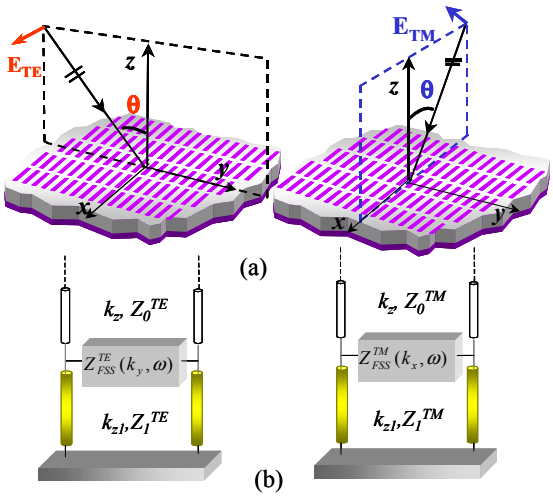

Figure 2

Figure 1 Geometry for a dipole-FSS printed on a grounded dielectric slab.

Figure 2 (a) Incident plane wave on the printed surfaces. Only the polarisations which interact with the FSS are shown.
(b) Transmission line networks for TE and TM polarizations.

For the validity of the network representation in Fig. 2, it is important to individuate the region of the dispersion diagram relevant t a single propagating FW. Indicating by *c* the free-space speed of light, and limiting the observation to positive value of k_x (negative values may be reconstructed by symmetry), the conditions for the TM case are (i) $k_x - 2\pi/d_x < -\omega/c$, (ii) $k_x < \omega/c$ (real angle of incidence). These relations are associated to the region shadowed at the right hand side of Fig. 3. For the TE case analogous conditions leads to the region shown at the left hand side of Fig. 3.

It is also worth noting that the properties of pole and zero of the impedance (also known as Foster properties) lead to the possibility to represent the impedance in a fast and efficient way by a rational function.

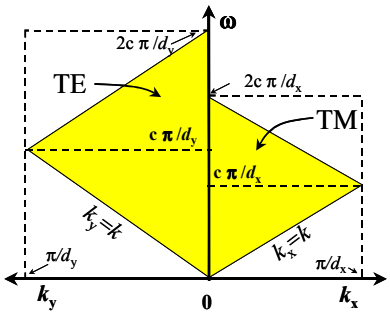

Figure 3 Region of validity of the single-mode transmission line network in the dispersion diagram k_x-ω (TM) and k_y-ω (TE) .

Assuming absence of losses, the equivalent FSS impedance is purely reactive for every k_x. We will postulate that $Z_{FSS}^{TM}(k_x,\omega)$ for every real k_x possesses the same properties of a passive "*driving point*" LC-function of frequency. These properties are [5]:

i) The driving point LC functions are rational function of frequency.

ii) Poles and zeros lie on the real ω axis, are *simple* and *alternate.*

iii) A pole or a zero must be at ω=0.

iv) The poles are symmetrically displaced w.r.t. the origin.

These properties imply that the frequency functions can univocally be determined by the positions of poles and zeros along the real ω axis. Since for the quasi-static limit the dipole-FSS behaves like a shunt capacitance in the transmission line (see Fig.2b), the FSS impedance exhibits a pole in the origin. The properties i)-iv) serves to provide analytical approximation of FSS impedance (see Sec.5.2.1.1)

References

[1] D. Sievenpiper, L. Zhang, F. Jimenez Broas, N. G. Alexopulos, E. Yablonovitch, "High-impedance electromagnetic surfaces with a forbidden frequency band", IEEE Trans. Microwave Theory Tech vol. 47, no. 11, pp. 2059-2074, Nov. 1999

[2] Fei-Ran Yan, Kuang-Ping M, Yongxi Qia, T. Itoh, "A novel TEM waveguide using uniplanar compact photonic-bandgap (UC-PBG) structure", IEEE Trans. Microwave Theory Tech, vol. 47, no.11, pp. 2092-2098, Nov. 1999

[3] Sergei Tretyakov, Analitical modelling in applied electromagnetics, Artech House, N.Y., 2003

[4] A. Grbic, G.V. Eleftheriades, "Periodic analysis of a 2-D negative refractive index transmission line structure", Special Issue on Metamaterial, IEEE Trans. Antennas Propagat, vol. 51, no. 10, pp. 2604- 2611, Oct. 2003

[5] Gobind Daryanani, Principles of active network synthesis and design, John Wiley & Sons, N.Y.,1976.

3.6 G1DMULT models for analysing one-dimensional (1D) multilayer (MULT) structures (Chalmers)

Planar, circular cylindrical and spherical multilayer structures have one property in common: the structure is homogeneous in two dimensions, and varies in the third dimension. For example, the cylindrical structure varies in radial direction and is homogeneous in axial and ϕ directions. Thus, we can call planar, cylindrical and spherical structures one-dimensional structures since they vary only in one dimension [1].

The problem of determining the E- and H-fields radiated by a source embedded in a one-dimensional structure can be simplified if we perform the two-dimensional (2D) Fourier transformation in the coordinates for which the structure is homogeneous. In the cylindrical case we perform the Fourier transformation in axial direction and the Fourier series in ϕ direction, and in the spherical case we perform the vector-Legendre transformation. For each spectral component of the source the excited electromagnetic field in two directions for which the structure is homogeneous has the same harmonic variation as the source. As a result, only the electromagnetic field variation in the normal direction is unknown. In other words, our original three-dimensional problem is transformed into a spectrum of one-dimensional problems, which is much easier to solve.

One representative of numerical algorithms that can determine the field distribution inside a multilayer structure is the G1DMULT algorithm [2] (the abbreviation G1DMULT stands for Green's functions of 1D multilayer structures). By means of a two-dimensional Fourier transformation, the three-dimensional excitation currents are transformed into harmonic current sheets (current tubes in the cylindrical case and current shells in the spherical case). The harmonic one-dimensional problem is solved by making use of equivalent problems, one for each layer. The unknowns are the tangential *E*- and *H*- fields at the layer boundaries. Since the variation of the *E*- and *H*- fields in the direction tangential to the boundaries is harmonic with known periodicity, we only need to determine the complex field amplitudes at the interfaces, i.e., we have four unknowns per boundary. The algorithm connects all equivalent subproblems into a system of $4\cdot(N_{layer}-1)$ linear equations with the same number of unknowns (N_{layer} denotes the number of layers).

Once the amplitudes of the tangential fields have been determined, it is easy to determine the field amplitudes anywhere in the multilayer structure by applying the homogeneous region equivalent principle for the layer inside which we want to determine the field value.

The advantage of the G1DMULT analysis method is that it is easy to implement homogenized boundary conditions for modeling various types of periodic structures, e.g. by assuming that the period is zero [3]. For example, corrugated surfaces, strip-loaded dielectric slabs and mushroom EBG structures were succesfully analyzed using this approach (see e.g. [2]).

References

[1] P.-S. Kildal and J. Sanford, "Analysis of conformal antennas by using spectral domain techniques for curved structures," Proceedings of COST 245 - ESA workshop on active antennas, Noordwijk, 1996, pp. 17-26.

[2] Z. Sipus, P.-S. Kildal, R. Leijon, and M. Johansson, "An algorithm for calculating Green's functions for planar, circular cylindrical and spherical multilayer substrates," Applied Computational Electromagnetics Society Journal, Vol. 13, No. 3., pp. 243-254, Nov. 1998.

[3] P.-S. Kildal, A. Kishk, Z.Sipus, "Asymptotic boundary conditions for strip-loaded and corrugated surfaces," Microwave and Optical Technology Letters, Vol. 14, pp. 99-101, Feb. 1997.

3.7 Conformal Models (TNO)

It must be underlined that only very few works have been presented in open literature regarding the modelling of curved conformal Frequency Selective Surfaces [1], [3]. On the contrary, an abundant literature is available on conformal antennas. Since these models could in principle be adopted also for the analysis of FSS, in order to offer a more complete picture, the overview presented hereafter will include all these different approaches. The different methods have been classified and subdivided into the following two categories: analytical and numerical techniques.

3.7.1 Analytical Techniques

The first theoretical works on rectangular and wraparound patch antennas on cylindrical surfaces were published in the early eighties [4]-[7]. These works are based on the so-called *cavity method*. The validity of such method is limited to thin cavities, where the substrate thickness is much smaller than the wavelength and the radius of curvature. The first rigorous full-wave approach was published only at the end of the eighties [8]. In the last twenty years, several other contributions have been published about the analysis of conformal microstrip antennas using full-wave methods [9]-[14]. Most of these analytical approaches are based on the derivation of the Green's function either in spatial or in spectral domain.

An attempt of generalisation of the Green's function approach is the *algorithm G1DMULT*, for calculating the Green's function in the spectral domain for planar, circular cylindrical and spherical multilayer structures [15]-[19]. All these three structures, in fact, have one property in common: they are homogeneous in two dimensions and vary in the third dimension. Therefore, the original three-dimensional problem is simplified into a one-dimensional problem and the corresponding Green's functions are determined performing a 2D Fourier transformation in the co-ordinates for which the structure is homogeneous.

Another method based on Green's functions is the so-called *Mixed Potential Integral Equation* (MPIE) approach [20]- [22]. The MPIE approach is simpler to implement and more efficient than the conventional electric field integral equation method because the Green's functions have the property to be less singular. In particular, this technique in evaluating the cylindrical Green's function involves subtracting off the appropriate flat-surface Green's function terms and deforming the path of integration into the complex plane to avoid the poles. This approach led to the development of Boulder Microwave Technologies Clementine® software.

A more general approach for the analysis of radiation and mutual coupling of antennas on smooth perfectly conducting arbitrary convex surfaces is the *Uniform geometrical Theory of Diffraction* (UTD) solution proposed in [23]-[29]. This technique allows computing radiation and surface fields for electric and magnetic currents in or on the coating on perfectly conducting arbitrarily shaped convex surfaces. This was achieved by developing asymptotic high frequency UTD solutions for a circular cylinder and a sphere from known eigenfunction series and then, by generalising those solutions to an arbitrarily shaped convex surface, via the local properties of electromagnetic wave propagation at high frequencies.

Another analytical method to analyse multilayer and multiconductor structures on quasi-cylindrical surfaces was presented in [30]. The dyadic Green's function for the unperturbed problem, derived in conventional circular-cylindrical coordinates, is the starting point for the solution of a perturbed problem corresponding to a quasi-cylindrical convex or concave structure. Deviations from the constant boundary are included into the analysis as a perturbation term for the dyadic Green's function of the circular cylindrical structure, which is found by using the vector Green's theorem in two dimensions.

Two specific works on the analysis and design of conformal patch based FSS can be found in [1] and [2]. These two works are conference papers and therefore limited information is available. In [1], a conformal dichroic subreflector structure has been first designed as a flat surface adopting classical dichroic techniques. In a second step, every element has been virtually transposed in the corresponding point of the hyperboloidal-paraboloidal sub-

reflector surface, deforming it in a suitable way in order to fit the exact tangential angle of the surface in the considered point. In [2], a numerical solution for coupling into and scattering from uniform array of patches or apertures conformed to a circular cylinder is presented. The work outlines some scattering features of cylindrical structures as frequency selective surfaces. The numerical technique of analysis is the conjugate gradient (CG) iterative scheme in conjunction with the fast Fourier transform (FFT).

At this point, it is worthwhile spending few words also for structures based on thick/thin slots on metallic surfaces.

The boundary value problem of radiation from a slot (with a sinusoidal distribution) on a metallic circular cylinder was solved exactly several decades ago [31]-[33]. The solution is a harmonic series of functions appropriate for the cylinder: Bessel and Hankel functions. Since then, several different modal approaches have been developed by different authors using a series for the azimuth poles in the Green's function, and integrals for the continuous spectrum, [34]-[40].

The similar problem of an array of infinitely long axial thin slots (slits) developed all around the cylinder have also been widely studied in [41]-[47], adopting the unit cell approach and consequently a Floquet's mode expansion, thanks to the periodicity and full symmetry of the structure. The unit cell approach was extended in [48]-[52], considering an infinitely long cylinder covered with a regular array of axial slots.

Asymptotic approaches, based on Ray Analysis, have been used for slots on cones [53], convex cylinders [54]-[57] and concave cylinders in [58],[59].

In [60] the authors present an integral equation approach based on the equivalence principle for the analysis of electromagnetic scattering by a cylindrically conformal waveguide-fed slot array. The integral equations are solved with the Method of Moments (MoM) with global sinusoidal basis functions. A number of numerical problems like derivation of the Green's functions, evaluation of singular integrals and slowly converging series are also addressed in this work.

The other work which presents the modelling of conformal FSS (in this case circular cylindrical thick perforated metal screens) is the one in [3]. Also this paper is a conference contribution but the underlying methodology is widely described in [61]. The work presents an efficient integral equation technique based on the *Multimode Equivalent Network (MEN)* formulation and the unit cell approach. It consents the analysis of structures like open-ended waveguide arrays and multilayer FSS on circular cylindrical surfaces as a cascade of multimode admittance matrixes. Thanks to the generality and modularity of this method, multilayer structures consisting of dielectric lay-

ers and frequency selective screens can also be efficiently analysed as standing alone as well as directly integrated in the array structure.

As was the case of arrays of elements on a cylinder, arrays of elements on a cone can be attacked either by harmonic series or by asymptotic methods, the latter for portions of the cone where the radius is large in terms of wavelengths [62]-[66].

An early work applying the harmonic (modal) series to a slot on a sphere was given in [62]. Much of the mutual coupling work for cones is, with minor changes, applicable to coupling of elements on a sphere. Both modal series and asymptotic methods have been used [67]-[70].

For more arbitrary surfaces, no analytic solutions are available and since the assumed dimensions compared to the wavelength are large, numerical techniques based on matrix methods may become impractical. The remaining choice is to use asymptotic techniques. Since the near field of the radiating elements are not known beforehand the asymptotic field computation is combined with the moment method, leading to a hybrid approach. In [71]-[73], such a method is used to analyse apertures on singly curved convex surfaces, but in general, the method can also be used for doubly curved surfaces.

3.7.2 Numerical Techniques

Over the past fifteen years we have witnessed an increasing reliance on computational methods for the characterisation of electromagnetic problems. Although traditional integral-equation methods continue to be used for many applications, one can safely state that in recent years the greatest progress in computational electromagnetic has been in the development and application of *partial differential equation* (PDE) methods such as the *Finite-Difference Time-Domain* (FDTD) and *Finite-Element Method* (FEM), including hybridisation of these with integral equation high frequency techniques. The major reasons for the increasing reliance on DE methods stem from their inherent geometrical adaptability and their capability to model heterogeneous (isotropic or anisotropic) structures. At the beginning of the nineties many researchers extended their numerical methods to conformal structures trying to overcome the limitations, in terms of structural complexity, of the traditional rigorous techniques involving integral equations.

The *Finite-Difference Time-Domain (FDTD) method,* in its original formulation, employs rectangular grid models to discretise space. However, when an irregularly shaped structure should be analysed, rectangular grid models must use fine division requiring correspondingly large amounts of time and memory. To overcome this drawback, several techniques have been elaborated and then used by some authors to model conformal radiating elements: *locally distorted grid models* [74], [75]; *globally distorted grid models* [76], [77] and *FDTD sandwich algorithm (SW-FDTD*) [78].

The other well-known approach is the one based on the *Finite-Element formulation*. The goal of any Finite-Element formulation is to obtain the solution of the electric field vector wave equation by means of the weighted residuals method by subdividing the volume enclosing the structure to be analysed as a collection of small elements. Within each volume element, the field can then be expanded in terms of proper set of edge-based shape or basis functions.

Over the past ten years, a lot of work has been done on the development of mesh truncation schemes. Exact boundary conditions provide an integral relation between electric and magnetic fields and the resulting formulation is referred as *Finite Element Boundary-Integral* (FE-BI). To alleviate the higher computational demands of the FE-BI method, absorbing boundary conditions (ABC's) and artificial absorbers (AA) can instead be used to terminate the mesh. In the case of ABC's, a local boundary condition in the form of a differential equation is applied on the surface to relate the electric and magnetic fields so that the surface appears as transparent as possible to the incident fields from the interior. The resulting method is referred to as the *Finite-Element ABC (FE-ABC) method*. In the *Finite-Element Artificial-Absorber (FE-AA) method* instead, the mesh is terminated by using a material absorber (typically not realisable in practice) to absorb the outgoing waves and suppress backward reflections.

In [79] and [80], the FE-BI method has been applied to the analysis of cavity-backed structures in an infinite, metallic cylinder, while in [81], the FE-AA method, with distorted triangular prism mesh elements, was adopted for the analysis of different *conformal patch antennas on spherical, conical and ogival platforms*.

Another numerical algorithm for the characterisation of microstrip conformal antennas, based on the *Method of Lines,* has been proposed in [82] and [83]. Generally, microstrip structures on multilayer conformal surfaces can be seen as concatenation of open waveguide sections and waveguide junctions. To describe the field propagation along the segments, *generalised transmission line equations* for the transverse electric and magnetic fields in inhomogeneous media have been developed. In each of the sections, radiation is taken into account by introducing absorbing boundary conditions (ABC) into the difference operators. The main advantage of this approach is in that all the formulations for various structures in different co-ordinate systems have formally the same form, which allows compact computer programs for all cases.

In [84], it has been proposed a new numerical approach based on the *Method of Auxiliary Sources (MAS)*. According to MAS, the EM fields in each domain of the structure under investigation are represented by a finite linear combination of analytical solutions of the relevant field equations, corresponding to sources situated at some distance away from the boundaries of each do-

main. The radiating "auxiliary sources" are chosen to be elementary dipoles located on the fictitious auxiliary surfaces, usually conformal to the actual surfaces of the structure. The displacement with respect to the boundaries eliminates the singularities of a typical MoM kernel, while there is no need for current integration at any stage of the solution. However this approach becomes inefficient in handling thin and open structures, and in order to overcame this limitation the standard version of MAS has been modified. According to the modified version (MMAS), instead of the EM fields generated by the fictitious current sources, the currents themselves and the charges on the auxiliary surfaces are used as unknowns. This method has been applied to the analysis of a cylindrical-rectangular microstrip patch [85].

References

[1] Floreani, M.G., Zich, R.E., Aulisio, G., Besso, P., Somma, A., "Design and experimental validations of a new FSS conformal subreflector structure for Cassegrain systems", Antennas and Propagation Society International Symposium, 2001. IEEE , Volume: 2 , 8-13 July 2001, Pages:304 - 307 vol.2

[2] Mokhtar, M., "Analysis of cylindrical frequency selective surfaces", Radio Science Conference, 1998. NRSC '98. Proceedings of the Fifteenth National , 24-26 Feb. 1998, Pages:B8/1 - B8/8.

[3] Gerini, G., Zappelli, L., "CAD of multilayer conformal cylindrical arrays", Antennas and Propagation Society International Symposium, 2001. IEEE , Volume: 3 , 8-13 July 2001, Pages:816 - 819 vol.3

[4] C.M. Krowne, "Cylindrical-Rectangular Microstrip Antenna", IEEE Trans. Antennas Propagation, Vol. AP-31, No. 1, pp. 194-199, Jan.1983.

[5] K.Y. Wu and J.F. Kaufman, "Radiation Pattern Computations for Cylindrical-Rectangular Microstrip Antenna", IEEE Antennas Propagat . Soc. Int. Symp. Dig., 1893, pp.39-42.

[6] J. Ashkenazy, S. Shrikman and D. Treves, "Electric Surface Current Model for the Analysis of Microstrip Antennas on Cylindrical Bodies", IEEE Trans. Antennas Propagation, Vol. AP-33, pp. 295-300, 1981.

[7] K.M Luk, K.F. Lee and J.S. Dahele, "Analysis of the Cylindrical-Rectangular Patch Antenna", IEEE Trans. Antennas Propagation, Vol. AP-37, No. 2, pp. 143-147, Feb.1989.

[8] S.M. Ali, T.M. Habashy, J.F. Kiang and J.A. Kong, "Resonance in Cylindrical-Rectangular and Wraparound Microstrip Structures", IEEE Trans. Microwave Theory and Techniques, Vol. MTT-37, No. 11, pp. 1773-1783, Nov.1989.

[9] F.C. Silva, S.B.A. Fonseca, A.J.M. Soares and A.J. Giarola, "Analysis of Microstrip Antennas on Circular-Cylindrical Substrates with a Dielectric Overlay", IEEE Trans. Antennas Propagation, Vol. AP-39, No. 9, pp. 1398-1404, Sept. 1991.

[10] T. Bertuch, G. Vecchi, L. Matekovits, M. Orefice, “Full-wave Analysis of Conformal Antennas of Arbitrary Shapes Printed on Circular Cylinders”, Proceedings of the 1st European Workshop on Conformal Antennas, Oct. 1999, Karlsruhe, Germany, pp.8-11.

[11] A. Svezhentsev, and G. Vandenbosch, “Incorporation of Conformal Structures Within the MAGMAS Framework”, Proceedings of the 2nd COST 260, Nov. 1999, Aveiro, Portugal, pp.25-30.

[12] D. Löffler, W. Wiesbeck and B. Johannisson, “Conformal Aperture Coupled Microstrip Phased Array on a Cylindrical Surface”, IEEE Antennas Propagat . Soc. Int. Symp. Dig., 1999, pp.882-885.

[13] K.L. Wong, Y.T. Cheng and J.S. Row, “Resonance in a Superstarte-Loaded Cylindrical-Rectangular Microstrip Structure”, IEEE Trans. Microwave Theory and Techniques, Vol. MTT-41, No. 5, pp. 814-819, May 1993.

[14] D. Löffler, W. Wiesbeck, “Dual Polarized Elements and Mutual Coupling in Conformal Array on Cylindrical Surfaces”, Proceedings of the Millennium Conference on Antennas & Propagation - AP 2000 (on CD-ROM), April 2000, Davos, Switzerland.

[15] P.S. Kildal and J. Sanford,”Analysis of Conformal Antennas by Using Spectral Domain Techniques for Curved Structures”, Proceedings of COST 245 – ESA Workshop on Active Antennas, 1996, Noordwik, The Netherlands, pp.17-26.

[16] Z. Sipus, P.S. Kildal, R. Leijon and M. Johansson, “An Algorithm for Calculating Green’s Functions for Planar, Circular Cylindrical and Spherical Multilayer Substrates”, Applied Computational Electromagnetics Society (ACES) Journal, Vol. 13, No.3, pp. 243-254, Nov. 1998.

[17] S. Raffaelli, Z. Sipus and P.S. Kildal, “Analysis of Patches on Multilayer Cylinders by Using G1DMULT”, Proceedings of the 1st European Workshop on Conformal Antennas, Oct. 1999, Karlsruhe, Germany, pp.12-30.

[18] Z. Sipus, P.S. Kildal, “Analysis of Conformal Antennas on Multilayer Circular Cylindrical and Spherical Structures Cylinders by Using G1DMULT”, Proceedings of the Millennium Conference on Antennas & Propagation - AP 2000 (on CD-ROM), April 2000, Davos, Switzerland.

[19] J. Bartolic, Z.Sipus, R. Zentner and D. Bonefacic, ”Design of Planar and Cylindrical Microstrip patch Antennas and Arrays for Wireless Applications”, Proceedings of the Millennium Conference on Antennas & Propagation - AP 2000 (on CD-ROM), April 2000, Davos, Switzerland.

[20] R.C. Hall, C.H. Thng, and D.C. Chang, “Mixed Potential Green’s Functions for Cylindrical Microstrip Structures”, IEEE Antennas Propagat . R.C. Hall and D.I. Wu, “Modelling and Design of Circularly-Polarized Cylindrical Wraparound Microstrip Antennas”, IEEE Antennas Propagat . Soc. Int. Symp. Dig., 1996, pp.672-675.

[21] W. Thomas, R.C. Hall and D.I. Wu, “Effects of Curvature on the fabrication of Wraparound Antennas”, IEEE Antennas Propagat . Soc. Int. Symp. Dig., 1997, pp.1512-1515.

[22] P.H. Pathak, W.D Burnside and R.J Marhefka, "A Uniform GTD Analysis of the Diffraction of Electromagnetic waves by a Smooth Convex Surface", IEEE Trans. on Antennas and Propagation, Vol.AP-28, No.5, pp. 631-642, Sept. 1980.

[23] P.H. Pathak, N. Wang, W.D. Burnside and R.G. Kouyoumijan, "A Uniform GTD Solution for the Radiation from Sources on a Convex Surface", IEEE Trans. on Antennas and Propagation, Vol.AP-29, No.4, pp. 609-621, July 1981.

[24] P.H. Pathak and N. Wang, "Ray Analysis of Mutual Coupling Between Antennas on a Convex Surface", IEEE Trans. on Antennas and Propagation, Vol.AP-29, No.6, pp. 911-922, Nov. 1981.

[25] P. Munk and P.H. Pathak, "A UTD Analysis of the Radiation and Mutual Coupling Associated with Antenna on a Smooth Perfectly Conducting Arbitrary Convex Surface with a Uniform Material Coating", IEEE Antennas Propagat . Soc. Int. Symp. Dig., 1996, pp.696-699.

[26] C. Demirdag and R.G. Rojas, "Mutual Coupling Calculations on a Dielectric Coated PEC Cylinder Using a UTD-based Greens's Function", IEEE Antennas Propagat . Soc. Int. Symp. Dig., 1997, pp.1525-1528.

[27] S. Chai, D. Yao and J. Mao, "An Improved Approach to the Mutual Coupling Calculation of Conformal Array", Proceedings of the 1997 National Aerospace and Electronics Conference, 1997, pp.873-877.

[28] R.W. Wills, "Mutual Coupling and Far Field Radiation From Waveguide Antenna Elements on Conformal Surfaces", Proceedings of 1987 International Conference on Radar, 1987, pp.515-519.

[29] M. Thiel and A. Dreher, "Perturbed Dyadic Green's Function for Quasi-Cylindrical Multilayer Microstrip Structures", Proceedings of the 1st European Workshop on Conformal Antennas, Oct. 1999, Karlsruhe, Germany, pp.32-35.

[30] P.S. Carter, "Antenna Arrays Around Cylinders", Proc. IRE, Vol. 31, pp.671-693, Dec. 1943.

[31] R.F. Harrington and W.R. Lepage, "Directional Antenna Arrays of Elements Circularly Disposed About a Cylindrical Reflector", Proc. IRE, Vol. 40, pp. 83-86, Jan. 1952.

[32] H.Knudsen, "Antennas on Circular Cylinders", Proc. IRE, Vol. AP-7, pp.S361-S370, Dec. 1959.

[33] L. Schwartzman and W.K. Kahn, "Maximum Efficiency for Cylindrically Disposed Multiple-Beam Antenna Arrays", IEEE Trans. on Antennas and Propagation, Vol. AP-12, No. 11, pp. 795-797, Nov. 1964.

[34] W.K. Kahn, "Efficiency of Radiating Element in Circular Cylindrical Arrays", IEEE Trans. on Antennas and Propagation, Vol. AP-19, No. 1, pp. 115-117, Jan. 1971.

[35] G.E. Stewart and K.E. Golden, "Mutual Admittance for Axial Rectangular Slots in a Large Conducting Cylinder", IEEE Trans. on Antennas and Propagation, Vol. AP-19, pp. 120-133, 1971.

[36] K.E. Golden and G.E. Stewart, "Self and Mutual Admittances for Axial Rectangular Slots on a Conducting Cylinder in the Presence of an Inhomogeneous Plasma Layer", IEEE Trans. on Antennas and Propagation, Vol. AP-19, No. 3, pp. 296-299, March 1971.

[37] K.E. Golden, G.E. Stewart and D.C. Primodore-Brown, "Approximation Techniques for the Mutual Admittance of Slot Antennas on Metallic Cones", IEEE Trans. on Antennas and Propagation, Vol. AP-22, No. 1, pp. 43-48, Jan. 1974.

[38] P.C. Bargeliotes, A.T. Villeneuve and W.H. Kummer, "Phased Array Antennas Scanned Near Endfire", Hughes Aircraft, Final Report No. P-76/232, Mar. 1976, AD-A028 781.

[39] P.C. Bargeliotes et al. "Conformal Phased Array Breadboard", Hughes Aircraft, Final Report, Jan. 1977, AD-A038 350.

[40] J.C. Sureau and A. Hessel, "Element Pattern for Circular Arrays of Axial Slits on Large Conducting Cylinders", IEEE Trans. on Antennas and Propagation, Vol. AP-17, No.11, pp. 799-803, Nov. 1969.

[41] J.C. Sureau and A. Hessel, "Element Pattern for Circular Arrays of Waveguide-Fed Axial Slits on Large Conducting Cylinders", IEEE Trans. on Antennas and Propagation, Vol. AP-19, No.1, pp. 64-74, Jan. 1971.

[42] J.C. Sureau and A. Hessel, "Realised gain Function for a Cylindrical Array of Open-Ended Waveguides", in Phased Array Antennas, A.A. Oliner and G.H. Knittel, Eds., Proceedings of the 1970 Phased Array Antenna Symposium, Polytechnic Institute of Brooklyn, New York, Artech House, pp. 315-322, 1972.

[43] A. Hessel and J.C. Sureau, "On the Realized Gain of Arrays", IEEE Trans. on Antennas and Propagation, Vol. AP-19, No. 1, pp.122-124, Jan. 1971.

[44] A. Hessel and J.C. Sureau, "Resonances on Circular Arrays With Dielectric Sheet Covers", IEEE Trans. on Antennas and Propagation, Vol. AP-21, No. 3, pp. 159-164, March 1973.

[45] A. Hessel, "Mutual Coupling Effects in Circular Arrays on Cylindrical Surfaces - Aperture Design Implications and Analysis", in Phased Array Antennas, A.A. Oliner and G.H. Knittel, Eds., Proceedings of the 1970 Phased Array Antenna Symposium, Polytechnic Institute of Brooklyn, New York, Artech House, pp. 273-291, 1972.

[46] S. Edelberg, A.A. Oliner, "Coupling Effects in Large Antenna Arrays: Part I-Slot Arrays", IRE Trans. on Antennas and Propagation, Vol. AP-8, No. 3, May 1960.

[47] A.D. Munger, J.H. Provencher and B.R. Gladman, "Mutual Coupling on a Cylindrical Array of Waveguides Elements", IEEE Trans. on Antennas and Propagation, Vol. AP-19, No.1, pp. 131-134, January 1971.

[48] G.V. Borgiotti and Q. Balzano, "Mutual Coupling Analysis of a Conformal Array of Elements on a Cylindrical Surface", IEEE Trans. on Antennas and Propagation, Vol. AP-18, No. 1, pp. 55-63, Jan. 1970.

[49] G.V. Borgiotti and Q. Balzano, "Conformal Arrays on Surfaces With Rotational Symmetry", in Phased Array Antennas, A.A. Oliner and G.H. Knittel, Eds., Proceedings of the 1970 Phased Array Antenna Symposium, Polytechnic Institute of Brooklyn, New York, Artech House, pp. 301-314, 1972.

[50] G.V. Borgiotti and Q. Balzano, "Analysis and Element Pattern Design of Periodic Arrays of Circular Apertures on Conducting Cylinders", IEEE Trans. on Antennas and Propagation, Vol. AP-20, No. 9, pp. 547-555, Sept. 1972.

[51] Q. Balzano, "Analysis of Periodic Arrays of Waveguide Apertures on Conducting Cylinders Covered by Dielectric", IEEE Trans. on Antennas and Propagation, Vol. AP-22, No. 1, pp. 25-34, Jan. 1974.

[52] S.W. Lee, "Mutual Admittance of Slots on a Cone: Solution by Ray Technique", IEEE Trans. on Antennas and Propagation, Vol. AP-26, pp. 768-773, 1978.

[53] S.W. Lee and S. Safavi-Nairi, "Approximate Symptotic Solution of Surface Field Due to a Magnetic Dipole on a Cylinder", IEEE Trans. on Antennas and Propagation, Vol. AP-26, No. 7, pp. 593-598, July 1978.

[54] T.S. Bird "Accurate Asymptotic Solution for the Surface field Due to Apertures in a Conducting Cylinder", IEEE Trans. on Antennas and Propagation, Vol. AP-33, No. 10, pp. 1108-1117, Oct. 1985.

[55] J. Shapira, L.B. Felsen and A. Hessel, "Ray Analysis of Conformal Antenna Arrays", IEEE Trans. on Antennas and Propagation, Vol. AP-22, No. 1, pp. 49-63, Jan. 1974.

[56] J. Shapira, L.B. Felsen and A. Hessel, "Surface Ray Analysis of Mutually Coupled Arrays on Variable Curvature Cylindrical Surfaces", IEEE Proceedings, Vol. 62, pp. 1482-1492, March 1974.

[57] B. Tomasic and A. Hessel, "Periodic Structure Ray Method for Analysis of Coupling Coefficients in Large Concave Arrays – Part I: Theory"; "Part II: Application", IEEE Trans. on Antennas and Propagation, Vol. AP-37, No. 11, pp. 1377-1385, 1386-1397, Nov. 1989.

[58] B. Tomasic, A. Hessel and H. Ahn, "Asymptotic Analysis of Mutual Coupling Coefficients in Concave Circular Cylindrical Arrays – Part I: Far-Zone"; "Part II: Near-Zone", IEEE Trans. on Antennas and Propagation, Vol. AP-41, No. 11, pp. 121-136, 137-145, Feb. 1993.

[59] G.X. Fan and J.M. Jin, "Scattering from a Cylindrically Conformal Slotted waveguide Array Antenna", IEEE Trans. on Antennas and Propagation, Vol. AP-45, No. 7, pp. 1150-1159, July 1997.

[60] G.Gerini, L.Zappelli, "Phased Arrays of Rectangular Apertures on Conformal Cylindrical Surfaces: a Multimode Equivalent Network Approach", IEEE Trans. on AP, vol.52, no.7, 2004.

[61] L.L. Bailin and S. Silver, “Exterior Electromagnetic Boundary Value Problems for Spheres and Cones”, Transactions IRE, Vol. AP-4, pp. 5-16, Jan.1956; corrections Vol. AP-5, p. 313, July 1957.

[62] D.C. Primodore-Brown, “Diffraction Coefficients for a Slot-Excited Conical Antenna”, IEEE Trans. on Antennas and Propagation, Vol. AP-20, No. 1, pp. 40-49, Jan. 1972.

[63] D.C. Primodore-Brown and G. Stewart, ”Radiation from Slot Antennas on Cones”, IEEE Trans. on Antennas and Propagation, Vol. AP-20, No. 1, pp. 36-39, Jan. 1972.

[64] K.K. Chan et al., “Creping Waves on a Perfectly Conducting Cone”, IEEE Trans. on Antennas and Propagation, Vol. AP-25, pp. 661-670, 1977.

[65] D.C. Primodore-Brown, “The Transition Field on the Surface of a Slot-Excited Conical Antenna”, IEEE Trans. on Antennas and Propagation, Vol. AP-21, No. 11, pp. 889-890, Nov. 1973.

[66] A. Hessel et al., “Mutual Admittance Between Circular Apertures on a Large Conducting Sphere”, Radio Science, Vol. 14 pp. 35-41, Jan.-Feb. 1979.

[67] M. Krairiksh, C. Phongcharoenpanich and K. Meksamoot and J. Takada, “A Circularly Polarized Conical Beam Spherical Slot Array Antenna”, Int. Journ. Electronics, Vol. 86, No. 7, pp. 815-823, July 1999.

[68] C. Phongcharoenpanich, M. Krairiksh and J. Takada, “Investigations of Radiation Characteristics of a Circularly Polarized Conical Beam Spherical Slot Array Antenna”, IEICE Trans. Electronics, Vol. E82-C, No. 7 pp. 1242-1247, July 1999.

[69] C. Phongcharoenpanich, M. Krairiksh and J. Takada, “Impedance Characteristics of a Circularly Polarized Conical Beam Spherical Slot Array Antenna”, Proceedings of the Millennium Conference on Antennas & Propagation - AP 2000, April 2000, Davos, Switzerland.

[70] P. Persson and L. Josefsson, “Calculating the Mutual Coupling Between Apertures on Convex Cylinders Using a Hybrid UTD-MoM Method”, IEEE Antennas Propagat . Soc. Int. Symp. Dig., 1999, pp.890-893.

[71] P. Persson and L. Josefsson, “Calculating the Mutual Coupling Between Apertures on Convex Surfaces Using a Hybrid UTD-MoM Method”, Proceedings of the 1st European Workshop on Conformal Antennas, Oct. 1999, Karlsruhe, Germany, pp.60-63.

[72] P. Persson and L. Josefsson, “Calculating the Mutual Coupling Between Apertures on Singly and Doubly Curved Convex Surfaces Using a Hybrid UTD-MoM Method”, Proceedings of the Millennium Conference on Antennas & Propagation - AP 2000, April 2000, Davos, Switzerland.

[73] S. Dey and R. Mittra, “A Locally Conformal Finite-Difference Time-Domain (FDTD) Algorithm for Modelling Three-Dimensional Perfectly Conducting Objects”, IEEE Microwave Guided Wave Lett., Vol. 7, No. 9, pp.273-275, Sept. 1997.

[74] J. Byun, B. Lee and F.J. Harackiewicz, "FDTD Analysis of Mutual Coupling Between Microstrip Patch Antennas on Curved Surfaces", IEEE Antennas Propagat . Soc. Int. Symp. Dig., 1999, pp.886-889.

[75] M. Fusco, "FDTD Algorithm in Curvilinear Coordinates", IEEE Trans. on Antennas and Propagation, Vol.AP-38, No.1, pp. 76-89, Jan. 1990.

[76] T. Kashiva, T. Onishi and I. Fukai, "Analysis of Microstrip Antennas on a Curved Surface Using the Conformal Grids FD-TD Method", IEEE Trans. on Antennas and Propagation, Vol.AP-42, No.3, pp. 423-427, March 1994.

[77] S. Albrecht and P. Edenhofer, "Modelling of Plain and Inclined Sandwich Structures Using the FDTD Technique", Proceedings of the 1st European Workshop on Conformal Antennas, Oct. 1999, Karlsruhe, Germany, pp.92-95.

[78] L.C. Kempel and J.L. Volakis, "Radiation by Patch Antennas on a Circular Cylinder Using the FE-BI Method", IEEE Antennas Propagat . Soc. Int. Symp. Dig., 1994, pp.182-185.

[79] L.C. Kempel and J.L. Volakis, "Scattering by Cavity-Backed Antennas on a Circular Cylinder", IEEE Trans. on Antennas and Propagation, Vol.AP-42, No.9, pp. 1268-1279, Sept. 1994.

[80] T.Özdemir and J.L.Volakis, "Triangular Prisms for Edge-Based Vector Finite Element Analysis of Conformal Antennas", IEEE Trans. on Antennas and Propagation, Vol.AP-45, No.5, pp. 788-797, May 1997.

[81] R. Pregla, "Efficient Modelling of Conformal Antennas", Proceedings of the 1st European Workshop on Conformal Antennas, Oct. 1999, Karlsruhe, Germany, pp.36-39.

[82] R. Pregla, "Efficient Modelling of Conformal Antennas With Anisotropic Material", Proceedings of the Millennium Conference on Antennas & Propagation - AP 2000 (on CD-ROM), April 2000, Davos, Switzerland.

[83] P. Shubitidze, R. Zaridze, D.P. Economou, D.I. Kaklamani and N.K. Uzunoglu, "The Method of Auxiliary Sources in Solving Cylindrical Shaped Conformal Antennas", IEEE Antennas Propagat . Soc. Int. Symp. Dig., 1999, pp.870-873.

[84] D.I. Kaklamani, H.T. Anastassiu and P. Shubitidze, "Analysis of Conformal Patch Arrays Via a Modified Method of Auxiliary Sources (MMAS)", Proceedings of the Millennium Conference on Antennas & Propagation - AP 2000 (on CD-ROM), April 2000, Davos, Switzerland.

4. DESIGN METHODS

4.1 Multi grid synthesis (POLITO)

In many cases it is not possible to satisfy the design requirements with a single array, especially when very stringent conditions are imposed. In these cases, one has to resort to multiple array configurations, where several FSS are packed together, forming a device similar to a multiple cavity filter.

The design of such structures is a difficult problem, often solved by optimisation techniques [1]. A filter-type approach, limited to the case of strip gratings, has been presented in [2].

The case of a two-array FSS structure has been treated by viewing it as a Fabry-Perot interferometer and a suitable synthesis method has been presented [3].

Recently a synthesis technique developed for waveguide filter design [4]-[5] has been adapted to the design of multiple array FSS. This synthesis technique is based on a distributed parameter model where each array is characterized by its scattering matrix. Typically, the metal patches are printed on dielectric layers that have a remarkable effect on the array response, since they reduce the resonance frequency. For these reasons it is important to compute directly the scattering matrix of each array in its real environment, i.e. including the support dielectric layers. In this way also the effects of strongly cut-off Floquet modes, present only in the array neighbourhood, is correctly accounted for.

The FSS design is based on a synthesis procedure [4] that needs the scattering matrix representation of each discontinuity: the array of patches, the dielectric support layers.

The synthesis method is based on an extraction procedure that uses as input the transmission matrix parameter $\mathbf{T_{21} = S_{11}/S_{21}}$ of the whole structure and yields the transmission coefficients $\mathbf{S_{21}}$ of the various discontinuities. In the synthesis procedure the parameter $\mathbf{T_{21}}$ is viewed as a polynomial of a complex variable $\boldsymbol{z}$, related to the frequency:

$$T_{11}(z) = \sum_{k=0}^{N} a_k \; z^{-k}; \;\; T_{21}(z) = \sum_{k=0}^{N} b_k \; z^{-k}$$

Two input parameters are generally enough to define the coefficients of the polynomial (typically Chebysheff): the transmission bandwidth and the relevant return loss. For this application, the transmission bandwidth parameter has been substituted with the magnitude of the transmission coefficient of the central discontinuity. In this way the procedure does not alter the geometry of the central array so that the position of the reflection band is maintained. In other words, the main role played by the other arrays is that of matching the central one, giving rise to the transmission band. As said above, the extraction procedure relies on the fact that the parameter $\mathbf{T_{21}}$ is a polynomial.

However, in practice, this is not the case due essentially to the array frequency dispersion, to the losses and to the multimodal interactions. Hence, the full wave analysis of the designed structure yields a $\mathbf{T_{21}}$ curve that is different from the desired one. These two functions can be considered as input and output signals in an abstract system that comprises the extraction procedure and the full-wave analysis of the designed structure. In [5] it is shown how to identify the parameters of this system, so that one can use (as a target to be synthesized) a pre-distorted version of the desired response curve.

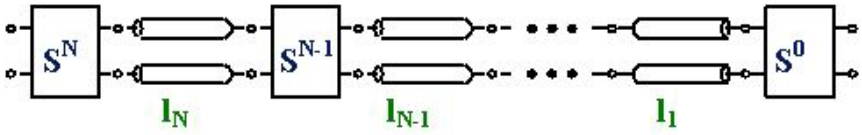

References

[1] J. W. Bandler and S. H. Chen, " Circuit Optimization: The State of the Art ", IEEE Trans. Microwave Theory Tech., Vol.MTT-36, pp.424-443, February 1998.

[2] D. Kinowski, M. Guglielmi and A. G. Roederer, "Angular bandpass filters: an alternative view point gives improved design flexibility", IEEE Trans. Antennas Propagat., Vol.AP-43, pp.390-395, April 1995.

[3] A.C. de C. Lima, E.A. Parker, "Fabry-Perot approach to the design of double layer FSS", IEE Proceedings Microw. Antennas Propag., Vol. 143, No. 2, April 1996.

[4] R. Tascone, P. Savi, D. Trinchero, R. Orta, "A procedure for the design of microwave filters based on a distributed parameter model", 1997 IEEE MTT-S Dig Int. Microwave Symp. Dig., pp. 643-646, 1997.

[5] R. Tascone, P. Savi, D. Trinchero, R. Orta, "Scattering Matrix approch for the design of microwave filters", IEEE Trans. Microwave Theory Tech. March, 2000.

4.2 Approximate models for scattering analysis (TICRA)

A scattering problem consists of a known incident field and a scatterer with known geometry and electrical surface properties. The goal is to compute the total radiated field.

If the surfaces of the scatterer are perfectly conducting the scattered field is generated by the induced surface currents on the scatterer. For non-perfectly conducting surfaces a set of equivalent electric and magnetic surface currents can be computed which exactly radiate the scattered field.

The scattering analysis can thus be considered as a three step procedure where the first step is to calculate the induced or equivalent surface currents, the second step is to calculate the radiated field by these currents and the third step is to add the incident and the scattered field to obtain the total field. Of these steps the first is the most difficult and in general it will involve techniques such as the method of moments that become very time-consuming for large scatterers. Physical Optics is a simple method that gives an approximation to the surface currents valid for perfectly conducting scatterers, which are large in terms of wavelength. In this approximation it is assumed that the surface current in a specific point on a curved, but perfectly conducting scatterer is the same as the surface current on an infinite planar surface, which is tangent to the scattering surface in this point.

If the surfaces of the scatterer are not perfectly conducting, but reflection and transmission coefficients are known, the Physical Optics method can be modified to give an approximation to the equivalent electric and magnetic surface currents.

When the scattering surface is curved and of finite extent the Physical Optics currents are an approximation to the exact equivalent currents. An important complication for the non-perfectly conducting surface is that the reflection and transmission coefficients usually depend on the angle of incidence, which means that it is necessary to know the direction of propagation of the incident field. This restriction is not necessary for the Physical Optics approximation on a perfectly conducting surface.

4.3 High frequency techniques for large surfaces (Radomes and Reflectors). (TICRA)

The Geometrical Theory of Diffraction (GTD) has proven to a very efficient analysis tool for reflector antenna systems that are electrically large. In the following it is illustrated how the conventional GTD approach can be modified to account for non-perfectly conducting reflector surfaces with known reflection and transmission properties.

One of the effects of the edge diffracted field is to create a continuous field across a reflection boundary (RB) and a shadow boundary (SB) of a scattering body, hence, where the reflected ray and the direct ray from the source are switched off. This situation is illustrated in Figure 1 for a perfect conductor.

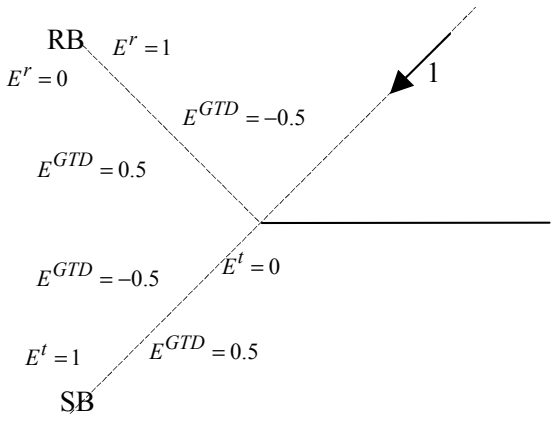

Figure 1 Diffraction on the edge of a perfect conductor

A ray with unity amplitude is diffracted in the left edge of a perfectly conducting plate. The reflected field, E^r, has unity amplitude inside the reflection boundary and is zero outside. The transmitted field has unity amplitude outside the shadow boundary and is zero inside the shadow boundary. To compensate for these discontinuities the diffracted field, E^{GTD}, must change from -0.5 to +0.5 across the boundaries.

If the perfect conductor is replaced by a partly reflecting and partly transmitting plate, the situation is as shown in Figure 2.

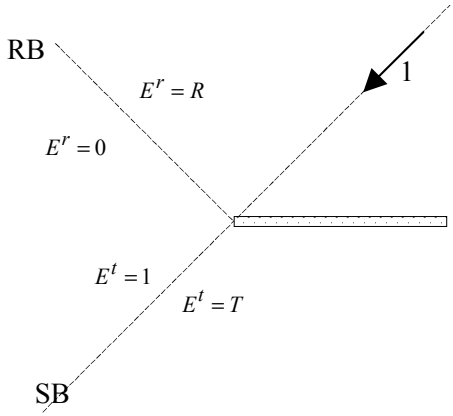

Figure 2 Edge diffraction on a non-perfectly conducting plate

The reflection/transmission coefficients are R and T; hence the reflected field inside the reflection boundary and the transmitted field inside the shadow boundary are modified accordingly.

The problem now consists in adapting the existing GTD algorithms, valid for perfect conductors, to surfaces that have specified reflection and transmission coefficients. Two separate cases, one for the reflection boundary and one for the shadow boundary, are considered. In Figure 3 the method for treating the reflection boundary is outlined.

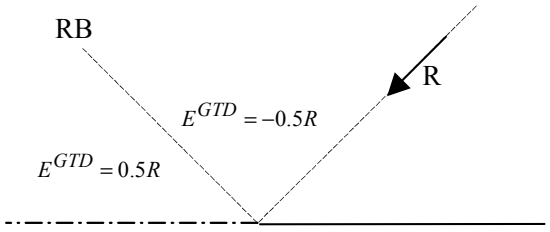

Figure 3 Diffraction at the RB edge of a non-perfectly conducting plate

As the reflected field inside the reflection boundary has the amplitude R, the existing algorithms for calculating the diffracted field can be used with the assumption that the incident field is scaled from unity to R.

As regards the shadow boundary the method is illustrated in Figure 4. The transmitted field, E^t, has unity amplitude outside the shadow boundary and the amplitude T inside the shadow boundary, hence, an amplitude change of 1-T. If the amplitude of the incident field is modified to 1-T, the diffraction coefficients valid for the perfect conductor case can be applied here.

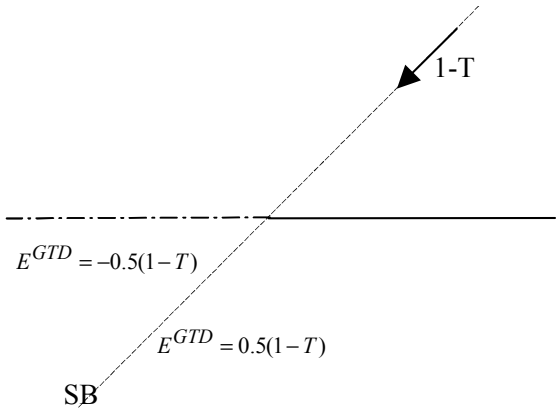

Figure 4 Diffraction at the SB edge of a non-perfectly conducting plate

In order to solve the discontinuity problem at the reflection and shadow boundaries of the non-perfectly conducting plate in Figure 2 the two approaches are used as illustrated in Figures 3 and 4. The dash-dot line in these two figures indicates where the switch from one approach to the other is done. This switch will give rise to a discontinuity in the GTD field; however, at the boundary line the GTD field is low compared to the direct field so the discontinuity in the total field will be negligible.

5. SPECIFIC SURFACE MODELING

5.1 Non-resonant surfaces

5.1.1 Strip grids

5.1.1.1 Simple analytical approach (TICRA)

A planar sample of a general reflector material is illustrated in the figure below. A material definition coordinate system, $x_d y_d z_d$, is introduced with the z_d-axis normal to the surface. The direction of an incident plane wave is given by the spherical coordinates (q_i, f_i), where q_i is measured from the positive z_d-axis and f_i from the positive x_d-axis.

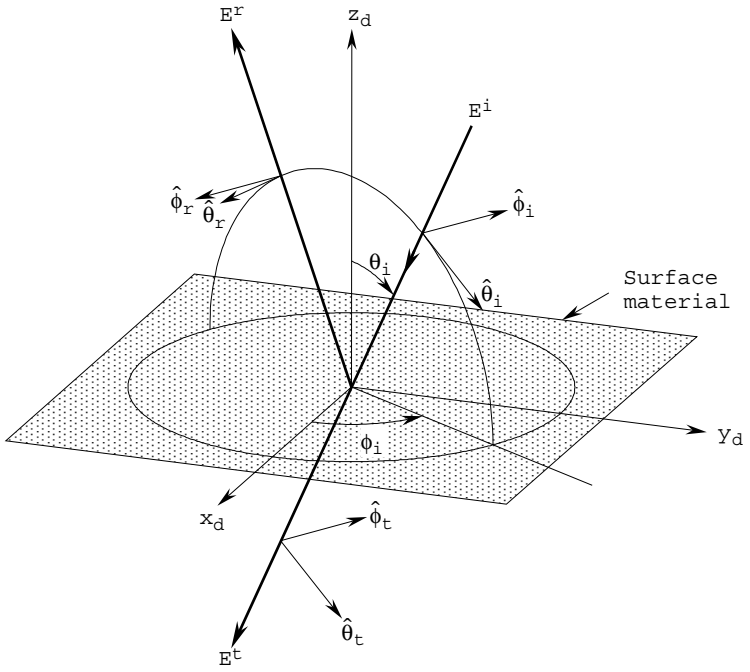

Unit vectors for the definition of reflection and transmission coefficients.

The incident plane wave can be decomposed as

$$\bar{E}^i = E^i_q \hat{q}_i + E^i_f \hat{f}_i$$

and is partly reflected and partly transmitted through the surface where the unit vectors of incidence, $\hat{q}_i$ and $\hat{f}_i$ are the usual polar vectors shown in the figure.

The reflected field is given by

$$\bar{E}^r = E_q^r \hat{q}_r + E_f^r \hat{f}_r$$

where

$$\begin{bmatrix} E_q^r \\ E_f^r \end{bmatrix} = \begin{bmatrix} R_{qq} & R_{qf} \\ R_{fq} & R_{ff} \end{bmatrix} \begin{bmatrix} E_q^i \\ E_f^i \end{bmatrix}$$

and the unit vectors of reflection, $\hat{q}_r$ and $\hat{f}_r$ are also shown in the figure and they are the negative mirror images of $\hat{q}_i$ and $\hat{f}_i$, respectively.

Similarly, the transmitted field is given by

$$\bar{E}^t = E_q^t \hat{q}_t + E_f^t \hat{f}_t$$

where

$$\begin{bmatrix} E_q^t \\ E_f^t \end{bmatrix} = \begin{bmatrix} T_{qq} & T_{qf} \\ T_{fq} & T_{ff} \end{bmatrix} \begin{bmatrix} E_q^i \\ E_f^i \end{bmatrix}$$

and the unit vectors of transmission $\hat{q}_t$ and $\hat{f}_t$ are defined by

$$\hat{q}_t = \hat{q}_i \quad , \quad \hat{f}_t = \hat{f}_i \quad .$$

A strip grid consists of parallel strips. Each strip has a width w and the spacing of the strips is s (the distance from the centre of one strip to the centre of the next).

The reflection and transmission coefficients are given by Nakamura and Ando (1988) for all angles of incidence. For a plane wave at normal incidence, $q_i = f_i = 0$, polarised parallel to the strips the reflection coefficient is

$$R_{qq} = \frac{1}{1 + jt}$$

$$t = - \frac{2s}{l} \ln \cos\left(\frac{p}{2}\left(1 - \frac{w}{s}\right)\right)$$

and for polarisation orthogonal to the strips one gets

$$R_{ff} = \frac{jt'}{1 + jt'}$$

$$t' = - \frac{2s}{l} \ln \sin\left(\frac{p}{2}\left(1 - \frac{w}{s}\right)\right)$$

where l is the wavelength.

The formulas by Nakamura and Ando have been compared to other methods and it has been found that good accuracy is obtained for $s/l < 0.3$.

The strip grid is applied to a reflector surface as follows: The constant strip grid parameters, s and w, are defined in the planar aperture of the reflector. The real strip grid on the reflector surface is now generated by projecting the planar grid along the antenna axis from the aperture to the surface. Since the reflector surface is generally curved it means that the local grid spacing and width will vary across the reflector. This approach is very important for practical applications since it corresponds to the laser etching technique where the strips are cut out of a continuous thin metal layer deposited on the surface.

References

[1] Nakamura, K. and Ando, M. (1988), "A full-wave analysis of offset reflector antennas with polarization grids", IEEE Trans. Antennas Propagat., Vol. 36, No. 2, pp. 164-170.

5.1.1.2 MoM based approach (POLITO)

A periodical arrangement of metallic strips can be seen as a Capacitive Frequency Selective Surfaces (FSS), having a two-dimensional arrangement of dipole patches with periodicities equals to the length and distance of the strips. For this reason, the general way a collection of strips can be analysed, as discussed in section 5.2.1.4.

5.1.2 Wire grids

5.1.2.1 Simple analytical approach (TICRA)

The wire grid material consists of a planar sheet of parallel circular cylindrical wires of spacing s. The diameter of the wires is d_0. It is assumed that $d_0 << s$.

The wire grid has many similarities with the strip grid and it can be shown that for polarisation parallel to the wires the reflection is equal to that of a strip grid where the strip width $w = 2d_0$ (Butler, 1982). For polarisation orthogonal to the wires the equivalent strip width is $w = \sqrt{2}\, d_0$ (Johnson and

Jasik, 1984, Ch.46). The angular dependence with q_i and f_i is the same as for the strip grid.

The wire grid is applied to a reflector surface in a similar way as for the strip grid. The constant wire grid parameters, s and d_0, are defined in the aperture of the reflector antenna. The real wire grid on the reflector is now generated by projecting the planar grid along the antenna axis to the surface. Since the reflector surface is generally curved it means that the local wire spacing will vary across the reflector. In contrast to the strip grid where also the strip width varies across the reflector, the wire diameter d_0 is kept constant for the wires on the surface.

References
[1] Butler, (1982), "The equivalent radius of a narrow conducting strip", IEEE Trans. Antennas Propagat., Vol. AP-30, No. 4, pp. 755-758.
[2] Johnson, R.C. and Jasik, H. (1984) "Antenna Engineering Handbook", McGraw-Hill Book company.

5.1.3 Dielectric sheets (TICRA)

The dielectric layer is a plate of dielectric material of thickness h and with a relative dielectric constant e_r. This type of material can be used to simulate the effects of a radome or it can be used in combination with other materials to model the sandwich support structure of a strip grid or the influence of thermal paint on a reflector.

The reflection and transmission coefficients are given by Born and Wolf (1983) and one obtains:

$$r = \frac{(p_2^2 - p_1^2)(1 - e^{-j2b})}{(p_1 + p_2)^2 - (p_1 - p_2)^2 e^{-j2b}}$$

$$t = \frac{4p_1 p_2 e^{-j(b - kh\cos q_i)}}{(p_1 + p_2)^2 - (p_1 - p_2)^2 e^{-j2b}}$$

$$p_1 = \cos q_i$$

$$b = kh\sqrt{e_r - \sin^2 q_i}$$

$$R_{qq} = -r$$

$$T_{qq} = t$$

$$with \quad p_2 = \frac{\sqrt{e_r - \sin^2 q_i}}{e_r}$$

$$R_{ff} = r$$

$$T_{ff} = t$$

$$with \quad p_2 = \sqrt{e_r - \sin^2 q_i}$$

where k is the free space wave number, $2p/l$. e_r may be complex to account for losses in the material. The dielectric material is isotropic and therefore the reflection and transmission properties are independent of f_i and all off-diagonal elements are zero.

References

[1] Born, M. and Wolf, E. (1983), "Principles of Optics", Sixth (corrected) edition, Pergamon Press, Oxford.

5.2 Resonant surfaces

5.2.1 Single layer Planar FSS, thin structures

5.2.1.1 Lund

Consider a frequency selective structure consisting of a periodic pattern of elements made up of thin strips (high aspect ratio). These can either be thin metallic strips, or thin slots in a metallic sheet. They can make element patterns consisting of straight sections and bends, such as crossed dipoles, tripoles, hexagons (loop type element) etc. The scattering problem is solved by a spectral Galerkin method [1]. It is necessary to set up basis functions to describe the currents on the strips, and the choice of basis functions strongly influences the total effectiveness of the algorithm.

In the papers [2-3], Poulsen develops an efficient set of basis functions for this kind of geometry. Starting by looking at the fundamental geometry of a V-dipole, i.e., two straight strips with an angle between them and joined in one of their respective endpoints, he develops a continuity condition for the current and defines a set of basis functions. The basis functions for the entire FSS element are then assembled by combining V-dipole functions for

each part of the geometry. As an example, the crossed dipole element looks like a plus sign (+), which can be constructed as four V-dipoles with 90 degrees angle. Several other possibilities are indicated in the figure below.

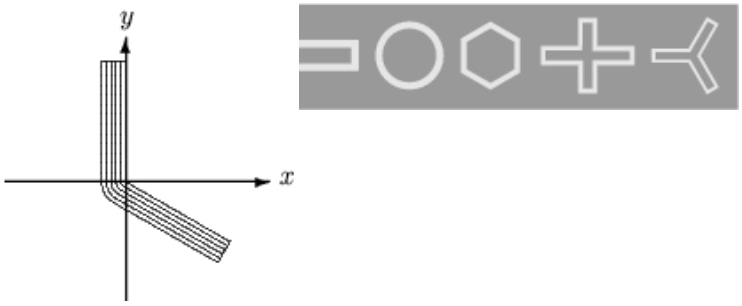

Figure 1 Geometry of the V-dipole, and some elements that can be constructed with it.

The method provides accurate results with a minimum of basis functions, which provides opportunities for treating larger and more complicated structures. For instance, the multiple layer algorithms in the following section benefit from a fast and accurate solution of the single layer FSS case.

References

[1] C.-H. Tsao and R. Mittra. Spectral-domain analysis of frequency selective surfaces comprised of periodic arrays of cross dipoles and Jerusalem crosses. IEEE Trans. Antennas and Propagat., Vol 32, No. 5, 478-486, 1984.

[2] S. Poulsen. Scattering from frequency selective surface: A continuity condition for entire domain basis functions and an improved set of basis functions for crossed dipoles. IEE Proc.-Microw. Antennas and Propag. Vol 146, No. 3, 234-240, June 1999.

[3] S. Poulsen. Scattering from frequency selective surfaces: An efficient set of V-dipole basis functions. IEEE Trans. Antennas and Propagat., Vol. 51, No. 3, March 2003.

5.2.1.2 TNO

The analysis of single layer FSSs is performed resorting to the Unit Cell approach [1] and an integral equation method [2] in combination with the Multimode Equivalent Network (MEN) approach [3],[4]. The MEN approach (see also section 3.3), which shows all its potentialities when applied to multilayer FSS structures, is also very efficient and accurate when applied to simpler single layer configurations. In fact, even in these cases, the structure may still consist of an FSS sandwiched between two dielectric layers. Fur-

thermore, the FSS is often used in combination with array antennas (feeds, phased arrays etc.) and therefore this approach offers the possibility to design the FSS not just as a standing alone element, but also as part of a system including also the array antenna. In this case, the FSS and the array can be analysed both in a strongly interacting integrated configuration as well as in a less interacting more conventional accommodation.

The FSS elements can be either arbitrarily shaped metallic patches or slots etched on a ground plane. The periodic structures under analysis are modelled resorting to the Unit Cell approach. This implies the introduction of the concept of Phase-Shift Wall Waveguides (PSWW), which represents the free space regions under the periodic conditions dictated by the array. Floquet's theorem provides a complete set of orthonormal modes to represent the field in these waveguides.

The overall structure is modelled as a cascade of uniform PSWWs connected through the common transition surfaces. In the formulation, it is also introduced the concept of "accessible" and "localised" modes. The accessible modes are the first modes (all the propagating modes plus first few non-propagating modes) excited by the discontinuity, which can "see" the successive transition, if any. The localised modes are all the infinite remaining modes confined in the neighbourhood of the discontinuity.

The FSS, which couples the modes in two opposite regions, is described by a multimode equivalent network. The MEN is derived imposing the proper boundary conditions of the electromagnetic field on the printed metallic elements or on the screen apertures. Depending on the kind of discontinuity, the transition networks are either in parallel or in series with respect to the Transmission Lines representing the uniform regions. This difference originates from the choice of the most suitable IE for representing the specific problem.

In the *patch formulatio*n [5], the problem is formalised in terms of an Electric Field Integral Equation (EFIE) and the unknown quantities are the differences between the magnetic fields in the half spaces defined by the FSS. Accordingly, these differences can be seen as currents flowing in a generalised load, located in parallel with respect to the transmission lines associated to the Floquet modes defined above and below the FSS discontinuity (shunt multimode admittance network).

In the *aperture formulatio*n, instead, the problem is formalised in terms of a Magnetic Field Integral Equation (MFIE). In this case the unknowns are the magnetic currents (electric field) on the apertures. Since the voltages across the transition are discontinuous, the equivalent generalised load can be seen in series (series multimode impedance network). The integral equations are solved resorting to a classical MoM method where sub-domain or ad hoc full-domains basis functions are used [6].

In Fig. 1a, it is shown an example of Frequency Selective Surface consisting of Jerusalem Cross dipoles embedded in a dielectric slab. Fig.1b shows a comparison between the reflection coefficients of the FSS for TE and TM polarised plane wave incidence, calculated with the MEN based theory and those available in open literature [7].

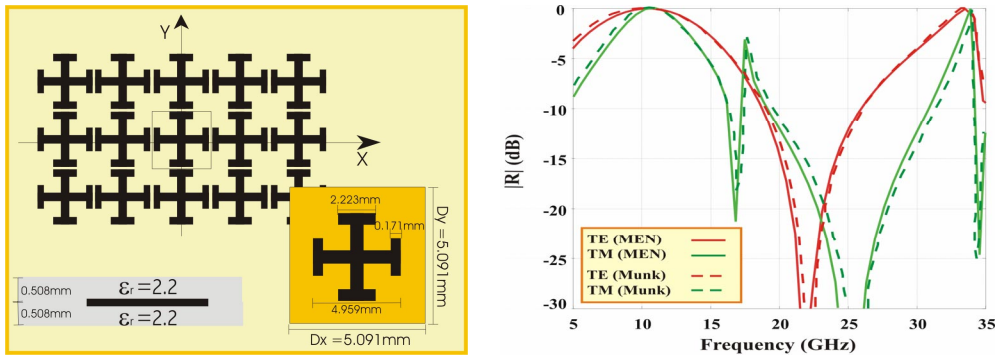

Figure 1 (a) FSS geometry. (b) comparison between the reflection coefficients of the FSS for TE and TM polarised plane wave incidence calculated with the MEN based theory, and those available in open literature (B. Munk) [6].

References

[1] H. A. Wheeler, "The radiation resistance of an antenna in an infinite array or waveguide," PROC. IRE, Vol. 36, pp. 478-487, April 1948.

[2] G. Gerini, M. Guglielmi, G. Lastoria, "Efficient Integral Equation Formulations for Admittance or Impedance Representation of Planar Waveguide Junctions", IEEE MTT-Symposium Digest, Anaheim, California, June 1998.

[3] M.Guglielmi and A.A.Oliner, "Multimode network description of a planar periodic metal-strip grating at a dielectric interface - part i: Rigorous network formulations," IEEE Trans. Microwave Theory Tech., vol. 37, no. 3, pp. 534–540, 1989.

[4] G.Gerini and M.Guglielmi, "Full-wave cad of a rectangular waveguide filter with integrated coaxial excitation," IEEE Trans. Microwave Theory Tech., vol. 49, no. 5, pp. 986–989, 2001.

[5] S. Monni, G. Gerini, A. Neto, 'Equivalent Network Analysis of Phased Arrays Integrated with Patch Based FSS Structures", 2002 IEEE International Antennas and Propagation Symposium, June 2002, San Antonio, Texas.

[6] G. Gerini, S. Monni, L. Zappelli, "Arbitrary shaped aperture/patch FSS's in planar phased arrays. Full Domain and sub domain basis functions",

2003 IEEE International Antennas and Propagation Symposium, June 2003, Columbus, Ohio.
[7] B.A.Munk, Frequency Selective Surfaces: theory and design. New York: John Wiley and Sons, 2000.

5.2.1.3 Siena

Reflectors constituted by FSS are often very complicated to be analysed due to the large dimension in terms of the wavelength, which renders inapplicable the conventional full-wave analysis. To this end, local approximation should be used, conceptually similar to the physical optics (PO) method for perfectly conducting surfaces. The equivalent currents to be distributed on the curved surfaces can be obtained from a multiparametric full-wave analysis. The parameters involved in the process are: frequency, direction of incidence and geometry. Calculating the reflection coefficient, amplitude and phase for each of these parameters in real time is inefficient, so that a precalculation of reflection coefficient is probably the more efficient way, especially when dealing with optimisation algorithm. To this end, it is extremely convenient to catch the full-wave multiparametric features from few runs and obtaining from this analytical expression of the reflection coefficient. The equivalent network introduced in Sec.3.5 is well suited to this purpose, and provides with few full-wave steps to a full analytical large bandwidth characterization of the FSS impedance.

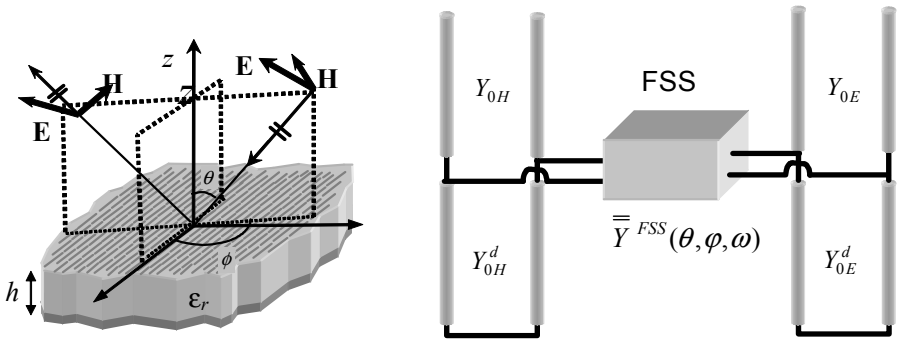

Figure 1 Geometry of a FSS of printed dipoles on a grounded dielec tric slab, illuminated by an incident plane wave (left), and relevant equivalent dual transmission line network (right).

To better illustrate the concept, let us consider the case of a FSS constituted by metallic patches printed on grounded slab, and illuminated by a plane wave with arbitrary direction of incidence (θ,φ) (Fig.1, left). The plane wave can be either transverse electric (TE) or transverse magnetic (TM) polarized.

In Sec 3.5 the particular case of incidence on the two principal cases has been considered which leads to two decoupled network z-transmission line networks for TE and TM cases. For oblique incidence with respect to the dipole direction a coupling between the two TE and TM is expected which yields the network illustrated in Fig.1, right.

The periodicity is assumed to be small enough so that only the dominant Floquet mode of the scattered field is propagating along *z*. Through a periodic Method of Moment analysis the response of the surface is characterized in terms of a frequency-dependent scattering matrix

$$\overline{\overline{\Gamma}}(\theta,\varphi,\omega)=\begin{bmatrix}\Gamma_{hh}(\theta,\varphi,\omega) & \Gamma_{eh}(\theta,\varphi,\omega)\\ \Gamma_{he}(\theta,\varphi,\omega) & \Gamma_{ee}(\theta,\varphi,\omega)\end{bmatrix} \tag{1}$$

where the subscripts *h* and *e* stand for transverse electric and magnetic, respectively. The first and the second subscript are associated to the polarization of the reflected and of the incident wave, respectively. The terms of the reflection coefficient dyadic can be associated to the equivalent *z*-transmission line network (Fig.1). The network is composed by two coupled transmission lines, associated to the TE and to the TM polarization, respectively. In Fig.1, $Y_{0e,h}$ and $Y^{d}_{0e,h}$ are the characteristic admittances of the free-space and dielectric transmission line sections, respectively; the lines are coupled by a two-port network characterized by admittance matrix.

$$\overline{\overline{Y}}^{FSS}(k_x,k_y,\omega)=\begin{bmatrix}Y^{FSS}_{hh}(k_x,k_y,\omega) & Y^{FSS}_{eh}(k_x,k_y,\omega)\\ Y^{FSS}_{he}(k_x,k_y,\omega) & Y^{FSS}_{ee}(k_x,k_y,\omega)\end{bmatrix}=\overline{\overline{R}}\cdot\begin{bmatrix}\widetilde{Y}_{11}(k_x,k_y,\omega) & 0\\ 0 & \widetilde{Y}_{22}{}^{FSS}(k_x,k_y,\omega)\end{bmatrix}\cdot\overline{\overline{R}}^{-1} \tag{2}$$

where the second equality could be simply obtained by a diagonalization process which implies the rotation matrix $\overline{\overline{R}}$.

When we have collected the functional dependence in terms of the k_x and k_y wavenumber, these wavenumber are related to the incidence angle by $k_x=k\sin\theta\cos\varphi$, $k_y=k\sin\theta\sin\varphi$. The two-port network is placed at the level of the FSS (z=0). This dyadic admittance simulates on a broad frequency band the response of the FSS surface by accounting for the local reactive energy associated to the evanescent Floquet modes. The off-diagonal elements of the dyadic take into account of the cross-polarization of z-transversalized fields due to the patches. We make here the assumption that the terms of the equivalent impedance dyadic are purely reactive due to the absence of losses in the electric conductor.

Following the theory illustrated in Sec 3.5, each term of the FSS admittance possesses the same properties of an LC driving-point impedance function of frequency. In network theory, it is well known that a LC-function can be uniquely determined by the positions of poles and zeros placed in the real ω axis and from the behaviour at $\omega = 0$ and infinity. On the basis of this assumption, the expression of the terms of the FSS admittance dyadic is:

$$\tilde{Y}^{FSS}(k_x,k_y,\omega) = j\omega C_\alpha(k_x,k_y)\frac{(\omega^2-\omega_{z1}^{\ 2}(k_x,k_x))\ldots(\omega^2-\omega_{zn}^{\ 2}(k_x,k_x))}{(\omega^2-\omega_{p1}^{\ 2}(k_x,k_x))\ldots(\omega^2-\omega_{pn}^{\ 2}(k_x,k_x))} \tag{3}$$

We note that poles and zeros are independent on the polarization. The key aspect of the method is then concerned with the identification of the poles $\omega_{pi}(k_x)$ and zeros $\omega_{zi}(k_x)$ as a function of frequency. The dispersion behaviour of poles and zeros of the admittance function can be retrieved from the full-wave data relevant to the scattering matrix on the frequency range under investigation.

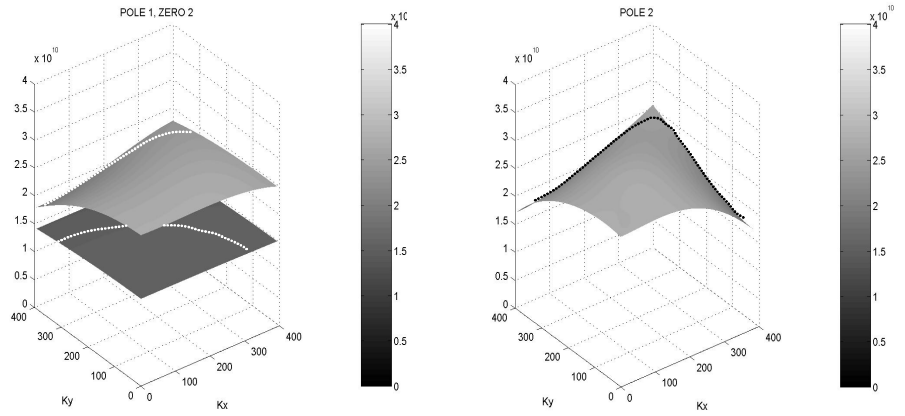

Fig. 2 2D dispersion curves of the of the first two poles, ω_{p1} and ω_{p2}, and of the zero ω_{z1} of the FSS admittance dyadic. The dashed line represents the intersection with the surface $\omega = c\sqrt{k_x^2+k_y^2}$. For value $\omega > c\sqrt{k_x^2+k_y^2}$ the data are extrapolated by analytical continuation.

As an example, the broad-band behaviour of the first two poles, ω_{p1} and ω_{p2} and of the zero ω_{z1} of $\tilde{Y}^{FSS}(k_x,k_y,\omega)$ is shown in Fig. 2 as a function of the transverse wavenumbers (k_x, k_y). It is apparent that the frequency associated to poles and zeros has a smooth variation with the transverse wavenumber in the visible range, thus, suggesting to interpolate the relevant curves in the wavenumber-frequency domain. It has been found convenient to realize the interpolation process in the polar variables (k_ρ,φ), with $k_\rho = k\sin\theta$, by using polynomial functions in k_ρ and trigonometric functions

in φ. Finally, by back substitution in the (k_x,k_y)-domain, the poles $\omega_{pi}(k_x,k_y)$ and the zeros $\omega_{zi}(k_x,k_y)$ are provided in analytical from the interpolation process. The surfaces $k_\rho = k$ is a zone in the dispersion diagram $\omega - (k_x,k_y)$ which crosses the dispersion surfaces of poles and zeros along the lines depicted in Fig.2

Once derived an analytical expression for $\tilde{Y}^{FSS}(k_x,k_y,\omega)$, one can use it in the equivalent circuit in Fig.1, thus calculating in analytical form the voltage and currents at the FSS level. This quantities are directly proportional to the tangential components of electric and magnetic fields; thus obtaining magnetic and electric PO currents to be distributed on the curved reflector surface. The overall process is rigorous, accurate and extremely fast w.r.t. the massive multiparametric full-wave analysis.

References

[1] D. Sievenpiper, L. Zhang, F. Jimenez Broas, N. G. Alexopulos, E. Yablonovitch, "High-impedance electromagnetic surfaces with a forbidden frequency band," IEEE Trans. Microwave Theory Tech., vol.47, no 11, Nov. 97, pp. 2059-2074, .

[2] Fei-Ran Yang, Kuang-Ping Ma, Yongxi Qian, T. Itho "A novel TEM waveguide using uniplanar compact photonic-bandgap (UC-PBG) structure," IEEE Trans. Microwave Theory Tech., vol. 47, no 11, Nov. 99, pp. 2092-2098.

[3] T. Zhao; D.R. Jackson, J.T. Williams, H.Y. Yang, "Radiation characteristics of a 2D periodic leaky-wave antenna using metal patches or slots," 2001 IEEE AP-S International Symposium, vol. 3 , pp. 260 – 263, 8-13 July 2001.

[4] S. Maci, R. Magliacani, A. Cucini, "Leaky-wave antennas realized by using artificial surfaces," 2003 IEEE AP-S International Symposium.

[5] S. Maci, M. Caiazzo, A. Cucini, M. Casaletti, "A network theory for EBG surfaces composed by FSS printed on a grounded dielectric slab," submitted to IEEE Trans. Antennas Propagat..

[6] S. Maci, P-S. Kildal, "Hard and soft gangbuster surfaces" submitted to URSI EMT, May 2004, Pisa, Italy

5.2.1.4 POLITO

FSS may be basically of two types, those that at low frequency are transparent (capacitive FSS consisting of an array of patches supported by dielectrics) and those that are reflecting (inductive FSS consisting of perforated screen). The behaviour at the resonance frequency is complementary: the capacitive FSS are reflecting whereas the inductive FSS are transparent. Typically, the polarization and the incident direction of the electromagnetic wave influence these properties. The analysis of FSS is carried out by a spectral technique. This technique is well suited especially when dielectric supports are present. In fact, in this case, the spectral representation of the

Green function is known in analytical form. This formulation allows us the introduction of a vector transmission line representation where voltages and currents are the two-dimensional Fourier transforms of the transversal electric and magnetic fields, respectively. Shunt current generators, whose strength is unknown, represent the currents induced on the metal region. The key point of this approach is the construction of a vector functional equation in the spectral domain. This equation relates the two unknown functions of the problem: the Fourier transform of the aperture electric fields (the vector voltage at the discontinuity section) and the Fourier transform of the current induced on the metal region (the vector current generator). The dielectric stratification, placed on both sides of the array are described, for each Floquet mode (propagating and evanescent), in terms of their scattering matrix. In this way, the relevant Green function is simply described by the dyadic load impedance seen by the current generator and the functional equation is obtained by means of circuit considerations. Even if the functional equation contains two unknowns, the problem can be solved. In fact, the inverse Fourier transforms of the two unknowns have complementary supports: the apertures for the transversal electric field and the metal region for the induced currents. By means of the Parseval Theorem this property yields the orthogonality between the two unknowns in the spectral domain. The orthogonality relationship can be seen as the second equation. Hence the problem can be solved by considering as primary unknown the current induced on the metallic region (patch approach) or the transversal electric field (aperture approach) according to the geometry of the discontinuity. When the metallic region has simple shape, for example strips, rings, crossed dipoles, tripoles, discs and so on, the patch approach is more convenient. Whereas the aperture approach is convenient in the case of perforated screens where the apertures have simple geometry (e.g. slots). For both the approaches the scattering problem is solved numerically in the spectral domain by the Galerkin method of moments.

The solution is given in terms of the Generalized Scattering Matrix in the Floquet mode base. Hence, it is possible to study any aspect of the scattering phenomenon: reflection and transmission coefficients, the depolarisation effects, scattering of higher order harmonics and so on. On the basis of this representation, the analysis of multiple array structures can be done by cascading the Generalized Scattering Matrices of each array. Obviously, The number of Floquet modes (propagating and evanescent) involved in the interaction depends on the spacing between the arrays. A key concept in this procedure is that of accessible Floquet modes and localized Floquet modes. This is, in turn, related to the two roles played by the Floquet modes in the analysis of the FSS. On one hand, the Floquet modes are used to represent the Green's function of the problem (this operator relates quantities defined in the same section of the discontinuity). On the other hand, the Floquet modes are used to represent the scattered fields from an array that, in the case of a multiple array configuration, are to be considered as incident fields

on the other arrays. It has to be remarked that the number of these Floquet modes is not necessarily the same of those used to represent the Green's function. The reason for this is that generally a finite distance exists between the array section and the one where the scattered field is of interest. Thus, a major role is played by the fact whether a mode is above or below cut-off. Hence, it is convenient to classify the Floquet modes as accessible or localized according to their attenuation between adjacent arrays being lower or higher than a specified threshold. Accessible modes, either propagating or evanescent, are responsible for the interaction through adjacent discontinuities. Localized modes are so attenuated that they do not `see' the other arrays and give rise only to energy storage if the dielectrics are lossless. In cascading the various GSM, only the accessible mode ports are involved, whereas the localized mode ports are disregarded. According to the definition of GSM, this amounts to terminate these with the input impedances of the dielectric loads. From a computational point of view, it may be convenient to decompose a multiple array FSS into single array cells where the dielectric stratifications are considered. In particular, the number of accessible modes may be different on the two sides of the array since the dielectric stratifications are generally different. The reference impedance is that of free space and the left reference plane is close to the grid, whereas the right one is close to the adjacent array. In other words, a dielectric spacer belongs always to the array located at its left. The ports corresponding to localized modes are loaded with the input impedances of the relevant dielectric stratifications. It can be noted that in the cascading procedure, the matrix to be inverted has a size that equals the number of accessible modes, since only these are responsible for the inter-array coupling. If the distance between the arrays is such that only a few Floquet modes are accessible, the cascading procedure is obviously very convenient. On the other hand, for very small spacing, a coupled equation technique is more efficient, since almost all Floquet modes, used in the characterization of each array, become accessible. These considerations explain why it is computationally very convenient to characterize each array directly in its dielectric environment, i.e. by using the application of the method of moments a Green's function that takes the dielectric structure into account. An alternative approach could be that of computing the GSM of the freestanding array and of the dielectric stratification separately and then combining them by a cascading procedure. In this case, however, being the conducting elements printed on the dielectric layers, all the Floquet modes used in the characterization would be accessible and the matrix to be inverted would be impracticably large.

In multiple array configurations, the various arrays (even if all with the same lattice) may be stacked with a transversal shift between each other. Obviously, the combination of the GSM of the various arrays can be carried out only if they are all referenced to the same origin. Instead of studying all the arrays in the same reference system, we evaluate the GSM's in the local

reference system of the corresponding arrays, which is more convenient, then they are transform to refer them to the general reference system.

When computing the field scattered from an FSS according to the formulation described above, two series expansions are involved: for the patch approach, for instance, they are the representation of the induced current in terms of basis functions and the representation of the Green's function in terms of Floquet modes. As for the basis functions, they may be entire domain or sub-domain types. The former can be used for regular geometries; the latter are more flexible and, in principle, may be used with very general configurations. An important point in the choice of basis functions is their ability to satisfy the conditions at the edges of the structure so that a small number of them are enough for an accurate numerical solution. However, it is to be noted that the elements of the scattering matrix can be considered as continuous linear functionals of the current distribution, which have a stationary point in correspondence of the solution of the scattering problem. For this reason, the accuracy of the reflection and transmission coefficients of the fundamental Floquet modes is always better than that of the representation of the current distribution.

Another point to be taken into account to reduce drastically the computer time requirements is, of course, the availability in closed form of the Fourier transforms of the basis functions. Furthermore, due to the particular shape of some frequently used patches, it is not necessary to model all the current components to get accurate results. In fact, for instance in the case of slender strips, it is the current component parallel to the strip that is responsible for the first resonance. Hence, it is the only one that needs to be expanded for this frequency range, whereas the other components may be safely neglected. Concerning the number of Floquet modes to take into account, essentially two approaches are possible. One consists in keeping a very large number of Floquet modes in order to obtain a representation of the Green's function as accurate as possible. Sometimes acceleration techniques for series summation have been used in the case of a freestanding array or simple dielectric stratifications. This strategy is appropriate when very specialized basis functions are used. The other approach is followed when more or less "general purpose basis functions" are used and then one tries to compensate for the inaccuracy in the unknown basis function representation with a corresponding inaccuracy caused by a truncated representation of the Green's function. The issue here is the relative convergence phenomenon. The key point is the best choice of the ratio between the number of terms retained in the two expansions. The case of a non-resonant iris in a rectangular waveguide has been studied in detail by numerical and analytical techniques. It has been shown that this ratio coincides with the ratio between the iris aperture width and the waveguide width when waveguide mode eigenfunctions are used to represent the aperture electric field. The cases that occur in the FSS analysis are much more complicated and no analytical

study can be applied. It is possible, however, to identify a criterion that is a generalization of the above mentioned one and that allows a correct analysis for very general patch or aperture shapes. In fact, one must recognize that the electric current induced on both sides of the metal elements is represented by means of two sets of functions, i.e. the basis functions and the Floquet modes. Indeed, the total induced current equals the magnetic field jump between the left and right faces of the metal elements. Similarly, in the case of the aperture approach, the aperture electric field is represented in terms of basis functions and of Floquet modes. In order to have a well-conditioned system matrix, it is important that the accuracy of the two approximations is comparable. A possible way to enforce this condition is to require that the spatial bandwidth of the two representations is the same. This is not a rigorous criterion, because the support of the basis functions in the spectral domain is not finite. However, as in many other problems, it is possible to define a measure of the spatial bandwidth and to choose the Floquet modes as those corresponding to the points of the reciprocal lattice that lie within this spatial band. The Fourier transforms of entire domain basis functions have an oscillatory behaviour with a maximum (main lobe) that moves further out the higher the order of the basis function. Therefore the spatial bandwidth of the representation, which in principle is infinite, can be defined in practice so as to include at least the main lobe of the highest order basis function considered.

As far as the design activity is concerned, our approaches allow us to derive a fundamental equivalent circuit of each array by a de-embedding procedure. This concept allows us the use of the standard matching procedures of microwave engineering to design the whole structure. Further details concerning the methods of the analysis, the design technique and applications can be found in the publications cited in the bibliography.

The patches on the arrays, or the apertures on the perforated screens, are periodically arranged in a skewed lattice defined by its basis vectors $\underline{d}_1$ and $\underline{d}_2$ in the xy-plane in the points:

$$\underline{\rho}_{pq} = p\underline{d}_1 + q\underline{d}_2$$

where $\underline{d}_1$ and $\underline{d}_2$ are the basis vectors of the direct lattice.

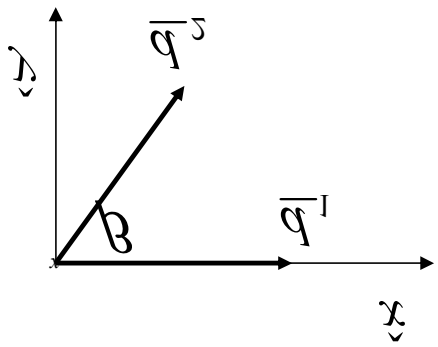

Figure 1 Lattice geometry

Consider two plane waves (progressive and regressive with respect to $\hat{z}$) whose incident directions are identified by the spherical coordinates θ_i and φ_i:

$$\underline{E}^{(+)} = \underline{E}_0{}^{(+)} \exp(-j\underline{k}^{(+)} \cdot \underline{r}) \qquad \text{and} \qquad \underline{E}^{(-)} = \underline{E}_0{}^{(-)} \exp(-j\underline{k}^{(-)} \cdot \underline{r})$$

where the wave vectors are

$$\underline{k}^{(\pm)} = \underline{k}_t \pm k_z \hat{z}$$

with

$$\underline{k}_t = K_0 \sin\theta_i (\cos\varphi_i \hat{x} + \sin\varphi_i \hat{y})$$

$$k_z = \sqrt{K_0{}^2 - |\underline{k}_t|^2}$$

The field scattered from the structure can be described in terms of Floquet modes, which forms a discrete spectrum of plane waves. The transversal electric field of the progressive and regressive waves can be written as:

$$\underline{E}_t^{(+)}(\underline{\rho}) = \sum_{pq} \left[V_{pq}^{(TE+)} \exp(-j\underline{k}_{pq} \cdot \underline{\rho})(\hat{z} \times \hat{k}_{pq}) + V_{pq}^{(TM+)} \exp(-j\underline{k}_{pq} \cdot \underline{\rho})\hat{k}_{pq} \right] \exp(-jk_{z,pq} z)$$

$$\underline{E}_t^{(-)}(\underline{\rho}) = \sum_{pq} \left[V_{pq}^{(TE-)} \exp(-j\underline{k}_{pq} \cdot \underline{\rho})(\hat{z} \times \hat{k}_{pq}) + V_{pq}^{(TM-)} \exp(-j\underline{k}_{pq} \cdot \underline{\rho})\hat{k}_{pq} \right] \exp(jk_{z,pq} z)$$

where $\underline{\sigma}_{pq} = \underline{k}_t + p\underline{\sigma}_1 + q\underline{\sigma}_2$

and

$$k_{z,pq} = \sqrt{K_0{}^2 - |\underline{\sigma}_{pq}|^2}$$

The vectors $\underline{\sigma}_1$ and $\underline{\sigma}_2$ are the basis vectors of the reciprocal lattice, related to those of the direct lattice by the following expressions:

$$\underline{\sigma}_1 = 2\pi \frac{\underline{d}_2 \times \hat{z}}{\underline{d}_1 \times \underline{d}_2 \cdot \hat{z}}$$

$$\underline{\sigma}_2 = 2\pi \frac{-\underline{d}_1 \times \hat{z}}{\underline{d}_1 \times \underline{d}_2 \cdot \hat{z}}$$

The Generalised Scattering Matrix (GSM) computed by the program CFSSS and IFSSS relates the power waves b_{pq} and a_{pq}. As is well known, b_{pq} and a_{pq} are associated to the scattered and incident modal voltages $V_{pq}^{(scatt.)}$ and $V_{pq}^{(inc.)}$.
For the propagating plane waves the GSM turns out to be the usual scattering matrix S. The relationship between the principal polarisations of the plane waves and the power waves becomes:

$$E_{pq}^{(TE,TM)} = \sqrt{\frac{Z_0}{\cos\theta_{pq}}} \left\{ b_{pq}^{(TE,TM)}, a_{pq}^{(TE,TM)} \right\}$$

where $Z_0 = \sqrt{\mu_0/\varepsilon_0}$ is the free space impedance, and θ_{pq} is the incident angle:

$$\cos\theta_{pq} = \sqrt{1 - \left(\frac{|\underline{\sigma}_{pq}|}{K_0} \right)^2}$$

The reference directions for the electric field are

$\hat{u}_{pq}^{(TE)} = \hat{z} \times \hat{\sigma}_{pq}$ for the TE polarisation

$\hat{u}_{pq}^{(TM)} = \hat{\sigma}_{pq} \sin\theta_{pq} \mp \hat{z} \cos\theta_{pq}$ for the TM polarisation

where the sign is related to the progressive and regressive state of the plane wave.

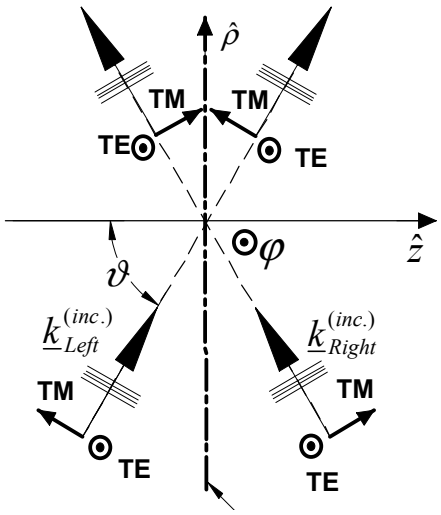

Figure 2 Plane of incidence. Reference Polarizations.

Usually only the TE_{00} and TM_{00} Floquet modes are propagating, whereas the other plane waves are evanescent. In this conditions, and according to the previous definitions, the scattering matrix relates the θ and φ components of the incident and scattered electric fields. Figure 1 shows the reference directions of the electric field in a generic plane of incidence $(\hat{\rho}, \hat{z})$ perpendicular to the unit vector $\hat{\varphi}$. CFSSS and IFSSS recognise in the angles θ and φ the direction of the wave vector $\underline{k}_{Left}^{(inc.)}$ corresponding to the incident progressive plane wave.

When $\theta = 0$ (normal incidence) the two fundamental Floquet modes degenerate and become TEM modes. In this case the labels TE and TM are assigned for continuity by considering the value of φ. For example, with $\varphi = 0$, the TE and TM labels correspond to the electric fields polarised along $\hat{y}$ and $\hat{x}$, respectively. Whereas with $\varphi = \pi/2$, these labels refer to the directions $-\hat{x}$ and $\hat{y}$, respectively.

References

[1] R.Orta, R. Tascone , R. Zich, ``Scattering from finite extent frequency selective surfaces illuminated by arbitrary sources", Electronics Letters, Vol.21, No.3 January 1985, pp.100-101.

[2] R. Orta, R. Tascone , R. Zich, ``Frequency selective surfaces: spectral characterization and application to multifrequency antenna systems", Annales des telecommunications, Vol.40, No. 7-8, July 1985, pp.378-386.

[3] S. Contu, R. Tascone , ``Scattering from passive arrays in plane stratified regions", Electromagnetics, Vol. 5, No. 4, 1985, pp.285-306.

[4] R. Orta, R. Tascone , R. Zich, ``A unified formulation for the analysis of general frequency selective surfaces", Electromagnetics, Vol. 5, No. 4, 1985, pp.307-329.

[5] R. Orta, R. Tascone , R. Zich, ``Efficient choice of basis functions in moment method analysis of frequency-selective surfaces", Electronics Letters, Vol.23 No.11, May 1987, pp.586-587.

[6] R. Orta, R. Tascone , R. Zich, ``Three-dimensional periodic arrays of thin conductors" Electromagnetics, Vol. 7, No. 2, 1987, pp.185-203.

[7] R. Orta, R. Tascone , R. Zich, ``Multiple-grid frequency-selective surfaces as periodically loaded structures", Electronics Letters, Vol.24 No.8, Apr. 1988, pp.449-450.

[8] R. Orta, R. Tascone , R. Zich; ``Multiple dielectric loaded perforated screens as frequency selective surfaces", IEE Proc. Vol. 135, Pt. H No. 2, Apr.1988, pp.75-82.

[9] R. Orta, P. Savi, R. Tascone , ``The effect of finite conductivity on frequency selective surface behaviour", Electromagnetics , Vol. 10, 1990, pp.213-227.

[10] R. Orta, P. Savi, R. Tascone , R. Zich, ``Multiple scale Frequency Selective Surfaces', in G. Franceschetti e R. Pierri (Eds.), Italian Recent Advances in Applied Electromagnetics , Liguori, Napoli 1991, pp. 267-280.

[11] M. Favreau, J. M. Goutoule, R. Orta, P. Savi, R. Tascone , ``Design of a 45-degree incidence millimeter wave diplexer'', Annales des telecommunications , Vol.47, No. 11-12, pp.539-540, Novembre-Dicembre 1992.

[12] M. Favreau, J. M. Goutoule, R. Orta, P. Savi, R. Tascone , ``A free-space double-grid diplexer for a millimeter-wave diplexer'', Microwave and Optical Technology Letters , Vol.6, No.2, Febbraio 1993.

[13] R. Orta, R. Tascone, D. Trinchero, J. C. Vardaxoglou, ``Dispersion curves and modal fields of a waveguide with FSS inserts'', Electronics Letters , Vol.31 , pp. 1073-1075, 1995.

[14] R.Orta, P.Savi, R.Tascone, "Multiple Frequency-Selective Surfaces consisting of ring patches", \it Electromagnetics , Vol.15, no.4, Luglio 1995, pp.417-426.

[15] R.Orta, P.Savi, R.Tascone, ``Numerical Green's function technique for the analysis of screens perforated by multiply connected apertures'', IEEE Trans. Antennas Propagat. , Vol. AP-44, pp. 765-776, Giugno 1996. bibitem BookFSS R. Orta, R. Tascone , Part II of the book J. C. Vardaxoglou, `` Frequency Selective Surfaces: Analysis and Design'', Research Study Press, John Wiley, 1997

[16] R. Orta, R. Tascone, R. Zich, ``Frequency selective surfaces: spectral characterization and application to multifrequency antenna systems'', (invited paper), JINA 1986 - Journees Internationales de Nice sur les Antennes , Nice, November 1984, pp.168-179.

[17] R. Orta, R. Tascone, R. Zich, ``Perforated screens as frequency selective surfaces. A scattering matrix approach'', IEEE Int. Symposium on Antennas and Propagation, AP-S 1986 , Philadelphia PA, pp.863-866.

[18] R. Orta, R. Tascone, R. Zich, ``Transmission characteristics of dielectric loaded perforated screens'', MONTECH'86, Conference on Antennas and Communications , September 1986, pp.19-23.

[19] R. Orta, R. Tascone, R. Zich, ``Parametric investigation of frequency selective surfaces'', JINA 1986 - Journees Internationales de Nice sur les Antennes , Nice, November 1986, pp.395-399.

[20] R. Orta, R. Tascone, R. Zich, ``General Frequency Selective Surfaces'', PIERS - Progress in Electromagnetics Research Symposium , Boston, Massachusetts, July 1989, p.308.

[21] R. Orta, R. Tascone, G. Tessitore, R. Zich; ``Frequency Selective Surfaces made of anisotropic material'' International Conference on Electromagnetics in Aerospace Applications , Torino, September 1989, pp.341-345.

[22] C. Cugiani, R. Orta, P. Savi, R. Tascone; ``A decomposition technique for the analysis of frequency selective sunfaces of complex shape'' International Conference on Electromagnetics in Aerospace Applications, Torino, September 1991, pp.59-62.

5.2.2 Multilayer planar FSS

5.2.2.1 Lund

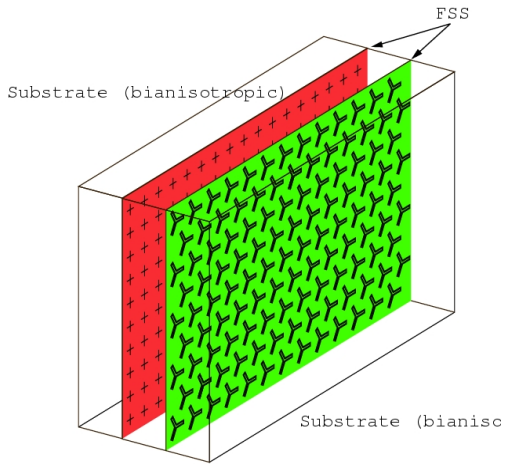

Figure 1 Geometry of a slab with two FSS's supported by arbitrary, general slabs.

A multilayered structure can be composed of thin FSS's separated by bianisotropic slabs, as in the figure above. To analyse this kind of structure, it is usually required to set up the currents on each thin FSS as free variables (a current sheet), and propagate the fields generated by these currents to the neighbouring sheets. This establishes a coupling between the different sheets, and the boundary conditions on the outmost sheets are used to determine the final distribution of the currents.

A general method for treating an arbitrary number of screens separated by arbitrary bianisotropic substrates is presented in [1-2]. The current sheets are represented in the spectral domain as a Fourier series, and the full tangential fields are propagated from one sheet to another using a propagator formalism, i.e., solving a system of ordinary differential equations for the unsplitted, total fields. This means the current sheets can be calculated directly from the outmost boundary conditions, and eliminates the need for cascading reflection and transmission matrices. The periodicity of the FSS's must be commensurate.

The propagator formalism allows the permittivity of the slabs to change continuously as well as discretely. This was used to analyse geometries such as pyramidal absorber-like structures used in anechoic chambers in [3].

References
[1] G. Kristensson, M. Åkerberg, and S. Poulsen. Scattering from a frequency selective surface supported by a bianisotropic substrate. Electromagnetic Waves PIER 35, Ed. J.A. Kong, pp. 83-114, EMW Publishing, Cambridge, Massachusetts, USA (2001).
[2] G. Kristensson, S. Poulsen, and S. Rikte. Propagators and scattering of electromagnetic waves in planar bianisotropic slabs – an application to frequency selective structures. Technical Report LUTEDX((TEAT-7099)/1-32/(2001), Lund Institute of Technology, Department of Electroscience, Electromagnetic Theory, Sweden, 2001. http://www.es.lth.se/teorel.
[3] O. Forslund, A. Karlsson, and S. Poulsen. Scattering from dielectric frequency selective structures. Radio Science, Vol 38, No. 3, 1-13, doi:10.1029/2000RS2566, 2003.

5.2.2.2 TNO

The integral equation formulation for both patch [1] and aperture based FSS, and the consequent derivation of the equivalent network representations (Fig.1), are described in section 5.2.1.2. The number of ports in these networks corresponds to the number of accessible modes necessary for an accurate modelling of the interaction between the different regions.

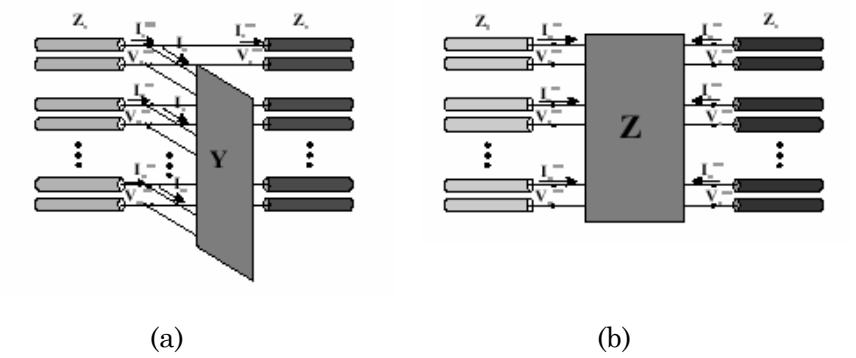

(a) (b)

Figure 1 (a) Multimode equivalent admittance network for the patch based FSS. (b) Multimode equivalent impedance network for the patch based FSS.

In this section, a particular emphasis is given to the MEN formulation [2], [3], which allows an efficient analysis of multilayer FSSs. The equivalent admittance or impedance representation of the single FSS is cascaded with those of the modal equivalent transmission lines representing the dielectric

layers separating the FSSs. In Fig.2, it is shown an example of multilayer structure with the corresponding network representation. This example shows the case of a patch based FSS. In this case, a shunt admittance representation is used. For the dual problem of an aperture based FSS, the dual representation in terms of a parallel impedance network must be used. The MEN approach is also perfectly suitable for the analysis of FSS panels integrated with array antennas. This particular aspect will be addressed in Section 5.5.1.

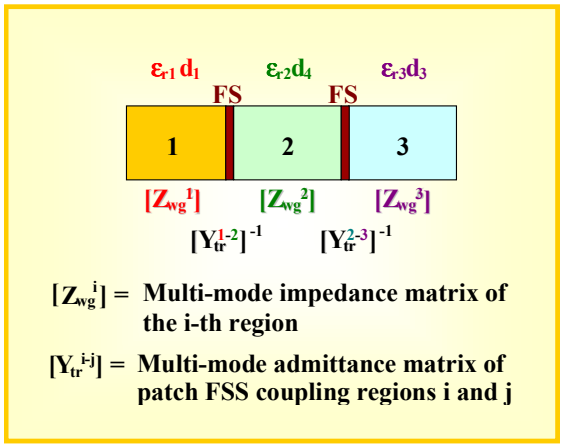

Figure 2 Schematic representation of a multilayer FSS problem (unit cell) and its pertinent multimode admittance/impedance representation.

The inherent modularity and flexibility of the approach is particularly useful in the design of complex multilayer structures. In fact, the preliminary design can be extremely simplified resorting to a single mode model. This can be derived starting from few full-wave simulations of the single FSS, where only the fundamental Floquet mode is taken as accessible mode. The equivalent admittance or impedance of the FSS, over the whole frequency band of interest, is then approximated with a proper Taylor series expansion. This first design is then successively refined with a full-wave multimode analysis of the overall structure. Even in this case, the tuning can be done in a very efficient way, thanks to the fact that only the part of the overall structure that is actually modified must be recomputed, while the model of the remaining unperturbed part, already available form previous simulations, can be simply reused.

Fig.3 shows an example of a double layer FSS of folded dipoles sandwiched between two matching dielectric layers [4]. The FSS core and the two matching layers have been realised gluing together several dielectric slabs

(Fig. 3a). A detail of the manufactured structure is shown in fig. 3b. Fig. 3c shows a comparison between experimental and theoretical results.

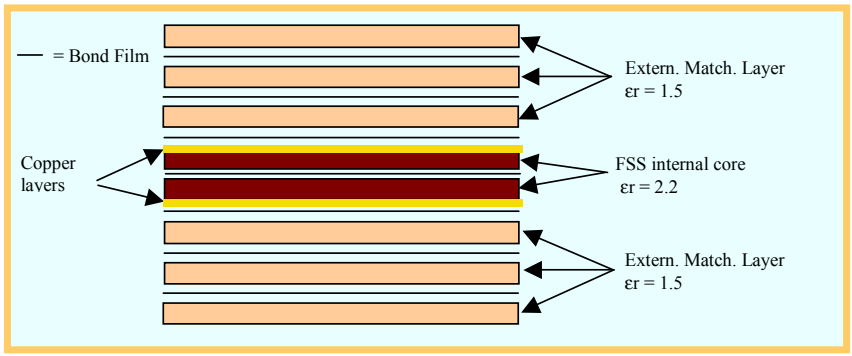

(a)

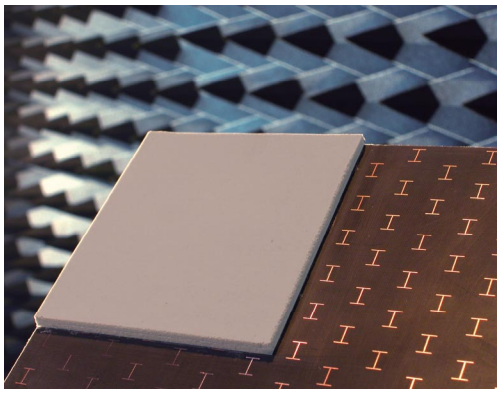

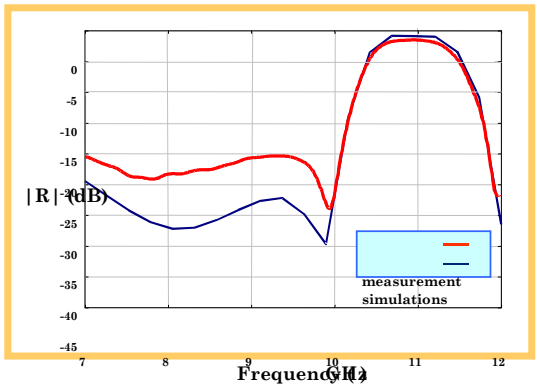

(b) (c)

Figure 3 Double layer FSS of folded dipoles sandwiched between two matching dielectric layers. The FSS core and the two matching layers have been realised gluing together several dielectric slabs (Fig. 3a). A detail of the manufactured structure is shown in Fig. 3b. Fig. 3c shows a comparison between experimental and theoretical results.

References

[1] S. Monni, G. Gerini, A. Neto, 'Equivalent Network Analysis of Phased Arrays Integrated with Patch Based FSS Structures", 2002 IEEE International Antennas and Propagation Symposium, June 2002, San Antonio, Texas.

[2] M.Guglielmi and A.A.Oliner, "Multimode network description of a planar periodic metal-strip grating at a dielectric interface - part i: Rigorous network formulations," IEEE Trans. Microwave Theory Tech., vol. 37, no. 3, pp. 534–540, 1989.
[3] G.Gerini and M.Guglielmi, "Full-wave cad of a rectangular waveguide filter with integrated coaxial excitation," IEEE Trans. Microwave Theory Tech., vol. 49, no. 5, pp. 986–989, 2001.
[4] S. Monni, G. Gerini, A. Neto, "Efficient Design of a Frequency Selective Surface for a Multi Functional Radar: Theory and Measurements", 34th European Microwave Conference 2004 Proceedings, Amsterdam, The Netherlands.

5.2.3 Planar FSS, thick structures (waveguide)

5.2.3.1 Lund

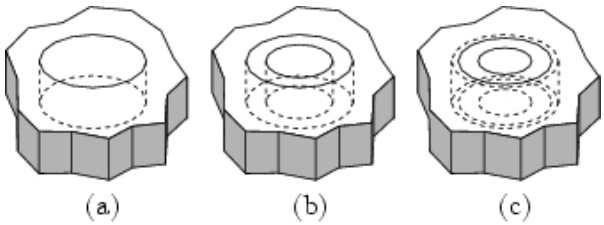

Figure 1 Some possible unit elements for thick-screen FSS applications

In a thick FSS, it is no longer possible to ignore the thickness of the metallic plate, which makes up the FSS. Referring to vacuum wavelengths, an FSS can be considered thin at least when it is less than λ/1000 thick [1]. A common design is when the metal is perforated by apertures, which is similar to an array of waveguides.

To solve for the scattering matrix from such an FSS, a mode matching technique is employed, where the Floquet modes of the surrounding medium are matched to the waveguide modes in the apertures. This results in a matrix equation, which can be solved when the boundary conditions for the incident and scattered fields are introduced. The waveguide modes are calculated by finite elements, and thus arbitrary cross sections can be analysed. The truncation of the Floquet series and the waveguide mode expansion is guided by the rule of thumb that the largest transverse wave number should be roughly equal in both series, which means both series must be equally accurate in describing the transverse variation of the fields. In [2], it is found that the bandwidth decreases when the thickness of the screen is increased, as shown in the figure below.

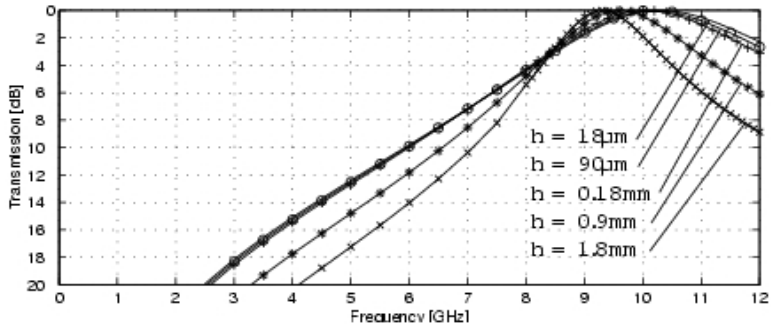

Figure 2 Transmission dependence of thickness for annular apertures [2].

References

[1] B. Widenberg. Thick Frequency Selective Structures. PhD Thesis, Dept. Electroscience, Lund Institute of Technology, Box 118, 221 00 Lund, Sweden. 2003.

[2] B. Widenberg, S. Poulsen, and A. Karlsson. Scattering from thick frequency selective screens. Journal of Electromagnetic Waves and Applications, Vol. 14, No. 9, pp. 1303-1328, 2000.

5.2.3.2 TNO

Thick FSSs consist normally of perforated metal screens of not negligible thickness. The corresponding apertures in the ground plane act as metallic waveguides of finite dimensions. Therefore a traditional field expansion in terms of waveguide modes is the most natural approach in the analysis of such structures.

The Multimode Equivalent Network technique, presented in section 3.3 and more detailed in 5.2.2.2, represents also in this case a very effective way of approaching the problem. In fact, already for the simplest configuration consisting of a single thick FSS, the structure can be seen as a cascade of three adjacent waveguides: the two phase-shift-wall waveguides representing the free space and the waveguide representing the aperture in the screen. The network representation is obtained resorting to a modal expansion of the fields in different regions (Floquet's modes for the open region and the waveguide modes for the metallic waveguide). By imposing the continuity of the electromagnetic field at the apertures, a set of integral equations (IE) can then be derived.

The unknown is represented by the electric field on the transition area (screen aperture). In the Method of Moment solution of the integral equations a crucial aspect in terms of accuracy and efficiency is the choice of the expanding functions for the unknown field.

The most flexible but not always the most efficient choice is given by sub-domain (piece-wise sinusoidal/linear) expanding functions. Their simplicity renders extremely efficient the evaluation of the coupling integrals in the kernel of the integral equations and also allows the analysis of any complex geometry. As drawbacks, it is normally required a rather large number of expanding functions to obtain an accurate field description and their large spectral content makes also the IE kernel slowly converging.

A less straightforward but sometimes very effective choice is given by full-domain modal representations. This last case becomes very attractive if used in combination with efficient techniques for the derivation of the eigenmodes of arbitrarily shaped waveguides (corresponding to the arbitrary geometry of the FSS apertures), like for example the BIRME [1] or BCMM (boundary contour mode matching) [2] methods. The same modes, in fact, are used also in the derivation of the equivalent network of the waveguide itself.

Furthermore, an accurate description of the field can be obtained with a relatively small number of functions and their small spectral contents make the IE kernel rapidly converging. On the other side, their evaluation is normally time consuming and their analytical complexity renders more difficult the evaluation of the coupling integrals with the Floquet's modes expansion of the external region. On the contrary, it is must be highlighted that since the expanding functions used at the interface coincide with the modes of the metallic waveguide, the evaluation of the coupling integrals with these modes is trivial thanks to the modal orthonormality property.

Basically the advantages and drawbacks in using these different expanding functions can be summarised as follows.

Eigenmodes expansions:
Advantages
- Smaller set of expanding functions
- Small spectral content: the kernel of the I.E. is more rapidly converging
- Aperture FSS: optimal choice for thick screens

Drawbacks
- Less flexible: eigenmodes derivation is time consuming
- Complex analytical form: onerous coupling coefficient evaluation

Subdomain expanding functions:
Advantages
- Very flexible: easy to use also for complex geometries
- Simple analytical form: fast coupling coefficient evaluation

Drawbacks

- Larger set of expanding functions
- Large spectral content: the kernel of the I.E. is slowly converging and therefore an acceleration technique is needed
- Aperture FSS: limitation to thin screens

In Fig.1 is shown a thick FSS (rectangular apertures) conformal to a circular cylindrical array of open-ended waveguides [3]. The reflection coefficient measured at the input port of the rectangular waveguide is shown in Fig.2 for different values of the FSS aperture dimensions.

In Fig.3 is shown an example of a cross-shaped aperture FSS, which has been modeled adopting full domain modal basis functions derived with the BCMM method. The relative reflection coefficient is shown in Fig.4.

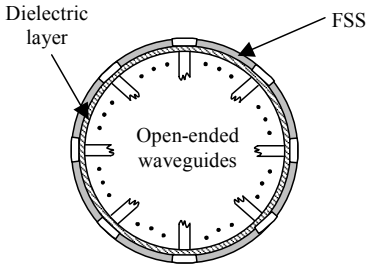

Figure 1 Thick FSS of rectangular shaped apertures conformal to a cylindrical array of open-ended waveguides.

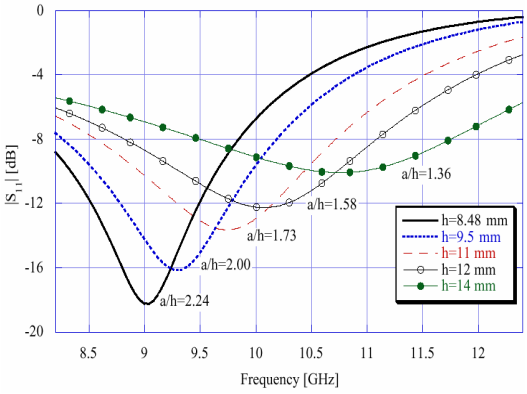

Figure 2 |S11| vs. frequency of the array shown in Fig. 1, for different values of the width 'a' of the aperture of the FSS (8.48 mm high, 2.5 mm thick). Cylinder radius: 0.75 m; Number of radiating elements in each row: 50.

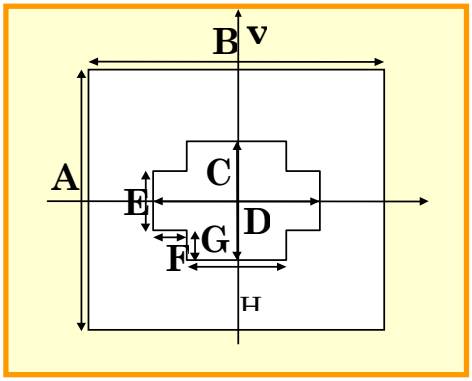

Figure 3 Example of cross-shaped aperture FSS. Drawing not in scale.(A=11.0mm, B=24.0mm, C=1.0mm, D=6.0mm, E=2.0mm, F=6.0mm, G=1.0mm, H=1.0mm)

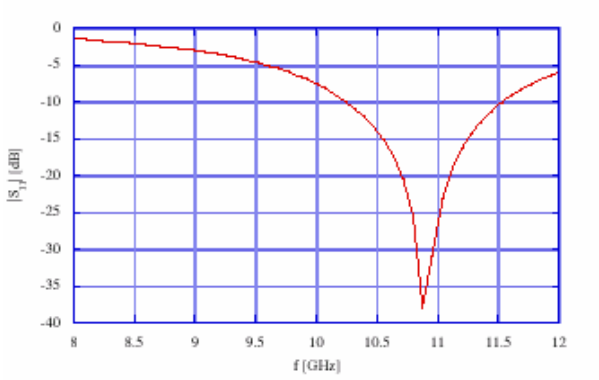

Figure 4 Reflection coefficient of the FSS shown in Fig.3.

References

[1] Bozzi, M.; Perregrini, L.; Weinzierl, J.; Winnewisser, C., "Efficient analysis of quasi-optical filters by a hybrid MoM/BI-RME method", IEEE Transactions on Antennas and Propagation, Vol.: 49 , Issue: 7 , July 200, pp. 1054 – 1064.

[2] F. Giese, J. M. Reiter, F. Arndt, "Modal analysis of arbitrarily shaped irises in waveguides by a hybrid contour-integral mode-matching method", 1995 IEEE International MTT Symposium, 16-20 May 1995, pp. 1359-1362.

[3] G. Gerini, L. Zappelli, "Cylindrical Conformal Arrays Loaded With Frequency Selective Screens", 31st European Microwave Conference 2001 Proceedings, 24-28 September 2001, London, U.K.

[4] G. Gerini, S. Monni, L. Zappelli, "Optimal choice of the E.M. expansion for arbitrary shaped aperture/patch FSSS in planar phased arrays", IEEE International Symposium on Phased Array Systems and Technology, 14-17 Oct. 2003, pp. 464 – 469.

5.3 Artificial and complex surfaces

5.3.1 Artificial PMC (Siena)

An artificial magnetic conductor (AMC) is an engineered electromagnetic material used to control surface currents in antenna and EMI applications [1],[2]. AMCs implement a lossless reactive surface whose surface impedance approximates an open circuit (high impedance) [3] over a specific bandwidth. As a periodic surface, they also exhibit a surface wave band gap [4]. AMC technology describes an electrically thin periodic surface, which has both

high-impedance and surface wave band gap properties, over similar but finite frequency bands. AMCs are typically realized as printed circuit periodic structures. An example is shown in Figure 1 whereby a capacitive frequency selective surface (FSS) is realized with conductive patches on the front side of the AMC, and conducting vias connect these patches to a conducting backplane (RF ground) on the back side of the AMC. Practical AMCs can be made as thin as $\lambda_0/50$ were lo is the free space wavelength at the AMC resonant frequency (defined by a 0° reflection phase).

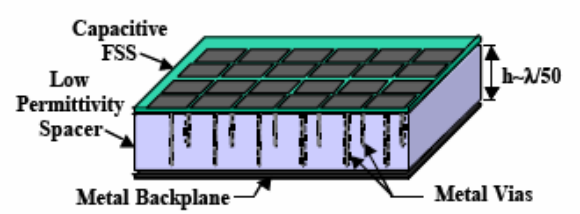

Figure 1. Anatomy of a typical AMC.

AMCs reflect plane waves in-phase at their resonant frequency, which is contrary to a metal surface that reflects plane waves out of phase. As a periodic structure, AMCs also suppresses bound surface waves over a range of frequencies known as a bandgap or a stopband. Thus, AMCs have application to limit the mutual coupling between adjacent antennas without absorbing power and degrading antenna efficiency [5],[6],[7].

References

[1] Y. Rahmat-Samii and H. Mosallaei, "Electromagnetic band-gap structures: Classification, characterization and applications," in Proc. Inst. Elect. Eng.-ICAP Symp., Apr. 2001, pp. 560–564.

[2] E. Yablonovitch, "Photonic crystals," J. Modern Opt., vol. 41, no. 2, pp. 173–194, 1994.

[3] D. Sievenpiper, L. Zhang, R. F. J. Broas, N. G. Alexopolus, and E. Yablonovitch, "High-impedance electromagnetic surfaces with a forbidden frequency band," IEEE Trans. Microwave Theory Tech., vol. 47, pp. 2059–2074, Nov. 1999.

[4] D. R. Jackson, J. T. Williams, A. K. Bhattacharyya, R. L. Smith, S. J. Buchheit, and S. A. Long, "Microstrip patch antenna designs that do not excite surface waves," IEEE Trans. Antennas Propagat., vol. 41, pp. 1026–1037, Aug. 1993.

[5] R. Gonzalo, P. Maagt, and M. Sorolla, "Enhanced patch-antenna performance by suppressing surface waves using photonic-bandgap substrates," IEEE Trans. Microwave Theory Tech., vol. 47, pp. 2131–2138, Nov. 1999.

[6] R. Coccioli, F. R. Yang, K. P. Ma, and T. Itoh, "Aperture-coupled patch antenna on UC-PBG substrate," IEEE Trans. Microwave Theory Tech., vol. 47, pp. 2123–2130, Nov. 1999.

[7] S. Sharma and L. Shafai, "Enhanced performance of an aperture-coupled rectangular microstrip antenna on a simplified unipolar compact photonic bandgap (UCPBG) structure," in Proc. IEEE AP-S Dig., vol. 2, July 2001, pp. 498–501.

5.3.2 1D EBG surfaces

5.3.2.1 Planar Strip Grating (TNO)

In Figure 1, the two possible ground plane configurations of a single dielectric slab loaded by a 1D periodic planar strip grating are shown with their relevant parameters. The procedure for the evaluation of the electric currents on the strip grating presented in [1] is based on an Electric Field Integral Equation (EFIE) approach adopting a spectral integration formulation. Both incident and scattered fields are expressed in the spectral domain, and the Poisson summation formula is adopted in order to perform an efficient evaluation of the series in the integral equation kernel. The method has been presented for the TM case, but it can be easily extended to the analysis of the TE case.

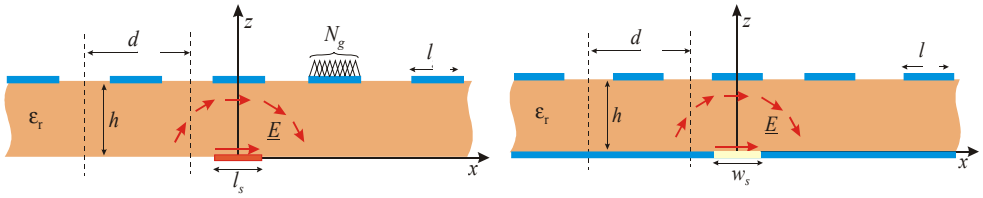

Figure 1 Planar Strip Grating a) Dielectric Slab. b) Grounded Dielectric Slab.

Once the EBG spectrum is obtained, a dispersion equation can be set up in order to analyze its polar singularities. These singularities define the modes that can propagate in the slab loaded by the strip grating. Figures 2a,b shows examples of the real and imaginary part of the dispersion equation solution. Varying two geometrical parameters, the grating periodicity and the strip dimension, the band-gap can be tuned.

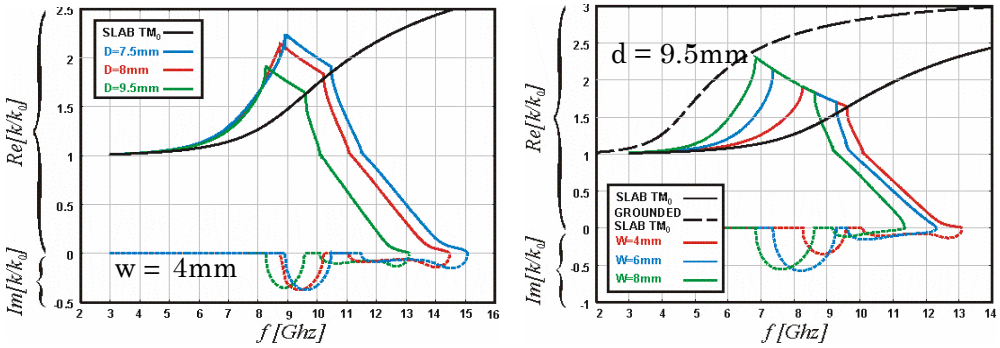

(a) (b)

Figure 2 Real and imaginary part of the TM_0 pole as function of the frequency for a dielectric slab (ε_r = 10, h =5mm). Dispersion diagrams for different periodicities (a); and for different strip widths (b).

References

[1] N. Llombart, A. Neto, G. Gerini, P. De Maagt, "Periodic structures excited by non periodic structures", Proceedings of the 27-th ESA/ESTEC Workshop on Innovative Periodic Antennas, pp. 601-607, March 2004.

5.3.2.2 Strips and corrugations (Chalmers)

Most common realizations of soft or hard surfaces (Chapter 2.2) are one-dimensional periodic structures that have band-gap or band-pass characteristic, i.e. usually they are realized as a corrugated structure or as a strip-loaded structure (Fig. 1). The rigorous analysis of the corrugated or the strip-loaded open surface can be performed by expanding the fields into Floquet modes or by expanding the currents into the basis functions (Chapter 3.1). In the latter approach the amplitudes of the Floquet modes are implicitly determined by calculating the unknown current [1]. The Floquet mode approach can be time-consuming if the source such as e.g. a dipole excites a spectrum of plane waves. Other rigorous approach is to take into account the finiteness of the structure and to use e.g. FEM or FDTD. Then, the computation time becomes large, but it will not depend on the type of source.

The analysis of the corrugated and strip-loaded surfaces can be simplified by using the asymptotic boundary conditions (Chapter 3.4 and [1]-[3]). In the model for corrugated surface the corrugated region is modelled by considering a parallel plate medium with incremental spacing between the parallel plates and with a metal shunt corresponding to the bottom of the corrugations. The field inside each incremental corrugation is not varying in the direction perpendicular to the parallel plate walls. However, the field in the

Eliminato: , such as e.g. a dipole

Eliminato: .

Eliminato: This approach is not so sensitive to

Eliminato: the tangential electric and magnetic fields are matched at the corrugated interface,

Eliminato: i.e.

Eliminato: ions

Eliminato: are

Eliminato: waveguide problem

Eliminato: inside the corrugations

total corrugated medium (encountering several incremental parallel plates) is matched to the outer field that generally varies in the direction perpendicular to the corrugations, and this will cause a discrete variation of the field from corrugation to corrugation in the corrugated medium. Similarly, the layer with metal strip grid can be modelled by setting the tangential parallel E-field component to zero over the whole grid, and by setting both the tangential perpendicular E-field and parallel H-field components continuous across the grid.

Eliminato: corresponding to
Eliminato: of the field
Eliminato: inner
Eliminato: region

In order to be able to analyse radiation properties of general sources above multilayer structures, the above-mentioned asymptotic boundary conditions have been implemented in the G1DMULT algorithm that calculates spectral-domain Green's functions of multilayer structures (Chapter 3.6 and [4]). More accurate boundary conditions for finite periods of strip-loaded and corrugated surfaces can be derived by a homogenization process [5], i.e. by averaging the electromagnetic fields of the fundamental Floquet mode.

Eliminato: analysis model
Eliminato: s

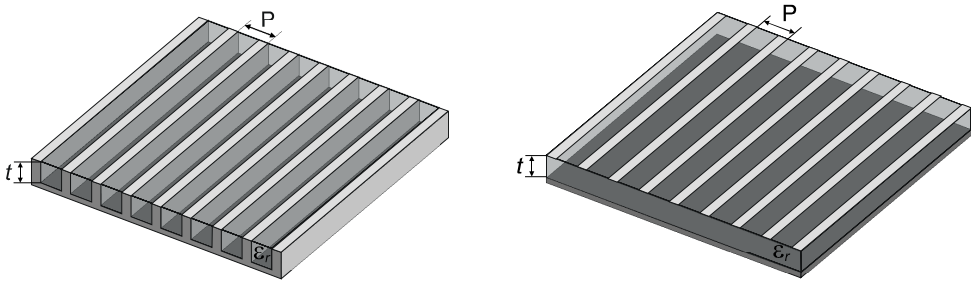

Figure 1 (a) corrugated surface, (b) strip-loaded surface

References

[1] Z. Sipus, S. Raffaelli, P.-S. Kildal, "Periodic strips on planar and circular cylindrical substrates: Exact and asymptotic analysis," *Microwave and Optical Technology Letters*, Vol. 7, No. 3, pp. 173-178, Feb. 1998.

[2] P.-S. Kildal, A. Kishk, Z.Sipus, "Asymptotic boundary conditions for strip-loaded and corrugated surfaces," *Microwave and Optical Technology Letters*, Vol. 14, pp. 99-101, Feb. 1997.

[3] Z. Sipus, H. Merkel, P.-S. Kildal, "Green's functions for planar soft and hard surfaces derived by asymptotic boundary conditions," *IEE Proceedings - Microwaves, Antennas and Propagation*, Vol. 144, pp. 321-328, Oct. 1997.

[4] Z. Sipus, P.-S. Kildal, R. Leijon, and M. Johansson, "An algorithm for calculating Green's functions for planar, circular cylindrical and spherical multilayer substrates," *Applied Computational Electromagnetics Society Journal,* Vol. 13, No. 3., pp. 243-254, Nov. 1998.

[5] [F. H. Bellamine, E. F. Kuester, "Guided waves along a metal grating on the surface of a grounded dielectric slab," *IEEE Trans. Microwave Theory Tech.*, Vol. 42, pp. 1190-1197, July 1994.

5.3.3 2D EBG surfaces

5.3.3.1 Siena

Recently, a lot of research efforts have been devoted to periodic planar surfaces used to generate new equivalent boundary conditions. These studies have stimulated various engineering applications in the field of microwave and antennas. In some applications, these surfaces constitute the modern version of transversely corrugated structures, often used to improve the performance of feed-horns. In the early nineties, the so-called "soft" and "hard" surfaces (terminology derived from acoustics) were introduced and their relationships with the classical corrugated structures were discussed [1]. The soft surface behaves like a perfectly electric conductor (PEC) for TE polarization and as a perfectly magnetic conductor (PMC) for the TM polarization; vice-versa for the hard surface. Various solutions were presented in the past for devising such surface properties, which are based on printed strips short-circuited to a ground plane. This paper present new solutions for hard and soft surfaces realized by printing a "gangbuster type" frequency selective surface (FSS) [2] on a grounded slab. Depending on the direction of wave propagation and on the nature – capacitive or inductive – of the printed FSS, these structures exhibit alternatively hard or soft properties. It is well known that perfectly magnetic and relevant bandgap properties can be realized by printing FSS on a grounded dielectric slab. The gangbuster FSS surface was introduced by B. Munk as anisotropic FSS with outstanding performance [2]. Nader Engheta suggested the use of this type of gangbuster dipoles for the realization of a metamaterial medium [3] as well as for obtaining equivalent magnetic conducting effects for certain polarizations [4]. The main purpose here is to show that the gangbuster FSS leads to artificial soft and hard properties depending on the propagation direction relative to the orientation of the slots or dipoles on the printed surface. To this end, consider first the structure in Fig. 1a, constituted by a dipole FSS printed on a grounded slab. Assume first that the direction of propagation is along the dipoles. The interaction with the structure is very different for the two polarizations.

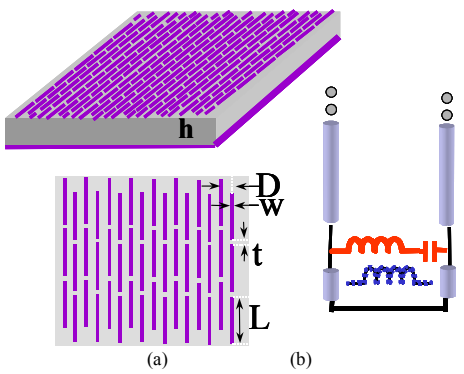

Fig. 1 Gangbuster dipole surface printed on a ground plane. (a) geometry: L=10mm, W=0,25 mm t=0,25 mm, D=5,127mm, h=1mm, epsr =4. (b) equivalent z-transmission line for the polarisation which interact with the FSS.

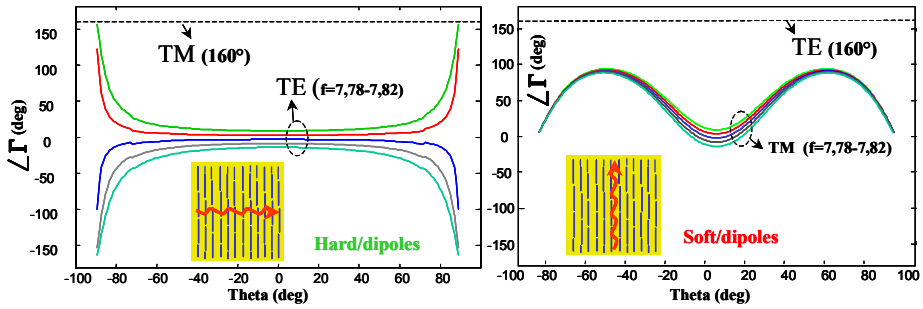

Fig 2 Phase of the reflection coefficient versus the incidence angle. (a) hard and (b) soft cases.

The TM wave possesses E-field along the dipoles and therefore strongly interacts with the FSS. The behaviour of the system is described by the simple equivalent circuit in Fig. 1b. There, the LC series circuit represents the global homogenized behaviour of the FSS in a z-transmission line with TM characteristic impedance. The loading of the ground plane represents a parallel inductance to the series circuits, which has a parallel resonant effect with the dipole capacitance, thus producing the PMC behaviour. For TE polarization, the dipoles (very thin) are orthogonal to the electric field, and do not interact with the FSS. Consequently, the behaviour is the same as that of a bare grounded slab with very small thickness, which is therefore only slightly different from a PEC. In summary, for propagation along the dipoles, and in a certain bandwidth, the surface exhibits high-impedance for TM polarization and low impedance for TE polarization, thus being artificially soft.

On the contrary, when the direction of propagation is orthogonal to the dipoles, the roles of TE and TM polarization are interchanged, because the TE wave now interacts with the dipoles; thus, realizing a hard surfaces. For this

case the equivalent z-transmission line is essentially that in Fig. 1b, but with TE characteristic impedances.

Fig. 2 presents the phase of the reflection coefficients versus the incidence angle θ with respect to the normal for the two directions of propagations and the two polarizations. The results have been obtained by using a full-wave method of moment analysis. For the parameters set in Fig. 1, the operative frequency is found to be 7,8 GHz. For the hard case (Fig. 2a, orthogonal to the dipoles) the phase is quite stable around 160° for TM case and around 0° for TE case, except near grazing angle of incidence where the frequency bandwidth is quite small. For the soft case (Fig. 2b), the phase of the reflection coefficient oscillates for TM case around 0° (with oscillation range within 90°) and remains stable at 160° for the TE case.

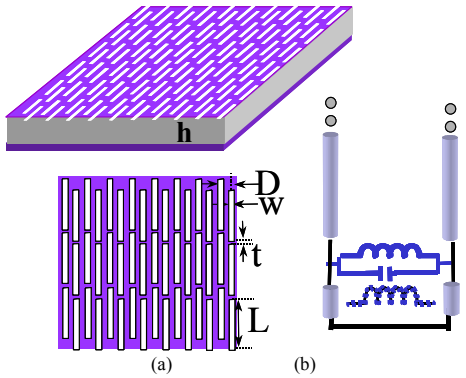

Fig. 3 Gangbuster slot surface printed on a ground plane. (a) geometry: L=10mm, W=0,25 mm t=0,25 mm, D=5,127mm, h=1mm, epsr =4. (b) equivalent z-transmission line for those polarizations which interact with the FSS

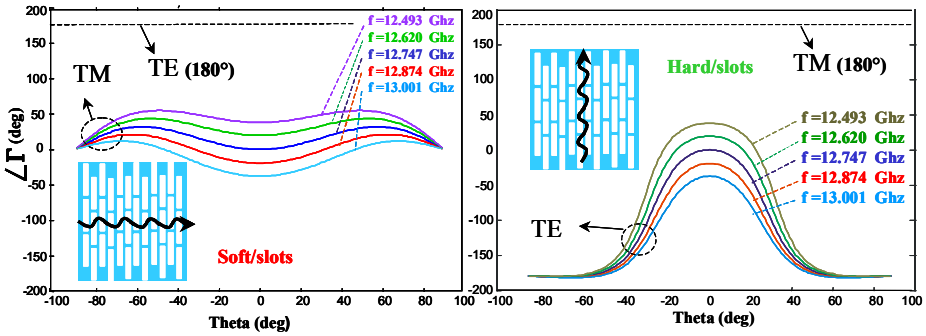

Fig 4. Phase variation with the incidence angle associated to the FSS-slot structures. (a) soft (b) hard

When the surface is realized with a slot-type gangbuster FSS (Fig. 3a), the behaviour of the structure is complementary. The surface is hard or soft dependent on whether the propagation direction is along the slot or orthogonal

to the slot, respectively. The equivalent z-transmission line for the case in which the wave interact with the slot is shown in Fig. 3b, and consists on a parallel LC circuit with an inductance loading due to the ground plane. The fact that the FSS circuit is in parallel in place of series (compare with Fig. 1b) implies an overall resonant frequency which is higher with respect to that for the dipole structure, being the thickness equal and FSS dimensions complementary equal.

For direction of propagation along the slot and TE polarization, the electric field is orthogonal to the slot, so that the wave interacts with the FSS and the structure realizes a high impedance surface. Since for TM polarization, the wave feels essentially a PEC ground plane, the surface is almost hard. On the contrary, when the direction of propagation is orthogonal to the slots, the roles of TE and TM polarization are interchanged, because the TM wave now interacts with the slot; thus, realizing a soft surfaces.

Fig. 4 presents the phase of the reflection coefficients versus the incidence angle θ with respect to the normal for the two directions of propagation and the two polarizations. For the parameters set in Fig. 3a, the operative frequency is found to be 12,7 GHz. The phase for the artificially soft case (Fig. 4a, orthogonal to the dipoles) is quite stable around 180° for TE case and oscillates around 0° for TM case, with a small dispersion with the frequency variation. For the hard case (Fig. 4b, parallel to the dipoles), the phase of the reflection coefficient remains stable at 180° for the TE case and is around 0° for TE case only for a limited range of incidence angle. In conclusion, the hard behaviour is ensured only for incidence angle near broadside and for a restricted range of frequency.

The EBG properties of this structure could be obtained by using the analytical representation of the Bangbuster structure as that shown in Sec. 5.2.2.1 To this end the resonant equation is formulated on the basis of the equivalent network in Sec 5.2.2.1 (Fig.1)

Through the admittance matrix formalism, the equivalent network is reconstructed as shown in Fig.5.

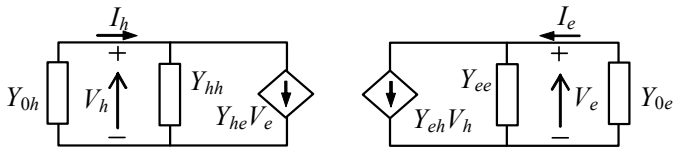

Fig. 5 Equivalent network for the resonance equation.

The equivalent current $\bar{I} = [I_h \quad I_e]$, associated to the transverse magnetic field, and voltage $\bar{V} = [V_h \quad V_e]$, associated to the transverse electric field, are related by the characteristic admittance of the free-space, that is $\bar{I} = -\bar{\bar{Y}}_0 \bar{V}$, with

$$\bar{\bar{Y}}_0 = \begin{bmatrix} Y_{0h} & 0 \\ 0 & Y_{0e} \end{bmatrix} \tag{4}$$

At the same time, current and voltage are related by the $\bar{I} = \bar{\bar{Y}}\bar{V}$ where

$$\bar{\bar{Y}} = \begin{bmatrix} Y_{hh}^{FSS} & Y_{eh}^{FSS} \\ Y_{he}^{FSS} & Y_{ee}^{FSS} \end{bmatrix} + \begin{bmatrix} Y_h^{cc} & 0 \\ 0 & Y_e^{cc} \end{bmatrix} \tag{5}$$

where $Y_{e,h}^{cc} = -jY_{0e,h}^{d} ctg(k_{zd} d)$. This leads to the relationship $\bar{I} = \bar{\bar{Y}}\bar{V}$. This equation admits non-trivial solutions when the determinant of the matrix is zero, leading to the following resonance equation

$$\det(\bar{\bar{Y}} + \bar{\bar{Y}}_0) = 0 \tag{6}$$

When searching for surface wave solutions, we assume that the expression of the FSS admittance is analytically continued in the non-visible region. This means that the pole and zero dispersion diagram is extrapolated for values of k_ρ greater that k until the limit of the Brillouin zone.

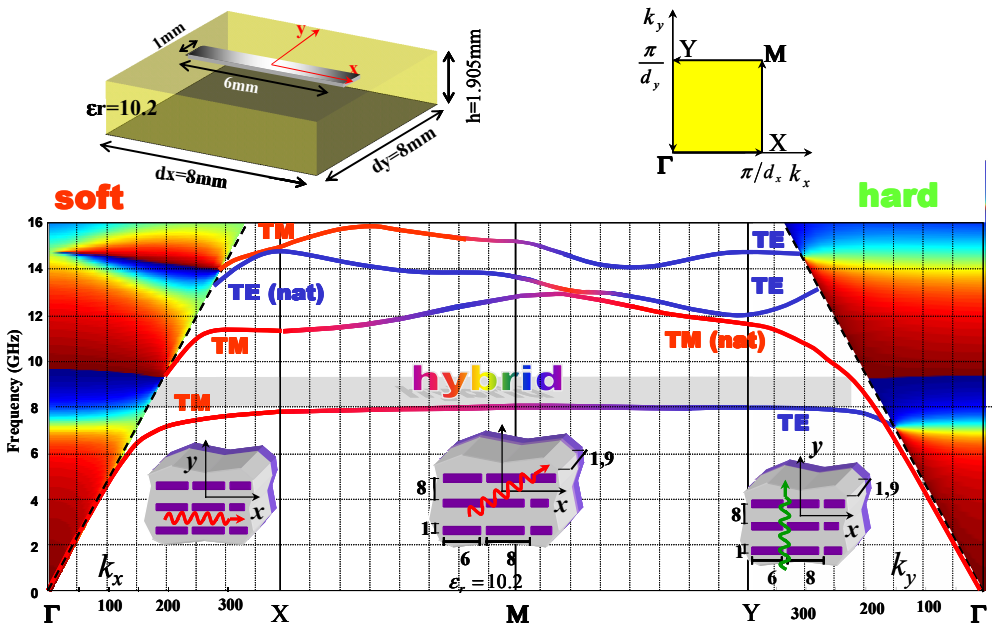

Fig. 6 Dispersion curve for surface wave mode for periodic printed dipoles. The basic cell is shown in the inset. The coloured region up to the light line represents the phase of the reflection coefficient for plane wave incidence.

The dispersion diagram along the square path of the k_x,k_y plane is shown in Fig.6, which shows the dispersion curve of both TE and TM mode. The TE and TM modes are supported only when the direction of propagation is parallel (soft case) or orthogonal (hard case) to the dipoles. In the intermediate region of wave-direction the modes are hybrid. The dispersion curves exhibit a partial, band gap for a large portion of the diagram.

To summarize, we have introduced two different types of structures, which behaves like soft and hard surfaces in a certain frequency bandwidth. The structures are realized by gangbuster FSS printed on grounded dielectric substrate without any vias to the ground, therefore providing a particularly easy manufacturing. Preliminary results have been presented to show the reflection properties of the structures. These results have confirmed the dipole-type gangbuster surface may exhibit both soft and hard surface characteristics, but with some uncertainty about the hard case near grazing aspects (fast frequency variations). The slot-type gangbuster surface behaves well for the soft case for all angles of incidence, but it does only represent a hard surface near normal incidence. Further investigations are presently concerned with the bandgap analysis and waveguide modal propagations. It is interesting to note that longitudinal dipoles generate the soft surface and transverse dipoles the hard surface, whereas the slots behave similar to corrugations in this sense, i.e. longitudinal slots (and corrugations) provide the hard surface and transverse ones the soft surface.

References

[1] Kildal, P-S., "Artificially soft and hard surfaces in electromagnetics", IEEE Transactions on Antennas and Propagation, vol. 38, 10, pp. 1537-1544, Oct. 1, 1990.

[2] B. A. Munk , Frequency Selective Surfaces:Theory and Design , Wiley, NY, 2000

[3] C.A. Moses, N. Engheta, “Electromagnetic wave propagation in the wire medium: a complex medium with long wire intrusion”, Wave Motion, Vol. 34, pp.301-317

[4] N. Engheta, URSI meeting, Boston, Massachusetts, July 8-13 2001, page 389.

5.3.3.2 Chalmers

Like in the case of 1D EBG surfaces (Section 5.3.2) the analysis of different EBG surfaces can be simplified using approximate boundary conditions (Chapter 3.4). **The grounded bed-of–nails** (Fig. 1a) can be considered as a uniaxial anisotropic media with permittivity and permeability tensors [1]. Due to anisotropy there is a fundamental difference in propagation of TE_z and TM_z waves. The TE_z waves do in principal not see the nails since the electric field is perpendicular to them. Therefore, TE_z waves propagate like

Eliminato: the

Eliminato: do

Eliminato: nails

in the ordinary slab with a little bit modified relative permittivity and permeability. For TM_z waves the bed-of-nails acts as a medium with negative effective permittivity. The separation into TE_z-TM_z modes is obtained in the spectral domain.

In principle, **the mushroom structure** consist of a grounded bed-of-nails and of a periodic patch array where each patch is attached on the top of one nail (Fig. 1.b). The array of patches forms a capacitive screen and therefore it can be simply analysed using grid impedance approach [2].

In order to be able to analyse radiation properties of general sources above different EBG surfaces, the analysis model has been implemented in the G1DMULT algorithm that calculates spectral-domain Green's functions of multilayer structures (Chapter 3.6). In this way mutual and self coupling of dipole antennas above different types of EBG structures have been analysed and compared with coupling above ideal PEC, PMC, soft and hard surfaces [3].

Eliminato: s

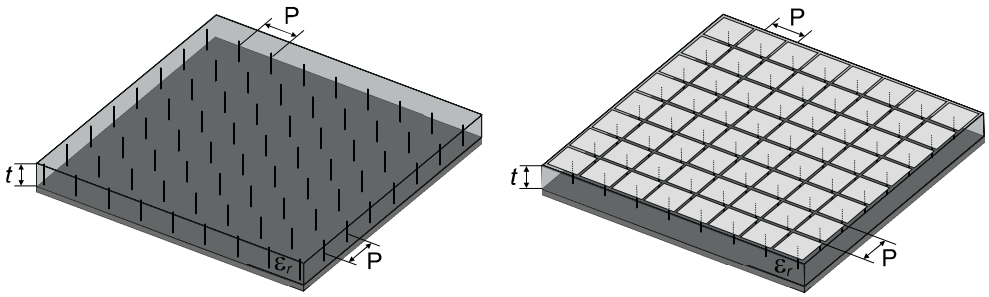

(a) (b)

Figure 1 (a) grounded bed-of nails structure, (b) mushroom structure

References

[1] R.J. King, D.V. Thiel, and K.S. Park, "The synthesis of surface reactance using an artificial dielectric," *IEEE Trans. Antennas and Propagat.*, vol. 31, pp. 471-476, May 1983.

[2] S.A. Tretyakov and C.R. Simovski, "Dynamic model of artificial reactive impedance surfaces," *J. Electromagn. Waves Applic.*, Vol. 17, pp. 131-145, 2003.

[3] Z. Sipus, P.-S. Kildal, "Full wave analysis of mutual coupling between dipoles over different EBG surfaces: AMC, soft and hard surfaces," *Proceedings of IEEE/URSI International Symposium on Antennas and Propagation*, Monterey, USA, 2004.

5.4 Special surfaces

5.4.1 Carbon Fibre Reinforced Plastic

5.4.1.1 Lund

Carbon Fibre Reinforced Plastic, CFRP, is an attractive alternative to metals as a structural material. Even though it generally has lower stiffness, its low density (almost half of aluminium, a fifth of steel) makes it an ideal material for space applications. CFRP is a composite material, essentially made up of conductive carbon fibres in a plastic matrix.

The physical properties of the material depend fundamentally on the amount and direction of fibres used, where the most important property for electromagnetics is the conductivity. When all the fibres are aligned in one direction, the conductivity is strongly anisotropic [1]. The conductivity along the fibres is simply the mean value of the respective conductivities, weighted by their respective volume fraction. The transverse conductivity depends on microscopic structure, and can be found by solving a two-dimensional version of the local problem defined in Chapter 3 Analysis methods, Homogenisation. For small volume fractions of the fibres the transverse conductivity varies linearly with the volume fraction, but when sufficiently many fibres are present, a percolation phenomenon occurs and the conductivity increases dramatically at a certain threshold. For fibres with identical radii, the critical volume ratio is about 67%, somewhat higher for fibres with a size distribution.

When homogenising conductive fibres, it is important to be very careful with the assumption about perfect conductivity, since the limits of vanishing microscopic scale (homogenisation) and infinite conductivity do not commute [2]. Starting with PEC fibres, the homogenised permittivity is smaller by a factor (1-*f*) compared to taking the PEC limit after homogenisation, where *f* is the volume fraction of the fibres. In [2] it is also shown that for small volume fractions, the permittivity along PEC fibres can be modelled as a plasma, i.e., $\hat{I} \approx 1 - (\omega_p / \omega)^2$ where ω_p is the plasma frequency.

References

[1] S. Torquato. Random Heterogeneous Materials: Microstructure and Macroscopic Properties. Springer-Verlag, New York, Inc, 2002.

[2] D. Felbacq and G. Bouchitté. Homogenization of a set of parallel fibres. Waves in Random Media, Vol. 7, pp. 245-256, 1997.

5.4.1.2 POLITO

Reflector antennas made of carbon-fibre-reinforced plastics (CFRP) are a source of intermodulation products (IMP), together with higher harmonics, because of the relatively nigh level or intrinsic non-linearity shown by graphite. This may cause serious problems in systems where an IMP or two transmitted frequencies is near to a received frequency, since the IMP power backscattered into the feed may have about the same level as the signal to be received.

The linear behaviour has been investigated, mainly experimentally, by several authors [1-3], while non linear effects have been considered only from a qualitative point of view among other sources of inter-modulation (joints, weldings, etc.) common also to metallic reflectors [4, 5]. Bulk non-linear effects in CFRP panels have received attention from a theoretical point of view [6, 7].

It is assumed that only a small fraction or the incident power is converted into higher harmonics, so that the non-linearity can be studied in a perturbative manner: therefore, if we assume that the field-current characteristics of the graphite is cubic, only third order harmonics and IMPs will be generated, according to the scheme of fig. 1.

Carbon-fibre panels used in reflector antenna technology are usually composed or a small number (e.g. 4) of plies made of unidirectional fibres immersed in an epoxy resin matrix whose relative dielectric constant is between 3 and 4. Single fibres (diameter of about 8-10μm) are grouped in yarns having a diameter of about 0.1 mm, which corresponds to the thickness or the ply. In fig.2 we show an example of this structure, which can be modelled, from an electromagnetic point of view, as a layered biaxial anisotropic (lossy and non-linear) material, whose permittivity matrix is given by:

$$\underline{\underline{\varepsilon}} = \varepsilon_0 \begin{vmatrix} \varepsilon_r + \sigma_{X'} / j\omega\varepsilon_0 & 0 & 0 \\ 0 & \varepsilon_r + \sigma_{Y'} / j\omega\varepsilon_0 & 0 \\ 0 & 0 & \varepsilon_r + \sigma_{Z'} / j\omega\varepsilon_0 \end{vmatrix} \qquad (1)$$

where the conductivity along x' (parallel to the fibres) is much greater than that along y' and z. Typical values for the former are 10-100 kS/m, while those suggested in the literature for the latter are: σ_{y1} = 100 S/m, σ_y = 40 S/m.

The linear model (originally proposed [3] for frequencies up to 1 GHz) has been validated also at higher frequencies by comparing the reflectivity for normal incidence of a panel 0/90/9010 with experimental data [2]. Good agreement has been found, as shown in fig.3.

The non-linear behaviour can be obtained starting from the following relationship between field and current density (both parallel to the fibres):

$$J_{x'} = \sigma_{x'} E_{x'} - \rho_1 \sigma_{x'}^4 E_{x'}^3 \tag{2}$$

Considering two incident plane waves at different frequencies, and computing the total field parallel to x', the current density can be obtained, with some manipulation, from (2). The backscattered field at the interface is then computed by using the Green's function of an anisotropic stratified structure [8] and by integrating the contributions from all sections of the panel. It can be shown that a multilinear relationship exists between the transverse components of the incident (i) and scattered (s) fields; on introducing a proper contracted-index backscattering tensor, this relationship can be written in the form (where $W_3=2W_1-W_2$):

$$\begin{vmatrix} E_x(\omega_3) \\ E_y(\omega_3) \end{vmatrix}^s = \begin{vmatrix} B_1 & B_2 & B_3 & B_4 & B_5 & B_6 \\ B_7 & B_8 & B_9 & B_{10} & B_{11} & B_{12} \end{vmatrix} \begin{vmatrix} E_x(\omega_1)E_x(\omega_1)E_y^*(\omega_2) \\ E_x(\omega_1)E_y(\omega_1)E_x^*(\omega_2) \\ E_y(\omega_1)E_y(\omega_2)E_x^*(\omega_2) \\ E_x(\omega_1)E_x(\omega_2)E_y^*(\omega_2) \\ E_x(\omega_1)E_y(\omega_2)E_y^*(\omega_2) \\ E_y(\omega_1)E_y(\omega_2)E_y^*(\omega_2) \end{vmatrix}^i \tag{3}$$

Tensor B is a function of several parameters: angle of incidence, frequency, physical characteristics of the panel. Fig. 4 shows the behaviour of B_1 and B_{12}, for normal incidence, on a structure 0/90/90/0, ply thickness 60 microns, W1≈W2≈W3. In this particular case, all other coefficients are zero. B_{12}, the coefficient for incidence perpendicular to the fibres of the first layer, is clearly dominant. This can be physically explained by noting that for parallel incidence the wave does not penetrate into the layers, giving therefore low intermodulation together with low losses. For oblique incidence, the other coefficients are non-zero but generally lower than the dominant ones, and will not be shown here for sake of brevity. Other structures (e.g. 0/±60) have a more complex behaviour: B_{12} is still dominant but all other terms are non-zero even for normal incidence: in particular B6 (parallel component backscattered from the perpendicular components of the incident fields) has some importance.

For an incidence angle not too for from the normal, the IMP level strongly depends on the frequencies involved, in particular when the beat frequency is low. In fig. 5 we show the amplitude of element B_{12} of the backscattering matrix, as a function of f_1 and f_2: it can be noted that it increases with f_3 and has a minimum when $f_3=0$. An approximate formula, empirically found, gives the dependence on the frequencies as:

$$|B_{12}| = C_1 f_1 + C_2 f_3^2 \tag{4}$$

where C_1 and C_2 are suitable constants. If $f_3 \approx 0$ (i.e. $2f_1 \approx f_2$) the first term dominates; when $|f_3|$ increases, the amplitude of B_{12} increases with the square of the frequency.

The dependence on the dielectric constant is neglig1ble. Computations made for values ranging from 3 to 4 have not shown significant changes. Finally, increasing the thickness of the ply leads to a slightly higher level of IMP, as shown in fig.6 for both configurations 0/90/90/0 and 0/±60.

For normal incidence, the backscattered power density can be expressed in logarithmic units as:

$$S_3 = 20 \log |B_i| Z_0 + S_2 + 2S_1 \tag{5}$$

both for parallel (i=l) and perpendicular (i=12) incidence, while the direction of propagation of the IMP backscattered wave can be derived from

$$\underline{k}_{t3} = 2\underline{k}_{t1} - \underline{k}_{t2} \tag{6}$$

As a consequence, the IMP wave has the same direction as the reflected waves only if f_1 and f_2 have the same incidence direction.

The IMP power backscattered from a reflector antenna into the feed can be computed with standard techniques for different configurations. Assuming, for sake of simplicity, $P_1=P_2$ at about the same frequency (so that feed gain and space attenuation are nearly frequency independent), and indicating with B the factor corresponding to the first term of (5), we get, for a center fed paraboloid:

$$P_r = \frac{\lambda^2 G^4}{(4\pi)^4 F^6} B P^3 \tag{7}$$

where F is the focal distance and G is the feed gain. For a hyperboloid we obtain:

$$P_r = \frac{\lambda^2 G^4 \delta^2}{(4\pi)^4 D^6} B P^3 \tag{8}$$

where D=a+c is the distance between feed and vertex, and δ=(e-l)/2e.

Similar, though more complicated expressions, can be derived for the offset case and/or for multi-feed configuration.

References
[1] K. M. Keen, El. Lett., Vol. 11, no. l1, p.234, 1975
[2] L. Heichele, AGARD Conf. Proc. no. 283, Paper 18, 1980
[3] D. C. Brewster, AGARD Conf. Proc. no. 283, Paper 5, June 1980
[4] J. C. Lee, ICC 80, Part II, Seattle, paper 25.6
[5] R. C. Chapman et al. ,AIAA/CASI 6th Camm. Sat. Sys. Conf. ,Montreal, 1976
[6] G. Ghione et al., Nat. Radio Sci. Mtg. Digest, Baston, 1984, p.167
[7] G. Ghione et al., Atti V Riun. Naz. Elettr. Appl., St.Vincent, 1984, p.363
[8] V. Daniele and R. Zich, Radio Sci., Vol. 8, Jan. 1973, pp.63-70

5.4.2 Honeycomb structure (Lund)

The honeycomb structure is a cellular, lightweight structure. It is usually made up of cylindrical, hexagonal unit cells, which provides mechanical strength using a small amount of material. When the cell material is highly conducting, the structure can be used as a reflector surface, but usually the material has low permittivity with small losses, and is intended as a distance material having small effective permittivity.

Provided the cell size is much smaller than the wavelength, the homogenisation technique described in Chapter 2 can be used. The complex permittivity for electric fields along the cylinder axis is exactly the mean value of the complex permittivities of the cell walls and the core, weighted by their respective volume fractions. The transverse permittivity is isotropic, and in the limit of thin walls it varies linearly with the thickness of the walls. If the walls are highly conducting compared to the core, we have the exact result $\sigma_{eff} / \sigma = f / 2$, where σ is the conductivity of the walls, and f is the volume fraction of the wall material [1].

References
[1] S. Torquato. Random Heterogeneous Materials: Microstructure and Macroscopic Properties. Springer-Verlag, New York, Inc, 2002.

5.4.3 Tricot meshes (TICRA)

The mesh grid consists of two orthogonal sets of wires as illustrated in the figure below. The spacing between the wires is s_x and s_y in the x_d- and y_d-direction, respectively. The wire diameter is d_0 and the two sets of wires are in electrical contact at all the intersection points.

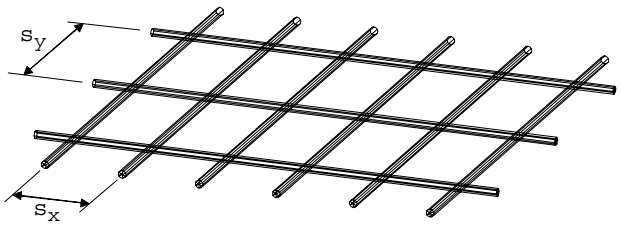

The reflection and transmission coefficients for the mesh grid are based on Astrakhan (1968). For incidence in one of the principal planes, for example $f_i = 0$, the reflection coefficients are practically identical to those for the wire grid, i.e. R_{qq} is the same as for the wire grid with spacing s_x and similarly for R_{ff} in the orthogonal plane.

One of the main purposes of the mesh grid is to model the electrical properties of the tricot mesh of unfurlable antennas. A real mesh is shown in the figure below. Although it is obvious that the pattern of the tricot mesh is far from being rectangular, it has been found (Pontoppidan, 1981) that it is possible to define an equivalent rectangular grid which, for any angle of incidence and polarisation, gives the same reflected and transmitted field as the real mesh.

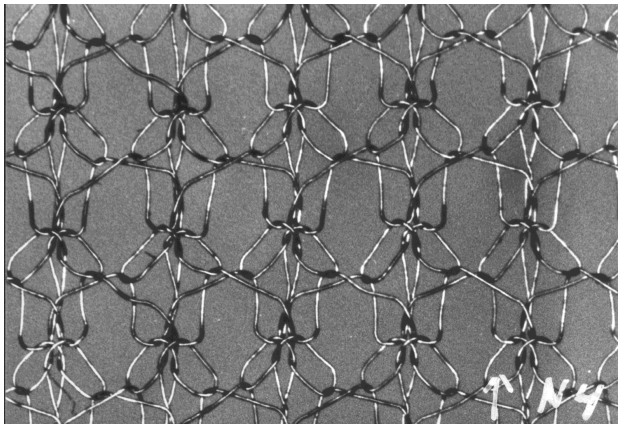

References

[1] Astrakhan, H.I. (1968), "Reflecting and screening properties of plane wire grids", Radio Engineering, Vol. 23, No. 1, pp. 76-83.

[2] Pontoppidan, K. (1981), "Study of offset unfurlable antennas - electrical design aspects", TICRA Report S-144-01.

5.5 Advanced topics

5.5.1 Combinations of FSS and arrays (TNO)

As already anticipated in section 5.2.2.2, the Multimode Equivalent Network Approach is very suited for the analysis of multilayer FSS structures, but also for systems where the FSS panels are directly integrated on top of the array aperture [1]. In particular, the FSS can be used in combination with the array in order to:

- improve the Radar Cross Section of the platform;
- improve the frequency selectivity of the antenna, by properly “shaping” (enlarging or reducing) the array bandwidth.

In the first case, it is not always sufficient to merely place the FSS in front of the array, but it must be properly shaped in order to get an effective reduction of the RCS.

In the second case, the FSS can be used to increase the bandwidth of the array, or create small stop-bands within the antenna bandwidth in order, for example, to reduce EMI problems in a complex platform environment containing several antennas [2].

The tool developed by TNO allows the analysis of open-ended waveguide arrays integrated with an arbitrary number of FSS panels. These latter may

consist of printed elements on dielectric substrates or perforated metal screens. Furthermore, the tool allows also the analysis of tuning or filtering elements and launchers inside the waveguide [3]. This gives the opportunity to design the array antenna as a whole (launcher, tuning or filtering elements in the waveguide, array apertures, FSSs), taking full advantage of the integrated structure and giving to the designer a number of different options and different degrees of freedom in the design process.

The MEN formulation looks at the overall structure as a cascade of uniform blocks coupled through common transition regions. For each uniform region (in Fig.1, it is shown, as an example, a compact radiating waveguide element with coax launcher), the multimode equivalent network is easily derived adopting a modal description of the field and using transmission line formalism.

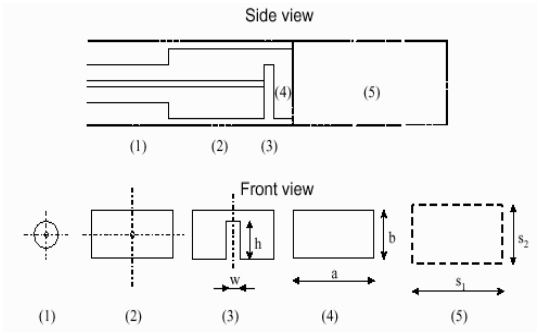

Figure 1 Example of decomposition of a complex structure (radiating waveguide element with coax launcher) into a cascade of uniform regions. The overall structure is studied with the MEN approach.

The corresponding representation of the transition region is on the contrary derived solving the set of integral equations obtained by imposing the continuity condition of the electromagnetic field and resorting again to the modal description adopted for the two adjacent regions [4]. An example of such FSS integrated array antenna structure is shown in Fig.2.

Fig. 3 shows the reflection coefficient of the FSS integrated array antenna of Fig.2, as a function of the frequency and for two different scanning angles. In the same picture, it is also shown a comparison with results obtained with the commercial software package HFSS [5]. The stop-band in the upper frequency band has been created in order to reduce the interference of an adjacent antenna system. The –10 dB useful bandwidth of the array between 8.0 and 10.5 GHz has been preserved.

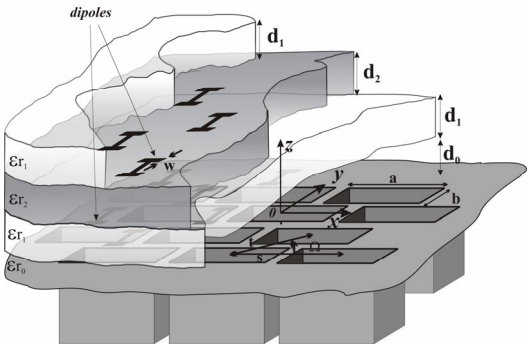

Figure 2 FSS integrated array antenna. The structure consists of the open-ended waveguide array and a multilayer FSS consisting of a core dielectric slab with printed FSS on both sides and two matching dielectric layers.

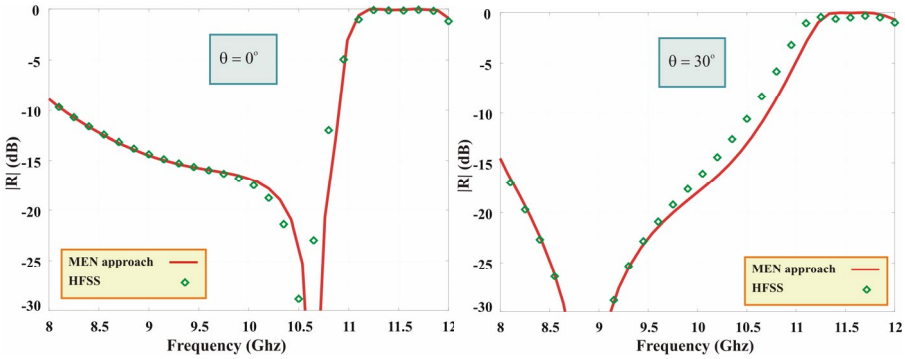

Figure 3 Magnitude of the reflection coefficient of the complete FSS cascaded with the array as in Fig. 2. Comparison between the MEN full-wave simulation and the result obtained using HFSS for different incidence angles.

References

[1] S. Monni, N. Llombart Juan, A. Neto, G. Gerini, "A closely spaced waveguide phased array integrated with a frequency selective surface: modeling and design", 2003 IEEE International Antennas and Propagation Symposium, June 2003, Columbus, Ohio.

[2] V. Galdi, G. Gerini, M. Guglielmi, H.J. Visser, F. d'Agostino, "CAD of Coaxially End-Fed Waveguide Phased Array Antennas", Microwave and Optical Technology Letters, vol. 34, No. 4, Aug. 2002

[3] S. Monni, G. Gerini, "A Novel Technique for the Design of Frequency Selective Structures Integrated with a Waveguide Array", 2004 IEEE International Antennas and Propagation Symposium, June 2004, Monterrey, California.

[4] G. Gerini, M. Guglielmi, G. Lastoria, "Efficient Integral Equation Formulations for Admittance or Impedance Representation of Planar

Waveguide Junctions", IEEE MTT-Symposium Digest, Anaheim, California, June 1998.
[5] Ansoft Corporation, ANSOFT HFSS-8.0.25 - User Guide Manual.

5.5.2 Curved surfaces

5.5.2.1 TNO

The type of structure that has been analyzed [1], [2] is reported in Fig. 1. It consists of an array of rectangular open-ended waveguides symmetrically developed all along an infinite metallic circular cylinder. Dielectric radomes and/or Frequency Selective Surfaces (FSS) can be placed in front of the apertures, in order to enhance some characteristics of the array, such as return loss and radiation pattern. The Unit Cell approach can be applied to such a structure under the hypothesis that all the apertures are placed symmetrically in both directions z and φ and are fed with the same amplitude, but with a progressive phase shift between two successive apertures. This assumption implies that radomes and/or FSS placed in front of the array must maintain the symmetry and the periodicity of the structure. Within each unit cell, as illustrated in a 3-d view in Fig. 2, we can identify the exciting rectangular waveguide, the radial phase shift wall waveguides (RPSWW), representing dielectric radomes or free space, and the metallic radial waveguides, representing the apertures in the FSS screens.

Assuming this representation, the problem is reduced to the analysis of a cascade of transitions between adjacent waveguides.

The electromagnetic field in the different regions is expanded in terms of eigenmodes. In general, in a radial waveguide, the electromagnetic field cannot be represented in terms of transverse to ρ vector modes.

The transverse field representation must consequently be effected on a scalar basis as a superposition of TE_z and TM_z modes w.r.t. the z-axis.

In the transverse directions φ and z the RPSWW and the metallic radial waveguide have different modal functions. These can be derived by imposing the proper boundary conditions dictated by the periodicity of the array for the RPSWW and by the metallic walls for the radial waveguide. In the radial coordinate, on the contrary, they have the same behavior, which can be described in terms of Hankel functions.

These functions (or the modified Bessel functions) represent forward and backward propagating (non-propagating) modes, respectively. A peculiarity of these waveguides is that forward waves "see" an enlarging radial waveguide, while the backward waves "see" a reducing radial waveguide. Hence, their characteristic impedances have different expressions and actually they are function of the radial coordinate.

Therefore, the same mode, at different sections of the radial waveguide, can be below cut-off (no propagation), or above cut-off (in propagation) passing through a transition region, the so-called gradual cut-off region, where the modal characteristic impedance gradually goes from a predominantly reactive to predominantly resistive behavior.

Once the modal spectra of the different regions are derived, the overall structure is analyzed resorting to the MEN approach and therefore cascading the multimode impedance matrix representations of the different regions and corresponding junctions.

A particular attention must be devoted to the transition between adjacent dielectric layers. In fact if this is trivial for the planar case, it is more complicated for the special case of radial waveguides. In fact, TE_z and TM_z modes in radial coordinates, employed in the transverse representation of the RPSWW, are separable with respect to the z axis (the axis of the cylinder), but propagating in the radial direction. With ordinary TE and TM modes in the direction of propagation, the air-dielectric or dielectric-dielectric interface would represent a simple junction between transmission lines, and the TE and TM modes would not be coupled together at the interface. On the contrary, the TE_z and TM_z modes used in the RPSWW do couple at this interface. For the characterization of simple or multi-layer dielectric radomes, it can be used the equivalent circuit representation shown in Fig. 3, [3], [4].

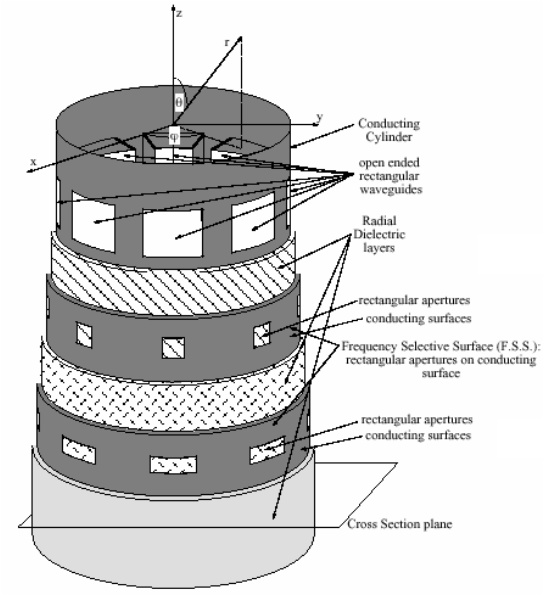

Figure1 Infinite array of open-ended waveguide radiators on a cylindrical surface loaded with dielectric layers and Frequency Selective Surfaces (FSS). The cylinder axis lies along z-axis.

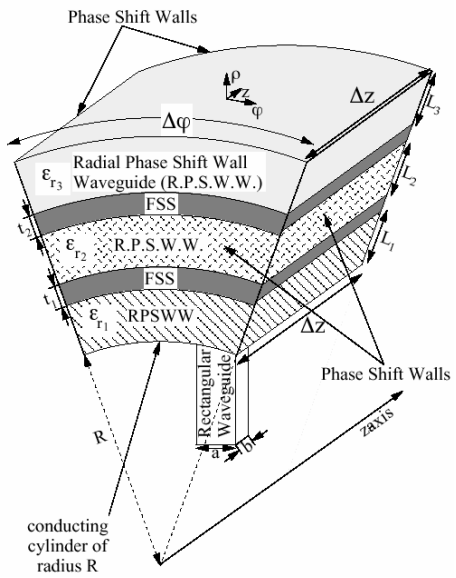

Figure 2 3-d view of the equivalent unit cell whose transverse-to-z section is shown in Fig. 1. A rectangular waveguide radiates through a conducting cylinder of radius R in the space and it is loaded with a cascade of Radial Phase Shift Wall Waveguide (RPSWW), filled with different dielectrics, and FSS

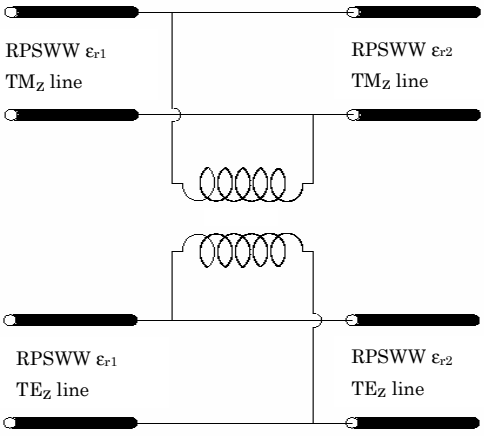

Figure 3 Equivalent circuit representing the coupling between TEz and TMz modes at the interface between two RPSWW with different dielectrics. TEz and TMz modes have the same combination of transverse indexes m and n

Fig. 4 shows the scattering parameters relative to the structure of Fig.2. The number of apertures (N) and the cylinder radius (R) are chosen in order

to maintain fixed the horizontal inter-element array $r\Delta\varphi$=24.247mm. This implies that: N=100 →R=0.386m, N=200 → R=0.772m, N=500 → R=1.929m. S_{11} refers to the reflection coefficient ``seen" from the TE_{10} mode of the horizontal WR90 rectangular waveguide. S_{12} represents the transmission coefficient to the fundamental TM_{00} mode. S_{13} represents the transmission coefficient to the first higher mode TM_{01}. TM_{00} and TM_{01} are above cut-off after the second FSS in the unit cell. TM_{01} mode is subject to the ``gradual" cut-off condition.

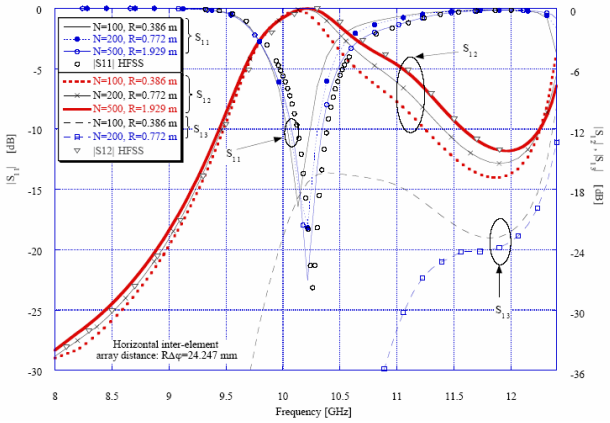

Figure 4 Scattering parameters relative to the structure shown in Fig. 2. The number of apertures (N) and the cylinder radius (R) are chosen in order to maintain fixed the horizontal inter-element array distance. S11 refers to the reflection coefficient ``seen" from the TE10 mode of the horizontal WR90 rectangular waveguide. S12 represents the transmission coefficient to the fundamental TM00 mode. S13 represents the transmission coefficient to the first higher mode TM01. TM00 and TM01 are above cut-off after the second FSS in the unit cell. TM01 mode is subject to the ``gradual" cut-off condition.

References

[1] G. Gerini, L. Zappelli, "Cilindrical Conformal Arrays Loaded With Frequency Selective Screens", 31st European Microwave Conference 2001 Proceedings, 24-28 September 2001, London, U.K.

[2] G. Gerini, L. Zappelli, "Multilayer Array Antennas with Integrated Frequency Selective Surfaces Conformal to a Circular Cylindrical Surface", accepted for publication on IEEE Trans. on Antennas and Propagation.

[3] P. J. B. Clarricoats and A. A. Oliner, "Transverse-network representation for inhomogeneously filled circular waveguide", Proc. of IEE , Vol. 112, No. 5, May 1965, pp. 883-894.

[4] A. Sanchez and A.A. Oliner, "A new Leaky Waveguide for Millimeter Waves Using Non-radiative Dielectric (NRD) waveguide - Part I: Accurate Theory", IEEE Trans on Microwave Theory and Techniques, Vol. MTT-35, No. 8, Aug. 1987, pp. 737-747.

5.5.2.2 Chalmers

Curved periodic structures have been used in reflector systems and radomes. The analysis of periodic strips and patches inside multilayer circular-cylindrical structures was performed by expanding the currents on the strips/patches in basis functions, and the amplitudes of the basis functions are determined numerically by the moment method (MoM) [1]. The electromagnetic field is in the form of Floquet modes due to the periodicity of the structure. It is sufficient to determine the current on one strip or patch, since the currents on the other strips are identical except for a phase difference. Similar type of analysis method was applied to spherical periodic structures [4].

If the source excites a full spectrum of plane or cylindrical waves, such as a dipole, the Floquet-mode expansion/MoM is a laborious process. A simpler approach is to use approximate boundary conditions. We have used two types of approximate boundary conditions for modelling the strips: the asymptotic strip boundary conditions and the boundary conditions obtained by the homogenization method (Chapter 3.4 and [1]-[3]). When applying homogenization method we have used a locally planar approximation, i.e. we assume that the surface where the strips are located is locally a plane surface. By this we can easily transform the boundary conditions from the rectangular coordinate system to the cylindrical one. The curved corrugated surfaces have also been analysed using the asymptotic boundary conditions [5].

Eliminato: one can suppose

Eliminato: also

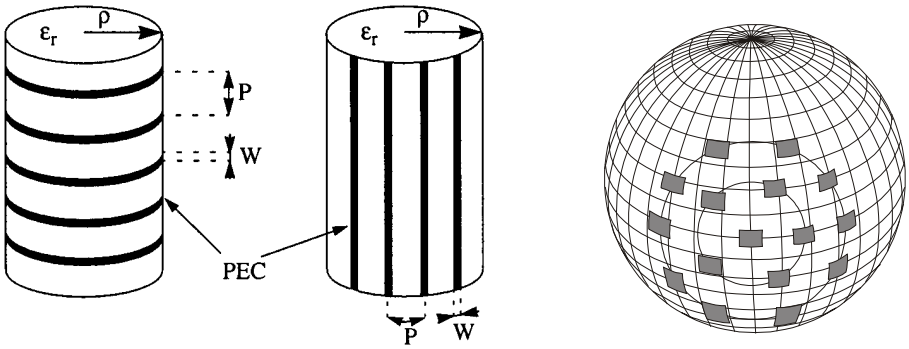

Figure 1 (a) cylindrical strip-loaded surface, (b) spherical periodical patch structure

References
[1] Z. Sipus, S. Raffaelli, P.-S. Kildal, "Periodic strips on planar and circular cylindrical substrates: Exact and asymptotic analysis," *Microwave and Optical Technology Letters*, Vol. 7, No. 3, pp. 173-178, Feb. 1998.
[2] P.-S. Kildal, A. Kishk, Z.Sipus, "Asymptotic boundary conditions for strip-loaded and corrugated surfaces," *Microwave and Optical Technology Letters*, Vol. 14, pp. 99-101, Feb. 1997.
[3] Z. Sipus, R. Zentner, J. Bartolic, "Validity of approximate boundary conditions for periodic strips on cylindrical substrates," *Proceedings of International Conference on Mathematical Methods in Electromagnetic Theory*, Kharkov, Ukraine, 1998, pp. 171-173.
[4] Z. Sipus, N. Burum, J. Bartolic, "Analysis of rectangular microstrip patch antennas on spherical structures," *Microwave and Optical Technology Letters,* Vol. 36, pp. 276-280, Feb. 2003.
[5] A. Kishk, P.-S. Kildal, A. Monorchio and G. Manara, "Asymptotic boundary condition for corrugated surfaces, and its application to scattering from circular cylinders with dielectric filled corrugations," *IEE Proceedings – Microwaves, Antennas and Propagation*, vol. 145, pp. 116-122, 1998.

5.5.3 Edge effects due to finite size of reflector or radome (Siena)

5.5.3.1 Truncated periodicity

The estimation of the reflection parameters in printed phased periodic surfaces is often based on the hypothesis of infinite structure; this allows the expansion of the fields in terms of Floquet waves (FW), thus reducing the analysis to that of a single cell of periodicity. As mentioned in Sec 5.2.1.3, the infinite surface approximation can be used to locally define equivalent currents to be used same way as Physical Optics. In this framework, the equivalent network introduced in section 5.2.1.1 can be adopted to synthesize the FSS behaviour with a moderate quantity of full-wave data. On the other hand, a rigorous analysis based on an element-by-element method of moments (MoM) becomes computationally prohibitive when the size of surface increases. An approximate while accurate alternative method consists of adding to the PO field an edge perturbation which may be rigorously estimated by solving via MoM an appropriate "fringe" integral equation [1], [2]. In this scheme, the perturbation field is expanded in terms of a few basis functions with domain on the entire surface aperture, which are derived by an efficient representation of the constituent locally tangent problem of semi-infinite periodic printed structure. Diffraction coefficients from this truncated periodicity problem can be obtained by superposing continuous equivalent FW source distribution extending over the semi-infinite array aperture [3], [4]. The asymptotic treatment of each FW aperture distribution

leads to a spatially truncated version of the infinite array FW expansion, plus FW-induced diffracted contributions from the edges of the array. Both the truncated FW series and the series of the corresponding diffracted field contributions exhibit excellent convergence properties so that the resulting representation is found extremely convenient with respect to the direct summation over the spatial contributions from each element of the array. This approach has been applied successfully to various canonical configurations, such as arrays of line sources in free-space [4] and on an infinite dielectric slab [5], as well as slits on a truncated ground plane [6]. Recently, the method has been extended to free-space semi-infinite phased dipole arrays [7], [8], and right-angle sectoral phased dipole arrays [9][10]. Invoking the localization principle of the diffraction phenomena at high frequency, these latter two canonical problems serve to construct the radiation from rectangular arrays as a superposition of edge and vertex FW-induced diffraction effects [11]. In [12], the three-dimensional (3-D) semi-infinite array treatment in terms of truncated FW is extended to an array of printed dipoles on a grounded slab (Fig. 1). This work generalizes the (two-dimensional) 2-D high-frequency solution presented in [5], to a 3-D case following the formulation used in [7], [8] for dipoles in free space. The rich variety of associated phenomena are investigated in [13] and [14], especially as concerned with the LW/SW-FW interaction as affected by various slab and array parameters, and with the corresponding generalized GTD wave physics which describes those effects. This high-frequency AGF can be used in the framework of the MoM scheme as in [4] for the analysis of patch phased arrays, as well as to approximate directly the field radiated by the array in the near zone.

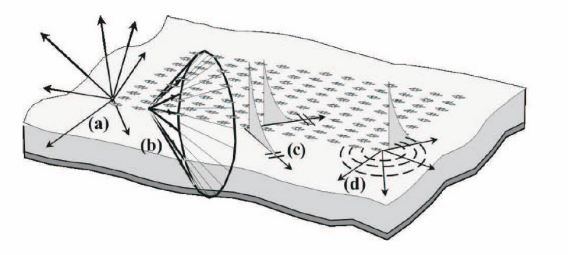

Figure 1 Waves excited by Floquet waves at a finite array of elementary dipoles printed on a grounded dielectric slab: (a) spherical vertex-excited (space) diffracted wave, (b) conical edge-excited (space) diffracted wave, (c) planar edge-excited surface wave, (d) cylindrical vertex-excited surface wave.

5.5.3.2 Truncated radomes

The analysis of the alteration of the radiation of an antenna system due to radome covers is a well consolidated field. There are books [15] and many contributions in scientific journals covering this topic [16]-[17]. Due to the typically large dimensions of the radomes in terms of the wavelength, their full wave analysis is usually restricted to axisymmetric structures [18],[19]. In more general cases, the analysis often resorts to high frequency techniques [20] such as Geometrical optics (GO), Geometrical Theory of Diffraction (GTD) or Physical Optics (PO). In particular PO [21],[22] is often selected as a general purpose tool since it does not suffer from the problems associated the presence of caustics in generically curved structures. A good reference for the comparisons between the different techniques can be found in [23]. A good approximation of the diffraction coefficients in dielectric structures can be obtained by a generalization of Physical Optics, which is concerned with the use of the Green's function of the stratified medium to estimate the equivalent current. This approach has been used in [24] and tested in [25] in comparison with full wave results. The "fringe integral equation" method presented in [26] has been proved as an efficient tool to test the accuracy of the diffraction coefficients derived from the above generalized PO.

References

[1] A. Neto, S. Maci, G. Vecchi, and M. Sabbadini, "A truncated Floquet wave diffraction method for the full-wave analysis of large phased arrays. Part I: Basic principles and 2D case," IEEE Trans. Antennas Propagat., vol. 48, Apr. 2000.

[2] A. Neto, S. Maci, G. Vecchi, and M. Sabbadini, "A truncated Floquet wave diffraction method for the full-wave analysis of large phased arrays. Part II: Generalization to the 3D case," IEEE Trans. Antennas Propagat., vol. 48, Apr. 2000.

[3] L. B. Felsen and L. Carin, "Diffraction theory of frequency and time domain scattering by weakly aperiodic truncated thin wire gratings," J.Opt. Soc. Amer., vol. 11, pp. 1291–1306, 1994.

[4] L. B. Felsen and E. G. Ribas, "Ray theory for scattering by two-dimensional quasiperiodic plane finite arrays," IEEE Trans. Antennas Propagat., vol. 44, pp. 375–382, Mar. 1996.

[5] L. Carin, L. B. Felsen, and T. T. Hsu, "High-frequency fields excited by a truncated arrays of nonuniformly distributed filamentary scatterers on an infinite dielectric slab: Parameterizing (leaky-mode)-(Floquet mode) interaction," IEEE Trans. Antennas Propagat., vol. 44, Jan. 1996.

[6] F. Capolino, M. Albani, S. Maci, and R. Tiberio, "High-frequency analysis of an array of line sources on a truncated ground plane," IEEE Trans. Antennas Propagat., vol. 46, pp. 570–578, Apr. 1998.

[7] F. Capolino, M. Albani, S. Maci, and L. B. Felsen, “Frequency domain Green’s function for a planar periodic semi-infinite phased array. Part I: truncated Floquet wave formulation,” IEEE Trans. Antennas Propagat., vol. 47, Jan. 2000.

[8] F. Capolino, M. Albani, S. Maci, and L. B. Felsen, “Frequency domain Green’s function for a planar periodic semiinfinite phased array. Part II: diffracted wave phenomenology,” IEEE Trans. Antennas Propagat., vol. 47, Jan. 2000.

[9] F. Capolino, S. Maci and L. B. Felsen, "Green's function for a planar phased sectoral array of dipoles", Radio Sci., Vol. 35, No 2, pp 579-593, arch-April 2000.

[10] F. Mariottini, F. Capolino, S. Maci, L. Felsen "Floquet wave diffraction Theory for a tapared planar angular sector array Green's function" IEEE Trans. on Antennas Propagat. to be published in 2004

[11] S. Maci, F. Capolino, L.B. Felsen "Three-dimensional Green's function for truncated planar periodic dipole arrays" Wave Motion, Vol. 34, pp. 263-279, 2001

[12] A. Polemi, A. Toccafondi, S. Maci, "High-frequency Green's function for a semi-infinite array of electric dipoles on a grounded slab. Part I: Formulation". IEEE Trans. on Antennas Propagat, Vol. 49, No. 12, pp. 1667-1677 December 2001

[13] S. Maci, A. Toccafondi, A. Polemi, L.B. Felsen "High-frequency Green's function for a semi-infinite array of electric dipoles on an infinite grounded stratified dielectric slab. Part II: Spatial Domain Parametrization" IEEE Trans. on Antennas Propagat.to be published in 2004

[14] L.B. Felsen, S. Maci, A. Polemi, A. Toccafondi, "High-frequency Green's function for a semi-infinite array of electric dipoles on an infinite grounded stratified dielectric slab. Part III: phase-matched wave interactions and numerical Results" IEEE Trans. on Antennas Propagat. to be published in 2004

[15] J. Kozakoff Analysis of Radome-Enclosed Antennas, Artech House Publishers, 1997

[16] R.K. Gordon, R. Mittra, " Finite Element Analysis of Axi-Symmetric radomes" IEEE Transactions On Antennas and Propagation, Vol. 41, July 1993, pg. 1975-980.

[17] M. A. Abdel Moneum, Z. Shen, J.L. Volakis, and O. Graham, "Hybrid Po-MoM Analysis of Large Axi-Symmetric Radomes" IEEE Transactions On Antennas and Propagation, Vol. 49, No. 12 December 2001, pg. 1657-1666.

[18] R. Orta, R. Tascone, R. Zich, "Performance Degradation of Dielectric Radome Covered Antennas" IEEE Transactions On Antennas and Propagation, Vol. 36, December 1988, No. 12 pg. 1707-1713

[19] Demetrius Paris, "Computer Aided Radome Analysis", IEEE Transactions On Antennas and Propagation, Vol. 18, No. 1, January 1970, pg.7-15

[20] D.C.F. Wu and R.C. Rudduck, "Plane Wave Spectrum-Surface Integration Technique for Radome Analaysis", IEEE Transactions On Antennas and Propagation, Vol. 22, May 1974, pg. 497-500

[21] Sembiam R. Regarajan, and Edmond Gillespie, "Asymptotic Approximations In Radome Analysis", IEEE Transactions On Antennas and Propagation, Vol. 36, No. 3 March 1988, pg. 405-414

[22] S. Maci, L. Borselli, L.Rossi "Diffraction at the edge of a grounded truncated dielectric slab", IEEE Transactions on Antennas and Propagation, Vol. 44, Issue 6, June 1996, pg. 862-873.

[23] S. Maci, L. Borselli, A. Cucurachi "Diffraction from a truncated grounded dielectric slab: a comparative full-wave / physical-optics analysis" IEEE Trans. on Antennas Propagat.,Vol. 48, No. 1, pp. 48-57, Jan. 2000.

[24] E. Jorgensen, S. Maci, A. Toccafondi, "Fringe integral equation method for a truncated grounded dielectric slab", IEEE Trans. on Antennas Propagat, Vol. 49, No. 8 pp. 1210-1217, August 2001.

5.5.4 Surface material defects and manufacturing tolerances (Lund)

The manufacturing process always induces errors in the design. Often the errors are modelled by random variables, and assuming a Gaussian error distribution the results for reflector surfaces and array antennas in [1-2] are employed to estimate the effect of the errors. For a general probability distribution, some corresponding formulas are derived in [3].

Usually, the effect of random errors is to decrease the deterministic (zero error) power by a typical factor $exp(-(k\delta)^2)$, where δ is the standard deviation of the errors in position. This decrease corresponds to the conversion of some deterministic power to a diffuse contribution proportional to the number of faulty elements. Often the errors are not Gaussian distributed, and for a general probability distribution the exponential factor is replaced by the Fourier transform, or characteristic function, of the probability distribution [3]. In the limit of small errors, there is no difference between different error distributions, unless the degrees of freedom are radically different between two distributions.

Manufacturing tolerances on surfaces and antenna elements can be estimated from analytical expressions as above, or by examining the sensitivity to perturbations in numerical simulations of the structure. In the latter case, it is important to have access to a code as general as possible, so that the code allows variation of the parameters needed to estimate the tolerances. When deciding on tolerance levels, it is important to have a clear understanding of the entire development chain of the antenna system, from the

numerical simulations guiding the design, to the final manufacturing process and the environment in which the antenna is supposed to operate.

References

[1] J. Ruze. The effect of aperture errors on the antenna radiation pattern. Nuovo Cimento Suppl., Vol. 9, No. 3, pp. 364-380, 1952.

[2] J. Ruze. Antenna tolerance theory – a review. Proc. IEEE, Vol. 54, No. 4, pp. 633-640, 1966.

[3] D. Sjöberg. Coherent effects in single scattering and random errors in antenna technology. Technical Report LUTEDX/(TEAT-7109)/1-21/(2002), Lund Institute of Technology, Department of Electroscience, Sweden, 2002. http://www.es.lth.se/teorel.